Inaugural dissertation

for

obtaining the doctoral degree

of the

Combined Faculty of Mathematics, Engineering and Natural Sciences

of the

Ruprecht - Karls - University

Heidelberg

Presented by

M.Sc. Natalia Sokolova

born in: Moscow, Russia

Oral examination: 17-11-2023

From progenitors to stem cells: emergence and characterization of adult retinal stem cells in medaka

Referees: Prof. Dr. Jochen Wittbrodt

Prof. Dr. Steffen Lemke

Abstract

Many vertebrate species show life-long growth facilitated by distinct and dedicated stem cell systems. Understanding the initial establishment and life-long maintenance of stem cells and their environment is, therefore, a key to understanding the transition between these species and mammals that have lost life-long growth capacity. In teleost fish, the retinal stem cell niche, called the ciliary marginal zone (CMZ), facilitates retinal growth and the proliferative behavior of stem cells and their progenitors, ensuring organ growth and functionality throughout life. The mature CMZ is found in the distal periphery of the retina, and it is composed of concentric rings containing stem (distal) and progenitor cells (more proximal), respectively. While stem and progenitor cells within the CMZ and their relative contribution to shape and function are well established, the origin of retinal stem cells (RSCs) remains obscure. Previous studies suggested the existing link between eye morphogenesis and RSC establishment and for a predefined RSC population at the early stages of eye development. Therefore, the objective of this thesis is centered on understanding the processes and mechanisms behind the development of adult RSCs in teleost fish. To describe RSCs in more depth, I conducted single-cell RNA sequencing of the medaka (Oryzias latipes) retina and unveiled novel markers for RSCs and retinal progenitor cells (RPCs). To address whether the establishment of RSCs is coupled to the optic cup morphogenesis, I inspected the pattern of RSC marker expression in the conditions of interrupted eye morphogenesis through either drug treatment or genetic mutations. I could show that stem cell marker expression is still initiated in the CMZ upon defected eye morphogenesis, indicating that all retinal progenitors retain the potency of acquiring retinal stem cell identity. Moreover, I analyzed the changes in the proliferative behaviour of retinal stem cell marker-expressing cells within the peripheral retina utilizing BrdU incorporation and tracing their progeny after Cre/loxP-mediated recombination. I observed that the fast-proliferating retinal progenitors in the retinal periphery switch to a slower proliferative behavior during the embryonic development of medaka. Via long-term clonal analysis, I showed when the retinal peripheral cells become clonal, i.e., bona fide stem cells. Taken together, my findings challenge the notion of a pre-existing early RSC population in eye development and argue for presence of mechanisms by which embryonic RPCs at the retinal periphery mature into adult stem cells in the medaka CMZ.

Zusammenfassung

Viele Wirbeltierarten zeigen ein lebenslanges Wachstum, welches durch spezielle, adulte Stammzellpopulationen ermöglicht wird. Das Verständnis der anfänglichen Etablierung und lebenslangen Aufrechterhaltung dieser Stammzellpopulationen ist daher wesentlich um Verständnis für den Übergang zwischen diesen Arten und den Säugetieren zu erlangen, die ihre lebenslange Wachstumsfähigkeit verloren haben. Bei den Knochenfischen ermöglicht die retinale Stammzellnische, die so genannte ziliare Marginalzone (CMZ), das lebenslange retinale Organwachstum und damit dessen anhaltende Funktionalität. Die reife CMZ befindet sich in der äußersten Peripherie der Retina und besteht aus konzentrischen Ringen, die Stammzellen (distal) sowie Vorläuferzellen (proximal) beinhaltet. Während die Lokalisation der Stamm- und Vorläuferzellen innerhalb der CMZ, sowie ihr relativer Beitrag zu retinaler Form und Funktion gut bekannt sind, ist der Ursprung der retinalen Stammzellen (RSCs) nach wie vor unklar. Frühere Studien legten nahe, dass ein Zusammenhang zwischen der Morphogenese des Auges und der Entstehung von RSCs besteht und dass es eine vordefinierte RSC-Population in den frühen Phasen der Augenentwicklung gibt. Daher ist das Ziel dieser Arbeit die ausführliche Untersuchung der Prozesse und Mechanismen hinter der Entstehung adulter RSCs bei Knochenfischen. Um die RSCs genauer zu charakterisieren, habe ich eine Einzelzell-RNA-Sequenzierung der Medaka (Oryzias latipes) Retina in verschiedenen embryonalen Entwicklungsstadien durchgeführt und damit neue Marker für RSCs und RPCs beschrieben. Um herauszufinden, ob die Etablierung retinaler Stammzellen an die Morphogenese des Augenbechers gekoppelt ist, untersuchte ich die räumliche Verteilung der Expression von RSC-Markern unter Bedingungen, bei denen die Morphogenese des Auges entweder durch medikamentöse Behandlung oder durch genetische Mutationen unterbrochen wurde. So konnte ich zeigen, dass die Expression von Stammzellmarkern auch bei gestörter Augenmorphogenese in der CMZ initiiert wird. Dies deutet darauf hin, dass alle retinalen Vorläuferzellen die Fähigkeit behalten retinale Stammzellidentität zu erwerben. Darüber hinaus habe ich Veränderungen im Proliferationsverhalten von Zellen, die retinale Stammzellmarker exprimieren, in der peripheren Retina mit Hilfe von BrdU-Inkorporationsexperimenten analysiert und ihre Nachkommenschaft nach Cre/loxP-vermittelter Rekombination verfolgt. Hier zeigte sich, dass die schnell proliferierenden retinalen Vorläuferzellen in der Netzhautperipherie während der

Embryonalentwicklung von Medaka zu einem langsameren Proliferationsverhalten wechseln. Mittels klonaler Langzeitanalysen konnte ich zeigen, wann die Zellen der Netzhautperipherie klonal werden, d.h. echte Stammzellen sind. Insgesamt widersprechen meine Ergebnisse die verbreitete Vorstellung einer bereits existierenden frühen RSC-Population in der Augenentwicklung und sprechen für das Vorhandensein von Mechanismen, durch die embryonale RPCs in der Netzhautperipherie zu adulten Stammzellen in der CMZ von Medaka heranreifen.

List of Abbreviations

opo *ojoplano.*

3D three-dimensional.

aldh aldehyde dehydrogenase.

ArCoS arched continuous stripe.

BrdU Bromodeoxyuridine.

BSA bovine serum albumin.

ccl25b chemokine (C-C motif) ligand 25.

cDNA complementary DNA.

CMZ ciliary marginal zone.

cndp1 carnosine dipeptidase 1.

col collagen.

CTP cytidine triphosphate.

DAPI 4,6-diamidino-2-phenylindole.

DMSO Dimethylsulfoxid.

dpf days post fertilisation.

dpr days post recombination.

E.coli Escherichia coli.

ECM extracellular matrix.

EdU 5-Ethynyl-2-deoxyuridine.

ERM embryonic rearing medium.

ERT2 selectively tamoxifen-sensitive estrogen receptor.

EtBr ethidium bromide.

FACS fluorescence-activated cell sorting.

FGF fibroblast growth factor.

GCL ganglion cell layer.

GFP green fluorescent protein.

HCR hybdridization chain reaction.

her human epidermal growth factor receptor.

hes hairy and enhancer of split.

HSC hematopoietic stem cell.

iArCoS induced ArCoS.

IGF insulin-like growth factor.

INL inner nuclear layer.

LB lysogeny broth.

Lgr5 Leucine-rich repeat-containing G-protein coupled receptor 5.

MG Müller glia.

mRNA messenger RNA.

NBT nitro blue tetrazolium chloride.

NR neural retina.

NSC neural stem cell.

ON optic nerve.

ONL outer nuclear layer.

PCNA proliferation cell nuclear antigen.

PFA paraformaldehyde.

PTW phosphate buffered saline plus Tween 20.

RGC retinal ganglion cell.

rNTP ribonucleoside triphosphate.

RPC retinal progenitor cell.

RPE retinal pigmented epithelium.

RSC retinal stem cell.

RSG red switch green.

rx retinal homeobox gene.

scRNA single-cell RNA.

sparc secreted protein acidic and rich in cysteine.

TAE Tris-acetate-EDTA-buffer.

TGFß transforming growth factor beta.

UV ultraviolet radiation.

V-SVZ ventricular-subventricular zone.

Wnt wingless-related integration site.

wph weeks post hatch.

Contents

1

Introduction

1.1 Adult stem cells in anamniotes and mammals

Adult stem cells are crucial for maintaining tissue balance and repairing damage in mammals and anamniotes. They are located in specialized environments known as stem cell niches, where interactions between the cells and their environment help sustain their presence (Ferraro et al., 2010; Li and Xie, 2005). While mammalian and anamniote adult stem cells share characteristics like self-renewal and the ability to differentiate into specialized cell types (Bond et al., 2015), there are notable distinctions in their functions. One such difference lies in the capacity of anamniotes to support continuous lifelong growth (Straznicky and Gaze, 1971). Mammalian adult stem cells primarily serve to replenish cells lost during homeostasis or regeneration in tissues like the intestines, blood, and skin (Barker et al., 2007; Lee and Hong, 2020; Milsom and Essers, 2023; Tumbar et al., 2004; Zhang et al., 2009). In contrast, anamniotes, including amphibians and teleost fish, possess adult stem cells that enable organ size to increase as the body grows proportionally (Hollyfield, 1971; Johns and Easter, 1977; William and Perron, 1998). This contrast is evident in the mechanisms regulating stem cells in these systems. While most mammalian adult stem cells remain dormant (Cheung and Rando, 2013; Urbán et al., 2019), the rapid postembryonic growth and maintenance of organ size in anamniotes necessitate a constant supply of adult stem cells (Kaslin et al., 2009; Roselló-Díez and Joyner, 2015). In teleost fish, specialized stem cell niches have been described in various organs, such as brain, neuromasts and gills (Grandel et al., 2006; Kaslin et al., 2009; Seleit et al., 2017; Stolper et al., 2019). Another notable example is the presence of RSC in fish, which contribute to ongoing neurogenesis and enable continuous growth of the retina (Centanin et al., 2011; Wetts et al., 1989). Conversely, in mammals, the RSCs hardly contribute to neurogenesis after birth (Bélanger et al., 2017; Moshiri and Reh, 2004).

1.2 Ciliary marginal zone as a model for studying adult RSCs

1.2.1 Ciliary marginal zone in anamniote species

A perfect example of a niche containing adult stem cells is a ciliary marginal zone located in the peripheral region of the retina (Figure 1.1A-B). As shown by BrdU treatment or proliferation cell nuclear antigen (PCNA), this region contains a pool of undifferentiated proliferating progenitors across different species (Centanin and Wittbrodt, 2014; Miles and Tropepe, 2021; Raymond et al., 2006). In anamniotes, such as teleost fish and amphibians, these cells serve as a pool, providing life-long postembryonic growth. Clonal analysis showed that the ciliary marginal zone of these species contains two major undifferentiated cell types – slowly dividing stem cells and fast-proliferating progenitors (Centanin et al., 2011; Ohnuma et al., 2002; Wan et al., 2016; Wong and Rapaport, 2009). RSCs are located at the most peripheral position and, upon asymmetrical division, produce retinal progenitor cell (RPC) positioned more centrally (Angileri and Gross, 2020; Becker et al., 2021; Reinhardt et al., 2015). Whereas in some species, the differentiation between stem and progenitor cells is relatively clear, in others, it is more challenging to distinguish them (Angileri and Gross, 2020; Becker et al., 2021; Centanin et al., 2014). Clonal lineage analysis of individually labeled cells was able to provide more insights into mechanisms by which stem and progenitor cells contribute to retinal growth: as stem cells give rise to so-called arched continuous stripe (ArCoS), which represent themselves life-long clones, whereas clones originating from progenitors are going to be disconnected from the CMZ (Becker et al., 2021; Centanin et al., 2014). Several studies also showed that RSCs serve as a source of growth not only for the neural retina but also for retinal pigmented epithelium (RPE) (Becker et al., 2021; Tsingos et al., 2019). Few markers are known to label adult stem cells in the teleost fish retina: *carnosine dipeptidase 1 (cndp1)* and *col15a1b* (previously known as *mz98*) in medaka and zebrafish, respectively (Angileri and Gross, 2020; Becker et al., 2021; Pujic et al., 2006). Besides, a Cre/loxP-mediated clonal analysis showed that a population of most peripheral cells in the CMZ of medaka expressing a cytokine, *ccl25b*, gives rise to continuous clones, called iArCoS (Eggeler, 2017). In turn, the middle part of CMZ of teleost fish, representing early progenitors, is marked by expression of *rx2*, *vsx2*, *gli3*, *pax6*, *hes1* and *six3* (Becker et al., 2021; Raymond et al., 2006; Reinhardt et al., 2015; Wan et al., 2016). Molecular markers of early progenitor cells are also expressed by RSCs. As progenitors divide, they produce

late RPCs expressing atoh7 and the F-actin binding protein anillin (Cepero Malo et al., 2017; Pérez et al., 2018).

1.2.2 Retinal architecture of the medaka eye

The result of a functioning retinal stem cell niche is the complex, constantly growing structure consisting of multiple neuronal cell types. Their interplay provides one of the major senses – the vision (Baden et al., 2019; Ptito et al., 2021). The mature retina contains seven cell types, including six neuronal and one glial cell types, distributed in 3 nuclei layers (Figure 1.1A). The light-sensitive photoreceptors in the outer nuclear layer (ONL) capture and transmit photons into electrochemical signals. These signals are then transferred along neurons of the inner nuclear layer (INL) - bipolar, horizontal and amacrine cells (BC, HC and AC, respectively) to the retinal ganglion cell (RGC)s, which nuclei reside in the ganglion cell layer (GCL) (Diamond, 2017; Ptito et al., 2021). Axons of retinal ganglion cells extend into the brain, forming the optic nerve (ON). The nuclei layers are separated by outer and inner plexiform layers (ONL and INL, respectively), where neuronal axons and dendrites form synaptic connections (Ptito et al., 2021). The glial cell type, Müller glia (MG), is located in the INL and serves many roles, such as maintaining retinal organization, promoting neuronal survival and regeneration and facilitating synaptogenesis (Bernardos et al., 2007; Lust and Wittbrodt, 2018; Tworig and Feller, 2022). The growth supporting such a complex structure is subjected to a specific spatiotemporal order (Centanin et al., 2011; Hollyfield, 1971; Straznicky and Gaze, 1971). As was shown in the medaka retina through BrdU incorporation experiments, proliferating cells of the CMZ incorporate BrdU (Figure 1.1C, left). With time, they get further centralized, being pushed out of the retinal periphery(Figure 1.1C, center). Thereby, the central retina represents older neurons that differentiated before BrdU application, while the peripheral retina is younger (Figure 1.1C, right).

1.2.3 CMZ in other vertebrate species

In other anamniotes, birds and mammals, the peripheral part of the retina also contains pools of undifferentiated proliferative cells (Table 1.1). The cells of CMZ in chick and quails in a postembryonic eye proliferate and contribute to certain retinal cell types, such as amacrine and bipolar cells, but not RGCs or photoreceptors (Fischer and Reh, 2000; Kubota et al., 2002; Morris et al., 1976). Until very recently there was little evidence that mammalian CMZ in vivo contains proliferative cells that can contribute to adult neurogenesis in vivo. Earlier studies showed the cells

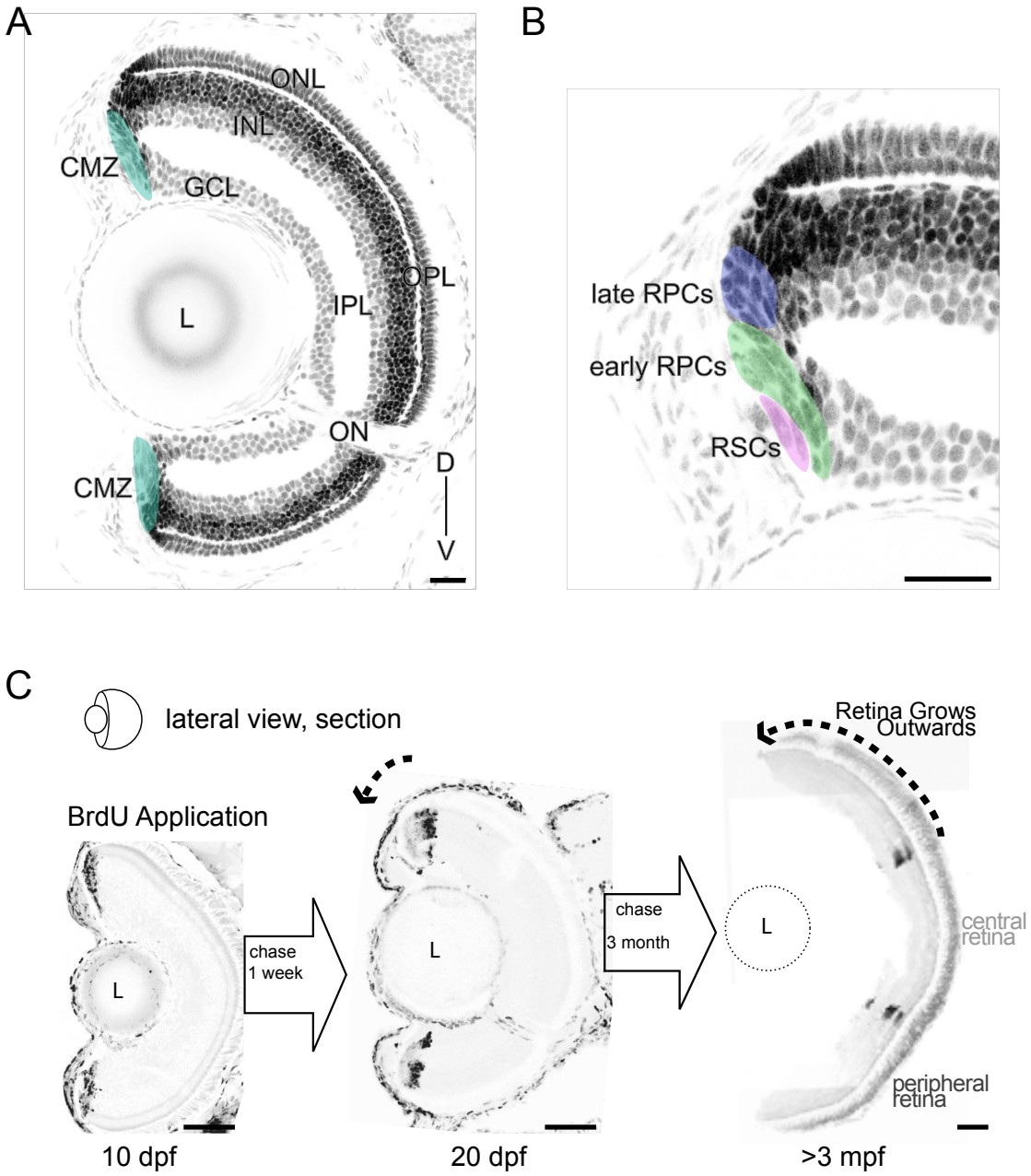

Figure 1.1. Structure and growth of the medaka retina.
(A) Transverse central cryosection of medaka retina at hatchling stage stained with nuclear stain 4,6-diamidino-2-phenylindole (DAPI) . Differentiated retina is organized in 3 nuclear layers: RGCs, INL, containing BC, HC, and AC and outer nuclear layer consisting of photoreceptors. The inner plexiform layer (IPL) separates GCL and INL, and outer plexiform layer (OPL) separates INL and ONL. The CMZ (in cyan) is located at the retinal periphery. L, lens. **(B)** Transverse central cryosection of medaka retina, showing dorsal CMZ, stained with DAPI . RSCs (magenta), early RPCs (green) and late RPCs (in blue) are schematically labelled. Scale bars for **(A)** and **(B)** are 20 µm.

Figure 1.1. **(C)** BrdU incorporation (black) by the cells of the CMZ reflects the accurate spatiotemporal order of medaka retina growth. When a BrdU pulse is succeeded by a 10-day chase, BrdU-labeled cells are observed in more central locations (center). After extending the chase to 3 months, these BrdU+ cells move to even deeper central positions (right). L, lens. Scale bar is 50 µm. Panel (C) is adapted from Centanin et al. (2011)

in the pigment epithelium of the ciliary body are able to proliferate and to form colonies consisting of several cell types, such as photoreceptors, bipolar cells and MG (Ahmad et al., 2000; Tropepe et al., 2000). Recently it was shown that the Msx1-positive proximal domain in the mouse CMZ contains progenitors that are proliferative and are able to give rise to both neural and non-neural lineages of the retina (Bélanger et al., 2017; Marcucci et al., 2016). While the neural lineage of the Msx1-positive progenitors includes all retinal cell types, this process is restricted to embryonic development and is lost in the postembryonic retina (Bélanger et al., 2017). Interestingly, the neurogenic activity of mammalian CMZ progenitors is extended when one allele of the Sonic hedgehog receptor patched is lost: CMZ progenitors can retain their ability to proliferate and maintain a stem cell-like gene expression profile for up to three months (Moshiri and Reh, 2004). Additionally, experiments involving the cultivation of cells of the pigmented ciliary body from adult mammalian retinas in vitro have demonstrated self-renewal and multipotent characteristics of these cells, as evidenced by the formation of neurospheres (Ahmad et al., 2000; Coles et al., 2004; Tropepe et al., 2000). However, the neurospheres' capability to generate all types of retinal cells, indicating their true multipotency, is not entirely clear, as they predominantly differentiate into only subset of the retinal cell types (as discussed in Frøen et al. (2013). Furthermore, it has not been confirmed whether fully differentiated neurons resulting from this process are postmitotic or capable of integrating into the neuronal circuitry (Frøen et al., 2013; Reh, 2002). Thus, the current understanding of proliferative progenitors of the CMZ in the mammalian retina suggests that they contribute to neurogenesis during embryonic development in vivo, while their "stem" characteristics can be observed post-embryonically only under specific in vitro conditions or genetic modifications. These findings suggest the existence of a mechanism that operates after embryonic development to restrict the full stem potential of CMZ cells in the mammalian retina in vivo.

1.3 Origin of adult RSCs

Emergence of adult RSCs is inextricably linked to eye morphogenesis. Retinal development has been extensively studied over several decades (Casey et al., 2021; Chow and Lang, 2001; Diacou et al., 2022; Fuhrmann, 2010; Martinez-Morales et al., 2017; Sinn and Wittbrodt, 2013). It starts with the specification of the eye field in the anterior neural plate and the subsequent evagination of the optic vesicle into an optic cup. As the optic cup is formed, the three main tissues of the eye are specified: , RPE surrounding the , and CMZ at the eye periphery (Fernández-Nogales et al., 2019). As the optic vesicle evaginates, it is composed of a pseudostratified epithelium (Heermann et al., 2015; Kwan et al., 2012). A complex interaction of the optic vesicle and surrounding tissues, such as surface ectoderm and periocular mesenchyme, is required for proper optic cup morphogenesis (Chow and Lang, 2001). It is accompanied by a spectacular change of shape for RPE and neural retina (NR) precursors, driven by pulsatile contractions of the cytoskeleton (Figure 1.2). The accumulation of actin and myosin on the basal side of retinal progenitors in the distal layer of the optic vesicle leads to gradual shrinkage of their basal surface and relaxation on the apical side. When applied to all retinal progenitors of the distal layer, this process generates force for NR inward bending (Figure 1.2). RPE precursors, in turn, also change their shape to a flatter one.

1.3.1 Optic cup morphogenesis in teleost fish

With microscopy advances of the last decade in vivo imaging of zebrafish and medaka eye development revealed essential details in the optic cup formation process (Heermann et al., 2015; Martinez-Morales et al., 2017; Sidhaye and Norden, 2017; Sokolova, 2019; Tang et al., 2017). Besides the basal constriction of retinal progenitors, active migration of cells was shown to significantly contribute to the optic cup formation in teleost fish (Figure 1.2A). This process, also called as “neuroepithelial flow” or “rim involution”, describes the flow of cells of the proximal layer migrating and contributing to the distal layer, which later differentiates into NR (Figure 1.1A-B) (Heermann et al., 2015; Nicolás-Pérez et al., 2016; Sidhaye and Norden, 2017; Sokolova, 2019). Meanwhile, a small domain of the proximal layer flattens and expands, thereby shaping the future RPE (Figure 1.2B) (Heermann et al., 2015). The rim involution has also been shown to depend on the BMP signaling pathway and extracellular matrix (ECM) integrity (Heermann et al., 2015; Nicolás-Pérez et al., 2016; Sidhaye and Norden, 2017). Genetic manipulations, perturbing ECM -related

genes, such as *laminin alpha 1* and *ojoplano (opo)*, led to impaired optic cup morphogenesis (Bryan et al., 2016; Martinez-Morales and Wittbrodt, 2009; Sidhaye and Norden, 2017; Soans et al., 2022). Interestingly, the treatment of zebrafish embryos with blebbistatin, a small molecule inhibitor of non-muscle myosin II (Straight et al., 2003), interfered with optic cup folding presumably by blocking basal constriction (Nicolás-Pérez et al., 2016).

1.3.2 Different modes of optic cup morphogenesis in teleost fish and mammals

In the meantime, the development of three-dimensional (3D) retinal organoid cultures allowed to capture the optic cup formation in the mammalian system (Eiraku et al., 2012, 2011). This process involves the invagination of the spherical vesicle through the flattening of the distal part and the formation of the hinge on the border between NR and RPE (Figure 1.2C). The molecular analysis of the formed optic cup confirmed the identities of the main domains as NR and RPE (Eiraku et al., 2011). The basal constriction of the NR progenitors mediated by rearrangement of the actomyosin network was found to be driving the NR invagination (Figure 1.2C) (Eiraku et al., 2012). As in zebrafish, disturbance of myosin activity via blebbistatin treatment affected the invagination process and formation of the hinge (Eiraku et al., 2011). While optic cup morphogenesis in both, fish and mammals, relies on the basal constriction of retinal progenitors, the rim involution seems to be the unique feature for the teleost fish (Table 1.1). As rim involution is independent of proliferation and faster than a single cell cycle in the optic vesicle neuroepithelium in zebrafish, it has been suggested to be adopted by fast-developing species to support the balance between NR and RPE and proper folding of the optic cup (Cardozo et al., 2023; Heermann et al., 2015; Li et al., 2000; Moreno-Mármol et al., 2021; Nicolás-Pérez et al., 2016). In amniotes, a slower speed of development allowed the optic cup layers to grow via cell proliferation, which is reflected in thicker RPE and the optic cup invagination failure upon mitotic arrest (Table 1.1) (Eiraku et al., 2011; Moreno-Mármol et al., 2021). Nevertheless, the different modes of optic cup formation led to invagination of the NR, wrapped by RPE with the CMZ domain stereotypically positioned at the border between NR and RPE.

1.3.3 CMZ specification during optic cup morphogenesis

In accord with differences in optic cup formation, distinct mechanisms for CMZ formation have been described. In zebrafish, backward individual cell tracking of

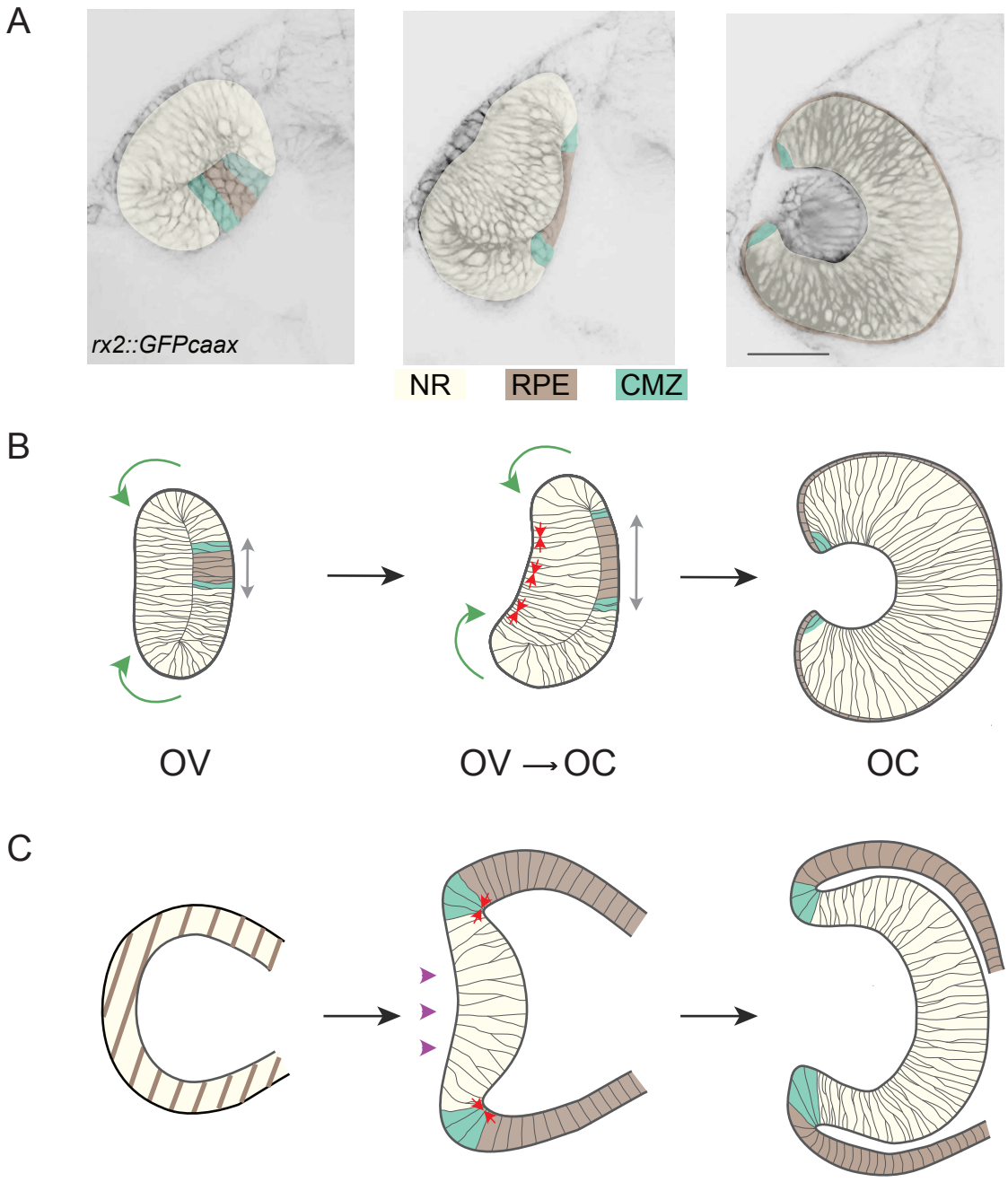

Figure 1.2. Structure and growth of the medaka retina.
(A) Successive steps of optic cup formation in zebrafish embryo. Rx2-expressing cells are labeled with membrane-tagged GFP (grey) (rx2::GFPcaax). (adapted from (Heermann et al., 2015). The NR (in beige), RPE (in brown) and CMZ (in green) domains are schematically labelled. **(A-B)** Rim involution (green arrows) of neuroepithelial cells into a distal layer of the optic vesicle (in beige) drives the optic cup formation. This process is accompanied by basal constriction of neural retinal progenitors (red arrows in **B**) and stretching (grey arrow) of the presumptive RPE (brown) cells.

Figure 1.2. The future CMZ cells (in green) originate from two distinct domains within the proximal layer at the optic vesicle stage (Heermann et al., 2015; Kwan et al., 2012; Li et al., 2000; Picker et al., 2009; Sidhaye and Norden, 2017). **(C)** Mouse early optic vesicle is bi-potent, able to give rise to NR as well as RPE (beige/brown stripes). Optic cup formation in mouse is driven by autonomously bending NR (violet arrowheads), largely depending on cell proliferation, apical relaxation of the developing NR layer and formation of wedge-shaped cells at the hinge region between NR and RPE (red arrows in **C**) (Eiraku et al., 2011). The CMZ markers appear at the junction between NR and RPE of the optic cup. Scale bar 50 µm. OV, optic vesicle; OC, optic cup. The figure is adapted from Sokolova et al. (2023)

CMZ cells revealed that RSCs originate from the set of retinal progenitors in the proximal layer of the optic vesicle (Heermann et al., 2015; Tang et al., 2017). As the rim involution proceeds and the RPE stretches, the future adult RSCs take their position at the retinal periphery (Figure 1.2A-B). It implicates a potential scenario where RSCs are predetermined early at the optic vesicle stage prior to the onset of optic cup morphogenesis (Heermann et al., 2015). In another anamniote species, *Xenopus*, the rim involution has not been examined yet, however, the optic cup folds independently of cell proliferation (Table 1.1) (Harris and Hartenstein, 1991). The scenario in which the RSCs would be predetermined in the optic vesicle found its proof in this species, as the retinal stem cell marker Hes4 was found at the NR / RPE border of the optic vesicle El Yakoubi et al. (2012). Moreover, the overexpression of Hes4 prevented NR and RPE differentiation and slowed down the cell cycle in Hes4-overexpressing progenitors El Yakoubi et al. (2012), which collaborates with the slow cell cycle kinetics of adult RSCs Ohnuma et al. (2001). In mammals, the first markers of the CMZ start appearing only after the formation of the optic cup (Martinez-Morales et al., 2001; Trimarchi et al., 2009). Studies performed in 3D organoid cultures suggest that the stem cell markers appear at the NR / RPE junction (or the hinge – Figure 1.2C) through the modulation of fibroblast growth factor (FGF) and wingless-related integration site (Wnt) signaling pathways. Interestingly, the fate of either domain could be reverted by tuning of FGF and Wnt signaling pathways (Kuwahara et al., 2015). When dissected and cultured in vitro, the CMZ cells from the NR / RPE junction confirmed their neurogenic potential by creating retinospheres (Kuwahara et al., 2015). The idea that interaction between FGF and Wnt signaling is required for the formation of CMZ has been recently

also addressed in the mammalian retina (Balasubramanian et al., 2021). Utilizing Cre/loxP-system and scRNA sequencing, Balasubramanian et al. (2021) were able to show in great detail that CMZ formation is dependent on the fine-tuning of FGF signaling. As the Wnt pathway is known for promoting stem cell fate in various systems, including vertebrate retina (Heavner et al., 2014; Liu et al., 2007), they also investigated the crosstalk between the two pathways and showed that constitutively active Wnt signaling transforms NR into CM, which upon removal of FGF receptors can be further transdifferentiated into RPE . In return, FGF overexpression leads to the transformation of RPE into CMZ (Balasubramanian et al., 2021). Such a flexible system suggested that CMZ is not really predetermined at the optic vesicle stage and appeared *in situ* as a result of singaling pathways' crosstalk.

Taken together, different modes of optic cup morphogenesis result in the formation of CMZ with variable stem potential. While further comparative studies are necessary to elucidate differences in the RSCs between fish and mammals, for now, it is not possible to rule out the possibility that the retinal stem cell precursors are inherently different in their neurogenic activity. Thus, it is alluring to suggest that the extended neurogenic potential of RSCs of lower vertebrates may be defined by the rim involution during eye morphogenesis. On the other side, it is also possible that the retinal stem cell identity is instructed in situ upon morphogenesis.

Table 1.1. Capacity to life-long growth and origin of RSCs in various species.

Species	Capacity to life-long growth	Presence of RSCs in adult retina in vivo in the CMZ	Optic cup formation	Origin of RSCs
Teleost fish (zebrafish, medaka)	+	++	Mediated through rim involution, RPE stretching (Heermann et al., 2015; Kwan et al., 2012; Sidhaye and Norden, 2017); Cell proliferation independent (Heermann et al., 2015; Kwan et al., 2012; Sidhaye and Norden, 2017);	RSCs originate from a set of cells in the lens-averted layer of the optic vesicle(Heermann et al., 2015; Tang et al., 2017)
Amphibians (Xenopus)	+	++	No evidence for rim involution; Cell proliferation independent (Harris and Hartenstein, 1991)	Markers of RSCs appear on the lens-averted layer of the optic vesicle (El Yakoubi et al., 2012)

Continued on next page

Table 1.1 – continued from previous page

Species	Capacity to life-long growth	Presence of RSCs in adult retina in vivo in the CMZ	Optic cup formation	Origin of RSCs
Chicken	-	+	Mediated through migration of cells, however not clear to which extent it resembles rim involution as in teleost fish (Kwan et al., 2012); No evidence on dependency on cell proliferation	Not known
Mammals	-	-	Driven by autonomous NR bending (Eiraku et al., 2011; Okuda et al., 2018); Cell proliferation dependant (Eiraku et al., 2011); CMZ formation is regulated by FGF and Wnt signaling pathways	CM-like zone develops on the NR - RPE border in in vitro human ES cell-derived organoid system (Kuwahara et al., 2015)

1.4 Mechanisms of adult stem cell emergence in other organs

Adult intestinal stem cells of mammalian gut are a well-studied system for investigating adult stem cells. Located at the bottom of the crypts of Lieberkühn, they express Leucine-rich repeat-containing G-protein coupled receptor 5 (Lgr5) marker (Barker et al., 2007; Post and Clevers, 2019). Recently, the origin of these cells has been addressed (Guiu et al., 2019). As fetal Lgr5 + cells were shown to give rise to adult intestinal stem cells, Guiu et al. (2019) asked if this population of Lgr5-positive cells was serving as a source of unique precursors for future adult stem cells. Using lineage tracing, modeling, and transplantations, the authors were able to conclude that all cells of the mouse intestinal epithelium are able to contribute to the pool of adult stem cells. This process was not dependent on the initial Lgr5 expression or their location and was rather based on the gross remodeling of the intestinal villi during embryonic development (Guiu et al., 2019). Developing technologies, such as scRNA sequencing, allowed to evaluate cell fates not only by the presence of certain markers but also by a global overview of the whole transcriptome. Such a study was performed in the context of a mouse cortex, where scRNA sequencing was performed at multiple developmental time points (Yuzwa et al., 2017). Neural stem cells (NSCs) of the adult mammalian brain reside within two niches: the ventricular-subventricular zone (V-SVZ) of the forebrain lateral ventricles and the subgranular zone of the hippocampus (reviewed by Lim and Alvarez-Buylla (2016)). While it had been already determined previously when the adult stem cell precursors slow down in their proliferation (Fuentealba et al., 2015), it was still unclear if the precursors share similarities with the adult stem cells on the molecular level. Having compared the scRNA sequencing datasets through a developmental timeline, Yuzwa et al. (2017) showed that while these embryonic radial precursors share a core transcriptional identity with adult NSCs, they acquired a quiescent adult NSCs identity during late embryogenesis (Yuzwa et al., 2017). Such evidence implies that stem cell identity is not fixed but is instead instructed upon.

1.5 Medaka (*Oryzias latipes*) as a model for studying adult RSCs

The freshwater egg-laying bony rice fish Oryzias latipes has emerged as a model organism since the first half of the last century. Today, due to established genetic resources and technologies, it has gained recognition as an outstanding model organism, particularly in genetics, developmental biology, toxicology, and evolutionary studies (Hilgers and Schwarzer, 2019; Lin et al., 2016; Shima and Mitani, 2004; Wittbrodt et al., 2002). Studies in medaka brought multiple insights to the mechanisms of eye formation, regeneration and functioning of CMZ (Becker et al., 2021; Centanin et al., 2014, 2011; Lust et al., 2016; Lust and Wittbrodt, 2018; Martinez-Morales and Wittbrodt, 2009; Pérez et al., 2018; Reinhardt et al., 2015; Rembold et al., 2006; Tsingos et al., 2019). Besides, the availability of markers exclusively labeling adult retinal cells is also essential for studying them (Becker et al., 2021; Eggeler, 2017). As most of the studies have been focusing on the postembryonic CMZ, there is still a lack of knowledge on how this zone, and particularly RSCs, is shaped during the embryonic development of the medaka. Thereby, in this thesis, I have focused on the fate determination of the adult RSCs in the medaka retina. During my PhD, I investigated whether stem cells are set aside or de-differentiated at a specific position from RPCs forming the optic vesicle. Based on the state-of-the-art research, I hypothesized two scenarios by which the retinal stem cell fate is instructed (Figure 1.3).

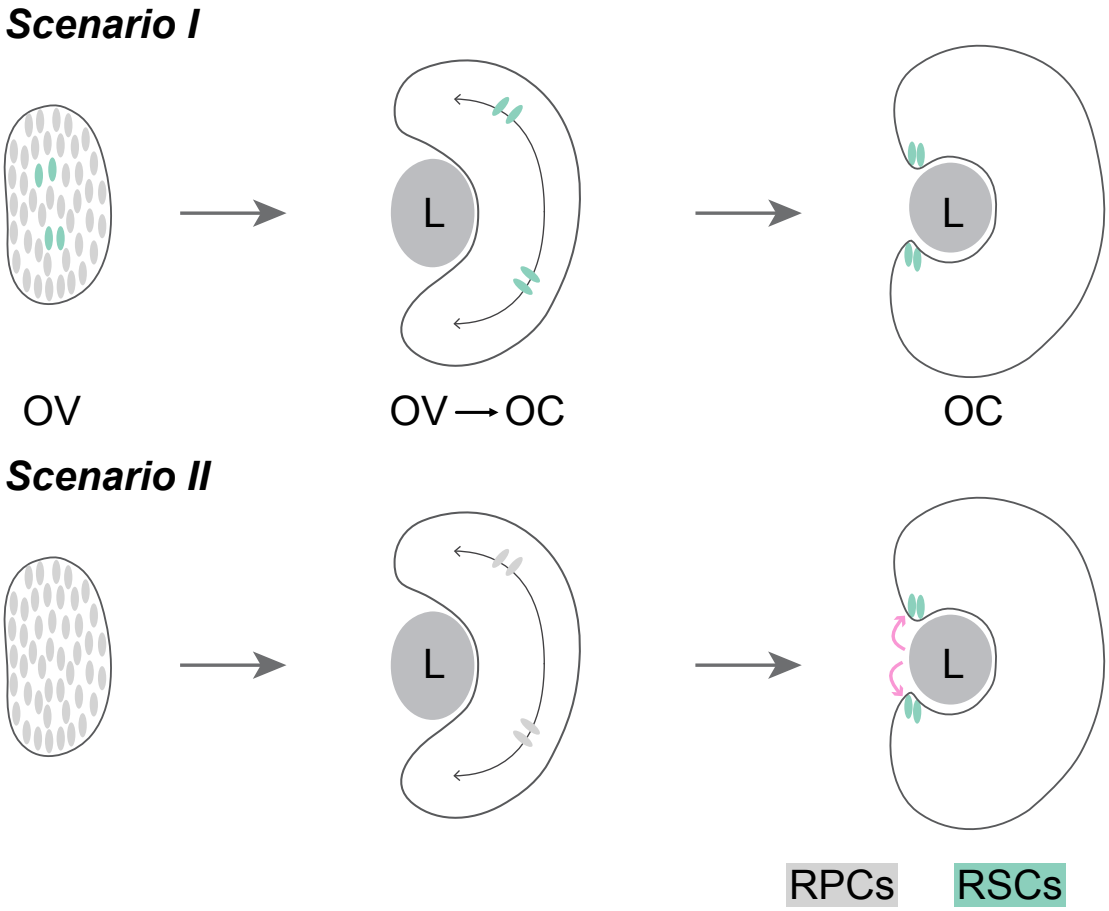

Figure 1.3. Schematic illustration of potential scenarios of adult retinal stem cell fate determination in the medaka eye.

In **Scenario I**, the fate of RSCs is predetermined at the optic stage. Following the rim involution, these cells are positioned at the retinal periphery. Such a hypothesis is based on studies in zebrafish and *Xenopus* (El Yakoubi et al., 2012; Heermann et al., 2015; Tang et al., 2017). **Scenario II** implements that the stem cell fate is not determined until after the eye morphogenesis is complete. As the optic cup is folded, RPCs acquire the stem cell identity through signals from the niche (pink arrows). L, lens.

2

Goals and objectives

The main goal of this study was to characterize the RSCs and to elucidate mechanisms governing the emergence of adult RSCs in teleost fish. While the function of this population has been investigated in several vertebrate species, the molecular and cellular mechanisms governing their formation have been poorly addressed. In medaka, the retinal stem and progenitor cell function within the CMZ has been well described; however, the origin of the RSCs remains obscure. Additionally, little is known about the molecular characteristics of the medaka retina stem cells. To achieve the general goal, I therefore focused on the following objectives:

1. To describe molecular characteristics of RSCs.

I compared the expression of two previously identified markers for adult RSCs in medaka to elucidate the level of their overlap within RSCs population. To discover more molecular markers labeling RSCs, I performed single-cell RNA sequencing and performed extensive validation of retinal stem cell cluster. I also explored patterns of retinal stem cell markers across early developmental stages to reveal the onset and the dynamics of their expression.

2. To investigate the expression of retinal stem cell markers in cases of disrupted eye morphogenesis.

To address whether the establishment of RSCs is coupled to the optic cup morphogenesis, I inspected the pattern of retinal stem cell markers expression in the conditions of interrupted eye morphogenesis using two approaches: treatment of embryos with non-muscle myosin II inhibitor blebbistatin and using previously established rx3 morphogenetic mutants.

3. To track the changes in the behavior of the retinal periphery cells with regard to their proliferation rates and ability to give rise to ArCoS during medaka embryonic development.

I analyzed the changes in proliferative behavior of retinal stem cell marker-expressing cells within the peripheral retina utilizing BrdU incorporation and by tracing their progeny after Cre/loxP – mediated recombination. To ascertain the onset of stem cell characteristics, especially their ability to generate ArCoS, I conducted a clonal analysis, leveraging BrdU incorporation as a temporal marker.

4. To uncover the molecular differences that govern changes in the behavior of retinal periphery cells through consequent stages.

Trying to unravel molecular differences between RSCs and their predecessors, I performed bulk and single-cell RNA sequencing analyses at corresponding stages.

3

Results

3.1 Molecular characterization of RSCs

3.1.1 RSCs in medaka are simultaneously marked by ndp1 and ccl25b.

In order to understand the emergence of a certain cell type, it should be well described with regard to its markers. While previously, both *cndp1* and *ccl25b* were shown to label RSCs in medaka (Becker et al., 2021; Eggeler, 2017), it remained to be seen whether they overlap and can be used interchangeably. To compare these two populations, I employed lineage tracing of ccl25b-positive cells in the background of a *cndp1* reporter line. For the lineage tracing, I used the line where the *ccl25b* promoter was driving the expression of inducible Cre recombinase while being already crossed with the GaudíRSG line, previously established in the lab (Centanin et al., 2014; Eggeler, 2017). Upon recombination induced by 4-hydroxytamoxifen (4-OH tamoxifen), the Cre protein translocated to the nucleus, facilitating recombination between the loxP sites flanking the mCherry gene. This recombination event led to the expression of H2B-eGFP, which is then inherited to the daughter cells (Centanin et al., 2014; Livet et al., 2007) (Figure 3.1A). This line was crossed with the *cndp1::mCherry-2A-oNTR* line, carrying a construct for nitroreductase (NTR) mediated cell ablation. I chose this line because of the distinguished high intensity of the fluorescent signal in the cytoplasmatic domain, which would differentiate the Cndp1-labeled cells from Ccl25b unrecombined, mCherry-positive ones. As these two lines were incrossed, I induced recombination with 4-OH tamoxifen at 3 days post fertilisation (dpf). Two (weeks post hatch (wph)) fish were sacrificed, retinas were dissected, and analysis via whole-mount immunohistochemistry was performed (Figure 3.1). I focused on the progeny of *ccl25b*-positive stem cells that were apparent as GFP-positive clones, which start with the mCherry-positive cell within the most peripheral part of the retina (Cndp1-positive RSCs). Quantification of the GFP-positive clones starting with the mCherry-positive cell in the CMZ region re-

vealed that 91.45 %±8.39 % of the GFP-positive clones originated within the cndp1 population (Figure 3.1D).

In the few cases (4/51 clones) where the GFP-positive clones did not have the cndp1-positive cell at their origin, the first cell in the clone was positioned more laterally within CMZ, potentially representing a starting footprint. However, since more than 90% of the clones started within the cndp1 expression domain, I conclude that the progeny of the Ccl25b-positive cells contributes to the formation of the iArCoS, originating within the Cndp1-positive RSCs domain.

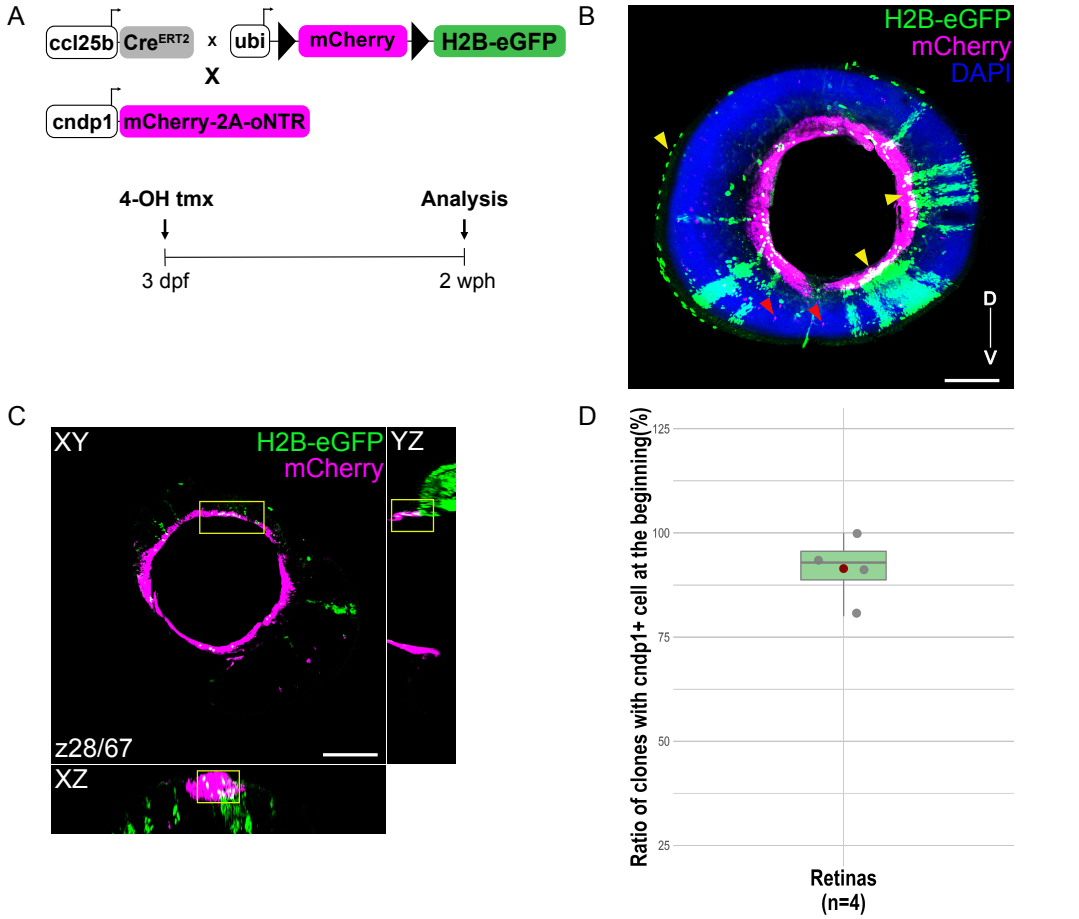

Figure 3.1. Cndp1 and Ccl25b mark identical population of RSCs in the medaka retina.

(A) Schematic representation of the constructs used for the reporter lines generation. In the *ccl25b::Cre*, *Gaudi*$^{redswitchgreen(RSG)}$ reporter line upon induction mCherry is floxed out resulting in *H2B-eGFP* being inherited by daughter cells. *cndp1::mCherry-2A-oNTR* marks the population of *cndp1*-positive RSCs. As these lines were incrossed, the offspring was recombined at 3 dpf with 4-OH tamoxifen and grown until analysis at 2 wph.

Figure 3.1. (B) Maximum projection of *cndp1::mCherry-2A-oNTR; ccl25b::Cre, Gaudí^{RSG}* retina stained against GFP (green) and mCherry (magenta), imaged from the front view. The RSCs express cndp1 (magenta) and give rise to recombined GFP-positive clones (green) spanning through all retinal cell types. The most peripheral cell of the clones is also cndp1-positive (yellow arrows). Besides expression in the CMZ, Ccl25b-recombined cells can also be detected in the choroid (white arrow). Single magenta cells (red arrows) represent non-recombined cells with a residual amount of mCherry coming from the GaudíRSG line. Scale bar is 100 µm. D, dorsal; V, ventral. **(C)** Orthogonal views of a single optical section depicting the same sample as in **(B)**. Cells, co-expressing Cndp1 and Ccl25b, are outlined in XY view (yellow rectangular). In YZ and XZ one can observe the RSCs being labelled by cytoplasmic mCherry (magenta) and nuclear GFP signal (green). Scale bar is 100 μm. **(D)** Quantification of the ratio of GFP-positive clones with cndp1-positive cell at the most peripheral position per retina (n = 4 retinas with 51 clones in total) confirms that Ccl25b and Cndp1 mark the same population of RSCs in medaka. The bold line indicates the median value, the red dot – mean.

3.1.2 Single-cell RNA sequencing revealed unique retinal stem cell markers

In order to find out more about molecular markers of the RSCs and their potential difference to RPCs, I performed single cell RNA sequencing of a medaka retina in joint effort with colleagues (see Contributions). Two right optic cups of stage 34 (Iwamatsu, 2004) medaka embryos were dissected and pooled together, and the single cell suspension was prepared using a mix of trypsin and dispase enzymes. The viability of the cells was assessed via Trypan Blue staining followed by quantification in the Neubauer chamber. The single-cell suspension with 88% of viable cells was submitted for sequencing with 10x Genomics. In the downstream pipeline, 6430 cells with 100-10000 features with less than 10% mitochondrial transcripts were analyzed. For clustering, the top 3000 features were used, with cell cycle or mitochondrial transcripts being regressed out. As a result, we obtained 17 clusters (Figure 3.2), which we then identified as the main retinal cell types based on the most upregulated markers and their known expression from the literature.

Based on fluorescence-activated cell sorting (FACS) analysis, I calculated that stem cells comprise only 0.2-0.5% of the total cell population in the medaka retina, making it challenging to find them in the single-cell dataset. There was no cluster in the dataset in which all known retinal stem cell markers (*ccl25b*, *cndp1*, *rx2*) were co-

expressed. However, I found a cluster (Figure 3.2, cluster 9) that had *ccl25b* and *gli3* co-expressed. To determine whether this cluster contains RSCs, I performed RNA in situ hybridization of the 27 most upregulated genes in this cluster (*sparc*, *TPM1*, *pcolcea*, *serpinh1b*, *fgfr3*, *ENSORLG00000009111* (*transforming growth factor beta (TGFß)3-like*), *igf2b*, *tnn*, *ENSORLG00000024891* (*syndecan-2B-like*), *id3*, *ndnf*, *cnmd*, *dcn*, *pcdh18b*, *collagen (col) 2a1a*, *CKM.1*, *si:ch211-156l18.7*, *osr2*, *aldehyde dehydrogenase (aldh)1a2*, *nexn*, *pitx1*, *TGFßi*, *ENSORLG00000007619* (*CD34-like*), *prrx1b*, *alx4b*, *id1*, *krt8*, via whole-mount RNA *in situ* hybridization.

I used heads of medaka embryos (n=5) for cryosectioning and antisense RNA probes, capturing the probe signal with a Nomarski differential interference contrast microscope (Figure 3.3 and 3.4). As controls for the signal in the RSCs I used the probes for already known markers *cndp1* and *ccl25b*. The *cndp1* messenger RNA (mRNA) was expected to be present in the RSCs and RPE to a lesser intensity. Interestingly, while its expression was evident in the RSCs (Figure 1.3A, left), the *cndp1* transcripts were not found in cluster 9. The *cndp1* transcription was present only in the RPE (Figure 3.3A, right). At the same time, the *ccl25b* transcripts, were found explicitly in cluster 9 (Figure 3.3B, right) but were not detected by alkaline phosphatase mediated RNA *in situ* hybridization (Figure 3.3B, left). As a result, 6 markers showed evident expression patterns in the CMZ region. mRNA of *sparc*, *col 2a1a*, *aldh1a2*, and the *TGFß3-like gene* (Ensembl ID: ENSORLG00000009111) were detected in the most distal part of the retina (Figure 3.3C-F), which contains RSCs. Besides, the expression of *sparc* and *col 2a1a* was also observed in the choroid surrounding the retina and lens epithelium (Figure 3.3C-D). The expression of two more markers, a novel *CD34-like* gene (Ensembl ID: ENSORLG00000007619) and *id1*, was detected in the broader domain of the peripheral retina, which would correlate to both RSCs and RPCs in the CMZ (Figure 3.3G-H, left panels). Additionally, *id1* is also expressed in MG cells located in the inner nuclear layer of the retina (Figure 3.3H, left). Such patterns are reflected in the scRNA sequencing data by the presence of the transcripts in corresponding clusters (Figure 3.3, right panels).

However, the expression of most of the genes upregulated in cluster 9 was not confirmed by RNA *in situ* hybridization (Figure 3.4). Some genes, such as *nexn* and *ndnf*, showed the expression in the MG , and other (*tfgbi*, *krt8*, *pmp22*, *alh4b*) in the epithelium. Expression in the cornea and lens epithelium for some of these genes was also quite distinctive (as the case for *ndnf*, *tnn*, *pcdh18b*, *si:ch211-156l18.7*, *CKM.1*, *TGFßi*, *pitx1*, *TPM1*, *dcn*, *syndecan-2B-like* and *prrx1b*). The antisense probe against *pcolcea* and *igf2b* provided only a minor background signal.

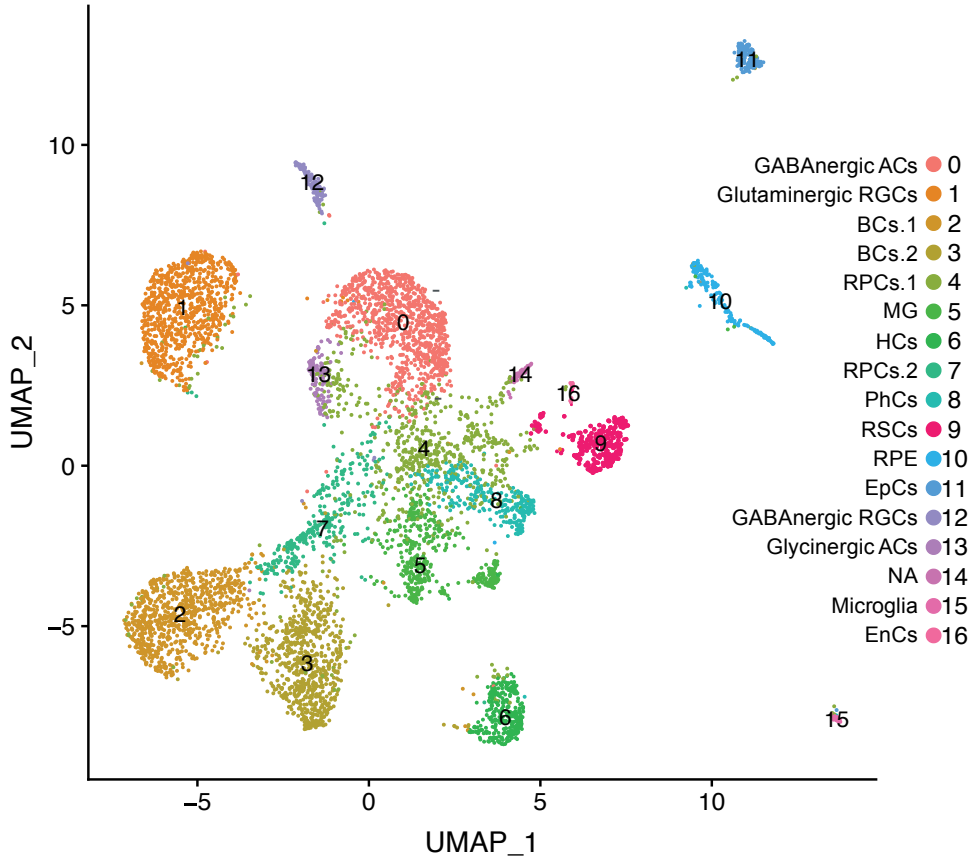

Figure 3.2. Cellular diversity of the retina in medaka.

UMAP plot showing 17 clusters of main cell types in the medaka retina. Single-cell suspension of the medaka stage 34 retina (Iwamatsu, 2004) was submitted for sequencing with 10x Genomics. The following workflow analysis identified 6430 cells with 100-10000 features with less than 10% mitochondrial transcripts. Clustering of the top 3000 features, with regression of cell cycle or mitochondrial transcripts, resulted in 17 clusters. ACs, amacrine cells; RGCs, retinal ganglion cells; BCs, bipolar cells; MG, Müller Glia; HCs, horizontal cells; PhCs, photoreceptors; RSCs, stem cells; RPE , retinal pigmented epithelium; EpC, epithelium cells; NA, not identified; EnC, endothelium cells.

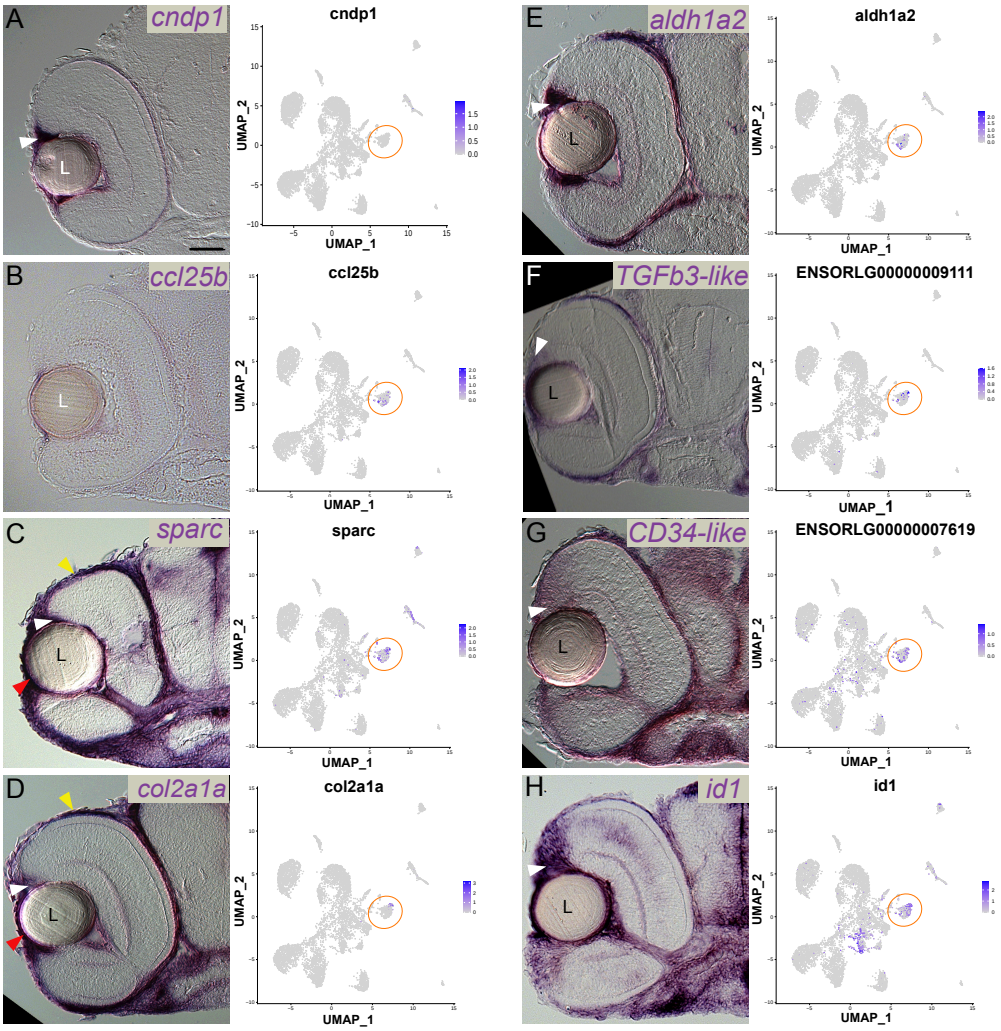

Figure 3.3. Single-cell RNA sequencing revealed new unique markers for RSCs.

(A) Stem cells take the most distal position of the retina, as marked by *cndp1* mRNA expression (left panel, white arrowhead marks the signal in the dorsal CMZ). However, *cndp1* transcripts were detected only in the cluster 10, enriched in the RPE specific genes, in the scRNA sequencing data (right panel). Scale bar is 50 μm. **(B)** *ccl25b* mRNA could not be detected in the RSCs (left panel). At the same time, its transcripts are present in cluster 9 (outlined in orange) of the scRNA sequencing dataset (right panel). **(C)** *sparc* mRNA marked the most distal part of the medaka retina (white arrowhead marks the signal in the dorsal CMZ) and the choroid (yellow arrowhead) and lens epithelium (red arrowhead) (left panel). Besides, its expression is also present in the RPE . The transcripts of *secreted protein acidic and rich in cysteine (sparc)* were detected in cluster 9 (outlined in orange) and also in cluster 10, representing RPE (right panel).

Figure 3.3. **(D)** *col2a1a* was observed to specifically label the most peripheral region of the medaka (white arrowhead marks the signal in the dorsal CMZ) retina as well as the choroid (yellow arrowhead) and lend epithelium (red arrowhead) of the eye (left panel). Its transcripts are present in cluster 9 (outlined in orange) (right panel). **(E)** *aldh1a2* mRNA (white arrowhead marks the signal in the dorsal CMZ) was present in the CMZ of the medaka retina as well as in the RPE (left panel). In the scRNA sequencing its transcripts were enriched in cluster 9 (outlined in orange) and to a lesser extent in cluster 10, representing RPE (right panel). **(F)** The mRNA of the novel *TGFß3-like* gene (Ensembl ID: ENSORLG00000009111) weakly marked the most distal part of the CMZ of the retina (white arrowhead marks the signal in the dorsal CMZ). At the same time, its transcripts were present in cluster 9 (outlined in orange) of the scRNA sequencing dataset (right panel). **(G)** The mRNA of the novel *CD34-like* gene (Ensembl ID: ENSORLG00000007619) marked the entire CMZ region (white arrowhead marks the signal in the dorsal CMZ) of the medaka retina (left panel). In turn, its transcripts were enriched in cluster 9 (outlined in orange) of the scRNA sequencing dataset and also present in clusters 4 and 7, representing RPCs (right panel). **(H)** *id1* mRNA was detected in the entire CMZ (white arrowhead marks the signal in the dorsal CMZ), as well as in MG cells (right panel). At the same time, its transcripts were enriched in cluster 9 (outlined in orange) of the scRNA sequencing dataset, as well as in cluster 5 representing MG population and to a lesser extent across clusters 4 and 7, representing retinal progenitor cell population (right panel). All left panels represent single optical sections of transverse sections (16 μm) of the medaka albino line *Heino* retina of stage 34. All right panels are UMAPs of the corresponding genes of the scRNA sequencing dataset of stage 34 medaka retina.

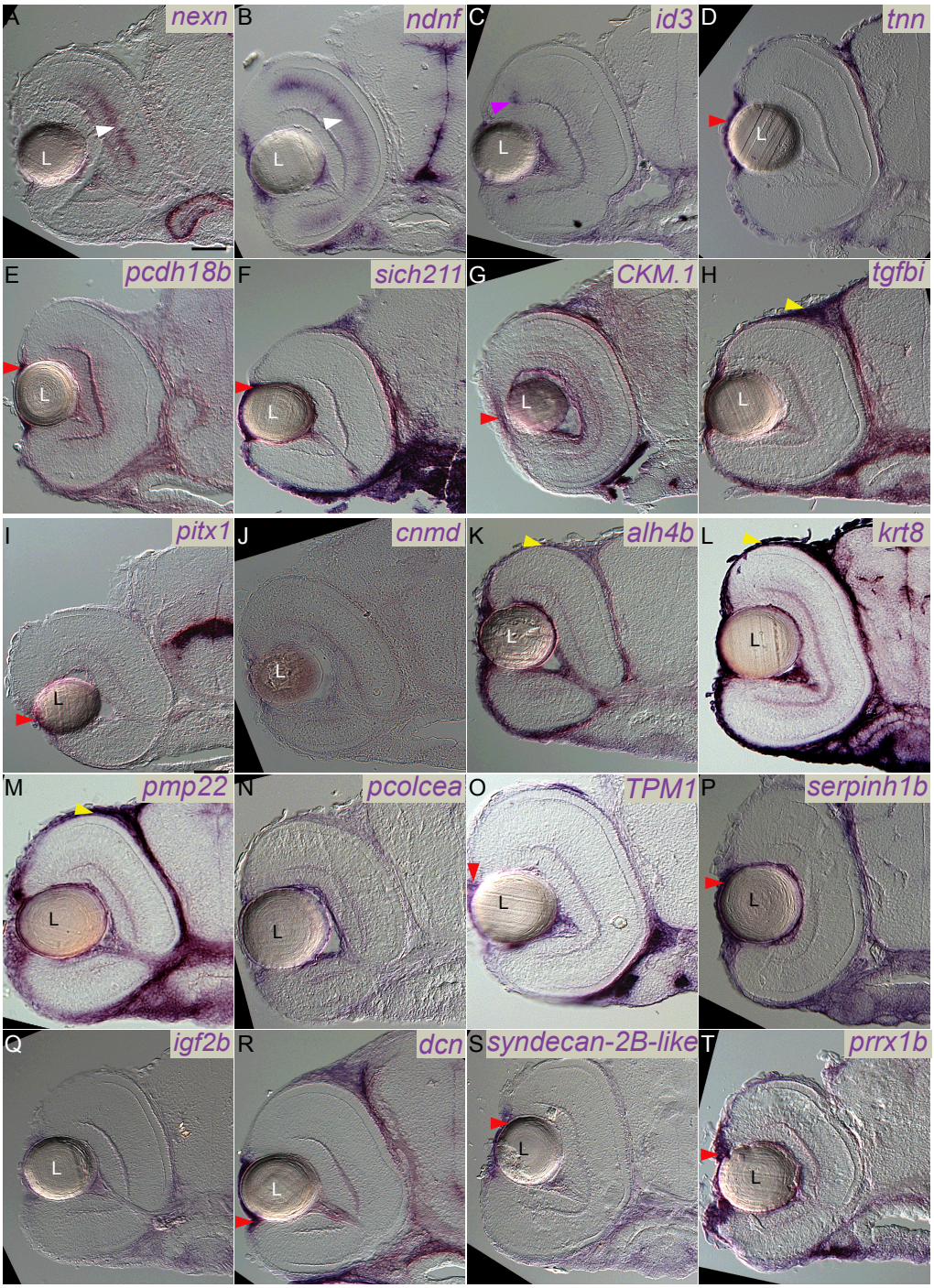

Figure 3.4. Expression of the majority of the genes upregulated in cluster 9 could not be verified through RNA *in situ* hybridization in the RSCs. Some genes, namely *nexn* **(A)** and *ndnf* **(B)**, were found to be expressed in the MG cells (white arrowheads). mRNA of *id3* was detected in the most proximal part of the CMZ , representing late progenitors (magenta arrowhead)

Figure 3.4. **(C)**. Others, such as *tfgbi* **(H)**, *alh4b* **(K)**, *krt8* **(L)** and *pmp22* **(M)** showed expression in the epithelium (yellow arrowheads). Additionally, certain genes exhibited distinct expression patterns in the cornea and lens epithelium (red arrowheads), notably *ndnf* **(B)**, *tnn* **(D)**, *pcdh18b* **(E)**, *sich211* **(F)**, *CKM.1* **(G)**, *TGFßi* **(H)**, *pitx1* **(I)**, *TPM1* **(O)**, *dcn* **(R)**, and *prrx1b* **(T)**. Besides, the antisense probes targeting *pcolcea* **(N)** and *igf2b* **(Q)** yielded only a minor background signal. All panels represent single optical sections of transverse cryosections (16 μm) of the medaka albino line *Heino* retina of stage 34. Scale bar is 50 μm.

3.1.3 HCR RNA-FISH confirms the identity of stem cell markers

As mentioned above, detecting *ccl25b* mRNA via conventional alkaline phosphatase in situ hybridization was challenging (Figure 3.3B). Since the reporter lines utilizing *ccl25b* regulatory element clearly show transgene activity in RSCs (able to give rise to ArCoS) (Figure 3.1), it was possible that there was an inconsistency between the endogenous expression of the gene and the tissue specificity of the *ccl25b* regulatory element. To resolve this question, I attempted to detect *ccl25b* transcripts by implementing a different method for mRNA detection, a fluorescent hybridization chain reaction RNA fluorescent *in situ* hybridization (HCR RNA-FISH) (Figure 3.5). As, in our laboratory, it has not been established performed on medaka, I had to optimize the protocol. During optimization, I observed that digestion with proteinase K did not provide the necessary permeabilization for whole-mount samples which led to the absence of fluorescent signal. However, when samples underwent CUBIC-mediated tissue clearing (Susaki et al., 2015; Tainaka et al., 2014), it was possible to achieve a robust fluorescent signal (Figure 3.5). The multiplex nature of the HCR RNA-FISH allowed me to simultaneously use two probes, one for *rx2* and one for *ccl25b* (Figure 3.5). As expected, the mRNA for *rx2* was detected in the CMZ , MG and photoreceptors (Figure 3.5). The signal for *ccl25b*, while being not very bright, was evidently present in the most peripheral part of the CMZ (Figure 3.5B-B', white arrowheads), providing additional evidence that *ccl25b* was indeed expressed in RSCs. As I discovered the new markers labeling the peripheral CMZ , I was interested in the exact pattern of their expression to address if they are explicit markers of RSCs, or if they are also expressed in the RPCs? To answer this question, I performed double HCR RNA-FISH on cryosections of medaka hatchlings (stage 40), combining a probe for *cndp1* as a reference for RSCs with probes for *sparc* , *col2a1a*, *aldh1a2* and the novel *TGFß-like* (Ensembl ID: ENSORLG00000009111)

to achieve the cellular resolution of their expression.

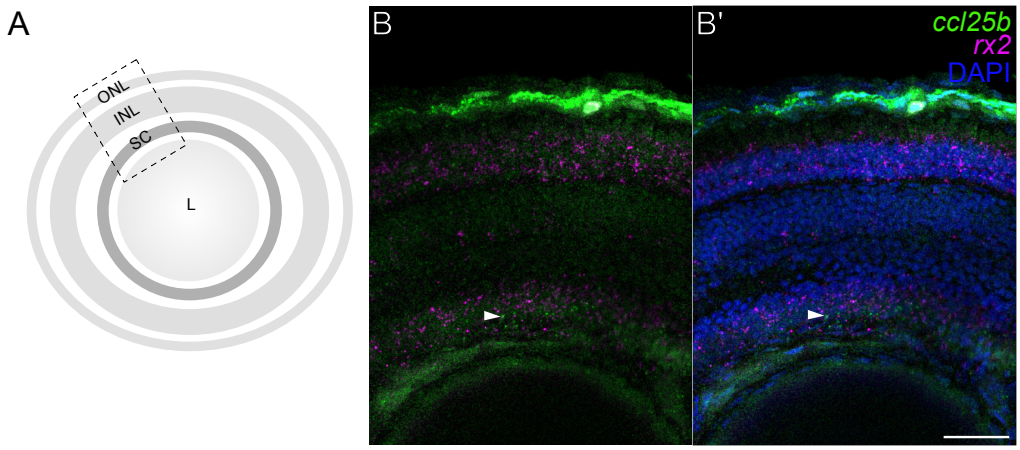

Figure 3.5. HCR RNA-FISH detects ccl25b mRNA in the CMZ of the whole-mount medaka retina.
(A) Scheme of the eye highlighting the area that is depicted in B-B'. L, lens. **(B)-(B')** Maximum projection of the medaka albino line *Heino* retina stage 40 stained against *ccl25b* mRNA (green) and *rx2* mRNA (magenta), imaged from the front view. mRNA of *ccl25b* was detected in the CMZ of the medaka retina (white arrows in the rectangle). mRNA of *rx2* labels RSCs and RPCs, MG , and photoreceptors in the medaka retina. The *ccl25b* transcripts were detected in the CMZ region, confirming the expression of the gene in the RSCs. DAPI staining (blue) was used for nuclei visualization. Scale bar is 50 μm.

All of the newly discovered markers (*sparc* , *col2a1a*, *aldh1a2* and the novel *TGFß-like* (Ensembl ID: ENSORLG00000009111) were detected in the peripheral CMZ of the medaka hatchlings, overlaying the *cndp1* expression (Figure 3.6). The patterns of *sparc* and *col2a1a* overlap with the *cndp1* in the RSCs (Figure 3.6B-B''', C-C'''), whereas aldh1a2 mRNA labels RSCs as well as RPCs (Figure 3.6D-D'''). The expression of the *TGFß3-like* gene, while being rather weak, also overlaps with the *cndp1* (Figure 3.6E-E'''). These results validate 4 novel genes as new markers for RSCs. Notably, the expression pattern of *sparc*, *col2a1a* and *TFGb3-like* accurately overlap with the *cndp1* mRNA signal. At the same time, *aldh1a2* mRNA labels RSCs as well as early RPCs (Figure 3.6D-D''').

3.1.4 Single-cell RNA sequencing revealed unique retinal progenitor cell markers

Besides identifying the stem cell cluster in our dataset, I was also able to identify a few genes specific to the progenitor population (Figure 3.7). Those showed up-

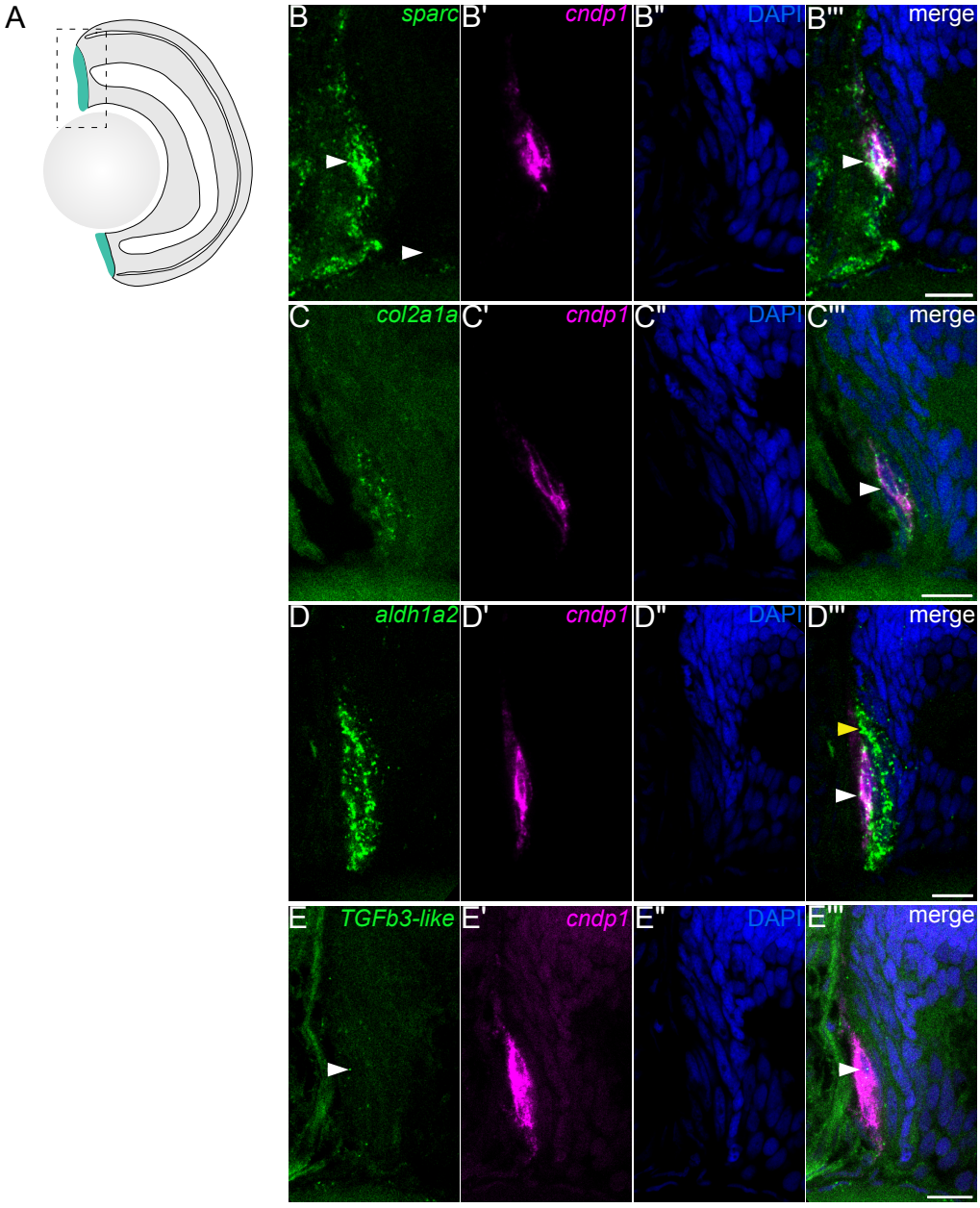

Figure 3.6. Novel markers label RSCs together along with cndp1.
(A) Scheme of the eye highlighting the area that is depicted in B-E'''. CMZ is highlighted in cyan. **(B)-(B''')** Dorsal CMZ of a hatchling medaka retina, stained against mRNA of *sparc* (green) and *cndp1* (magenta). The expression of *sparc* coincides with *cndp1* expression in the most distal region marking RSCs (white arrows). **(C)-(C''')** Dorsal CMZ of the medaka retina of stage 40, stained against mRNA of *col2a1a* (green) and *cndp1* (magenta). The expression pattern of *col2a1a* aligns with the expression of *cndp1* in the region of RSCs (white arrows).

Figure 3.6. (D)-(D'") Dorsal CMZ of a hatchling medaka retina, stained against mRNA of *aldh1a2* (green) and *cndp1* (magenta). This gene is expressed in the broader domain of the CMZ , marking both RSCs (white arrows) and early RPCs (yellow arrow). **(E)-(E'")** Dorsal CMZ of a medaka retina at stage 40, stained against mRNA of the novel *TGFß-like* gene (Ensembl ID: ENSORLG00000009111) (green) and *cndp1* (magenta). This gene weakly labels the RSCs in the medaka retina, overlapping with *cndp1*. All panels are single optical sections of transverse cryosections (16 μm). DAPI (blue) is used to visualize the nuclei. Data obtained from two independent experiments (n=6 retinas). Scale bars are 10 μm.

regulation in cluster 7 of the scRNA sequencing dataset (Figure 3.2). *hairy and enhancer of split (hes)6* and *gaddgb45.1* were among these genes. Like for RSCs I validated the expression of *hes6* and *gaddgb45.1* in the CMZ by whole-mount RNA in situ hybridization on the stage 34 medaka embryos. The results confirmed the expected expression pattern in the retina (Figure 3.7). Both *hes6* and *gadd45gb.1* mRNA were prominently expressed in the proximal region of the CMZ, while they were notably excluded from the peripheral region containing the RSCs. Taken together, based on scRNA sequencing data I identified new markers for the whole CMZ, as well as exclusively for RSCs and RPCs.

3.1.5 Expression of CMZ markers during retina formation

The cell tracking experiments hypothesized the existence of RPCs in the proximal layer of the optic vesicle that give rise to the adult RSCs (Heermann et al., 2015; Tang et al., 2017). As *ndp1* labels the most peripheral stem cell-containing part of the CMZ (Becker et al., 2021), I hypothesized that establishing its expression during retinogenesis could provide insights on the mechanisms of RSCs emergence. To address this, I examined the *ndp1* expression pattern within the retina field, from the optic vesicle stage to the fully differentiated retina (Figure 3.8). The *cndp1* mRNA could not be detected in the optic vesicle and early stage of optic cup formation at stages 20-22 (Figure 3.8A-C). The first indication of *cndp1* expression in the developing retina becomes evident at stage 23 (Figure 3.8D), where it is observed in the developing RPE (Figure 3.8D, yellow arrows). By stage 24, the stage when major steps of optic cup formation is completed *cndp1* becomes more localized to the retinal periphery (Figure 3.8E), white arrow). As the retina matures, *cndp1* expression becomes more prominent in the CMZ while still faintly labeling the RPE (Figure 3.8F-H). These results show that the RSCs marker is not present

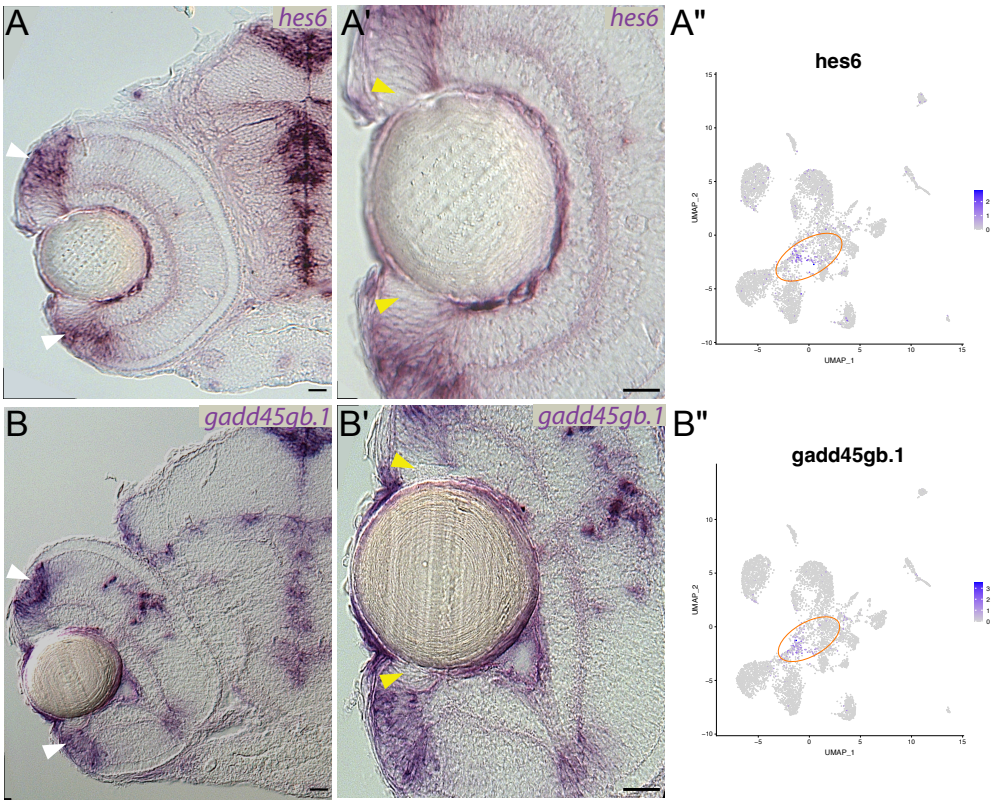

Figure 3.7. Single-cell RNA sequencing revealed new unique markers for RPCs.

(A)-**(A')** RNA in situ hybridization showing restricted expression of *hes6* to the proximal region of CMZ , representing RPCs (white arrowheads). The signal was not detected in the distal domain of the CMZ containing RSCs (yellow arrowheads). **(A'')** Transcripts of *hes6* were enriched in cluster 7 (outlined in orange), representing RPCs. **(B)**-**(B')** Expression of *gadd45gb.1* was shown to be exclusive to the RPCs in the medaka CMZ (white arrowheads) and was not detected in the RSCs (yellow arrowheads). **(B'')** Transcripts of *gadd45gb.1* were found in cluster 7 (outlined in orange), indicating its association with RPCs. Panels **(A)**, **(A')**, **(B)**, **(B')** represent single optical sections of transverse cryosections (16 μm) of whole-mount *in situ* hybridization against *hes6* and *gadd45gb.1* mRNA performed on the medaka albino line *Heino* retina of stage 34. Scale bars are 20 μm. Panels (A") and (B") represent UMAPs of the corresponding genes of the scRNA sequencing dataset of stage 34 medaka retina.

in early eye development and gets restricted to the CMZ only later upon optic cup formation.

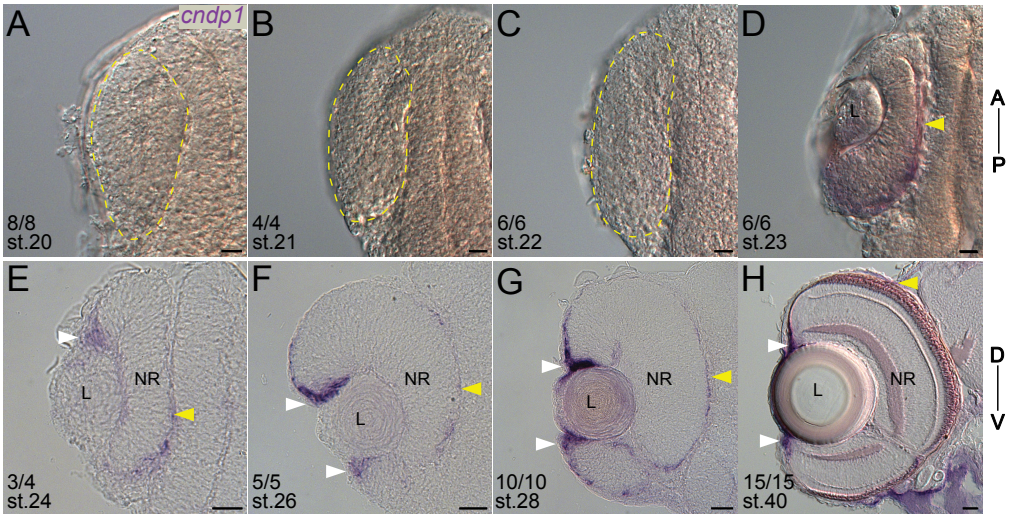

Figure 3.8. *cndp1* expression during retinogenesis.
(A) *cndp1* transcripts are not present in the optic vesicle and early stages of optic cup invagination **(B)**-**(C)**. The first indication of *cndp1* expression in the optic cup (yellow dashes) starts at stage 23 **(D)** in the developing RPE (yellow arrows). At stage 24, *cndp1* is more confined to the retinal periphery as indicated by a white arrow in **(E)**. Once the retina matures, the *cndp1* expression gets more evident in the CMZ white arrows in **(F)**-**(H)** while still faintly marking the RPE (yellow arrows). Panels **(A)**-**(D)** depict single optical sections of the whole-mount RNA *in situ* hybridization against *cndp1* mRNA at corresponding stages. A, anterior; P, posterior. Panels **(E)**-**(H)** depict single optical sections of transverse cryosections (16 μm) of whole-mount RNA *in situ* hybridization against *cndp1* mRNA at corresponding stages. A, anterior; P, posterior; L, lens; D, dorsal; NR, neural retina; V, ventral. Scale bars are 20 μm.

Taking advantage of the newly identified CMZ markers, I asked how their expression profile changes during the retina formation. For that, I used three markers: *id1* as a marker labeling entire CMZ , *aldh1a2* as a marker for RSCs, and *hes6* as a marker for RPCs (Figure 3.9). In the newly formed optic cup at stage 24, the *id1* is expressed widely throughout early retinal progenitors (Figure 3.9A). As these retinal progenitors start differentiating just before stage 28, the expression of *id1* stays in the undifferentiated cells. The first differentiated cells – RGCs – do not express this gene (Figure 3.9A'). With the maturation of the optic cup at stages 32-34, *id1* mRNA was observed in the CMZ and the MG of the medaka retina (Figure 3.9A"). In contrast, *aldh1a2* mRNA was present only in the distal parts of

the optic cup at stage 24 (Figure 3.9B). As the optic cup undergoes differentiation and maturation, *aldh1a2* expression becomes limited to the most peripheral region of the CMZ, specifically labeling RSCs and early RPCs (Figure 3.9B-B"). Interestingly, the marker of RPCs *hes6* and the marker of RSCs *aldh1a2* show mutually exclusive expression patterns (Figure 1.9 C). The *hes6* transcripts are present in the proximal part of the optic cup at stage 24 (Figure 1.9 C). With the progression of retinal development, *hes6* expression is getting excluded from differentiating cells, similarly to *id1* (Figure 3.9C'). As the retina matures, *hes6* gets restricted to the proximal part of the CMZ (Figure 3.9C"), marking the RPCs of the CMZ.

Overall, these results demonstrate an interesting interplay of CMZ markers during retinal development. Together with the *cndp1* pattern expression, this data suggests a bimodal mechanism of RSCs determination: while *cndp1* at first was detected in the RPE at st.23, the expression of *aldh1a2* at first was present in the distal optic cup, which are NR precursors. Later in development both *cndp1* and *aldh1a2* converge in the most peripheral region of the CMZ (Figures 3.6, 3.8, 3.9). The absence of *cndp1* mRNA in the optic vesicle does not corroborate the hypothesis that RPCs in the proximal layer of the optic vesicle are predefined to become RSCs (Figure 3.8).

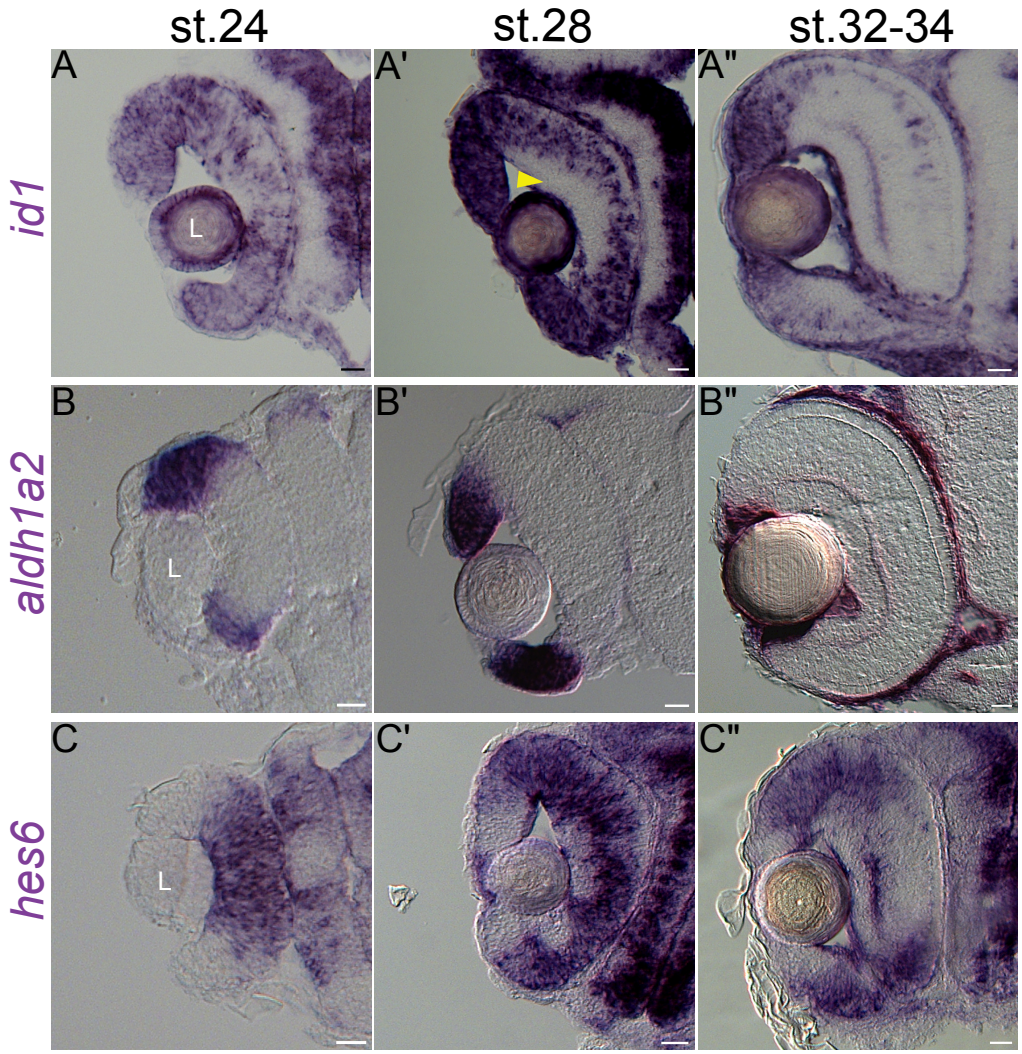

Figure 3.9. Markers of CMZ , RSCs, and RPCs during retinogenesis. **(A)-(A")** In the early optic cup of stage 24, *id1* is expressed throughout the retinal progenitors. As the retinal progenitors of the optic cup start to differentiate just before stage 28, the *id1* expression is restricted to the undifferentiated cells. The first undifferentiated cells in central retina – RGCs – stop expressing this gene (yellow arrowhead). With the maturation of the optic cup at stages 32-34, *id1* is expressed in the CMZ and MG in the medaka retina. **(B)-(B")** The expression of *aldh1a2* labels the distal parts of the optic cup at stage 24. As the optic cup differentiates and matures, the *aldh1a2* gets restricted to the most peripheral part of the CMZ, labeling RSCs, and early RPCs. **(C)-(C")** *hes6* marks the proximal part of the optic cup at stage 24. At later stages, it is present only in undifferentiated cells of the CMZ, except, however, the most distal part of the CMZ containing RSCs. All panels depict single optical sections of transverse cryosections (16 μm) of whole-mount RNA *in situ* hybridization against corresponding genes at stages 24, 28, and 32-34 (Iwamatsu, 2004). Scale bars are 20 μm.

3.2 RSC identity is established in the medaka CMZ despite morphogenetic defects

3.2.1 Blebbistatin treatment results in perturbed optic cup morphogenesis

Live imaging of optic cup development and cell tracking experiments in zebrafish have indicated the existence of a distinct population of cells within the proximal layer of the optic vesicle. These cells reach the retinal periphery region with the rim involution process and subsequently contribute to the adult RSCs (Heermann et al., 2015; Tang et al., 2017). The phenomenon of rim involution has also been documented in medaka (Sokolova, 2019). However, a question remains unanswered: does morphogenesis play a crucial role in the specification of adult RSCs? To address this question, I employed two different approaches. The first one involved the treatment of embryos with blebbistatin, a general myosin II ATPase inhibitor that blocks myosin in an actin-detached state (Kovács et al., 2004; Ramamurthy et al., 2004). Previously, it was shown that treatment of zebrafish embryos in blebbistatin interferes with optic cup folding via presumably blocking the cell constriction (Moreno-Mármol et al., 2021; Nicolás-Pérez et al., 2016). The treatment of dechorionated Cab wild-type medaka embryos from stage 20 (an optic vesicle stage) to stage 28 (2.5 dpf, an optic cup has formed and starts to differentiate) led to the absence of the ventral part of the optic cup (Figure 3.10A-B).

3.2.2 RSCs marker expression is initiated upon disturbed optic cup morphogenesis in medaka retina

Given that the blebbistatin treatment disrupts the rim involution process (Figure 3.10), the presumably predetermined population of RSCs would remain entrapped in the proximal layer of the optic vesicle. To address this, I tested the retinal periphery of blebbistatin treated embryos for the presence of *cndp1* mRNA. The Cab embryos were incubated from stage 20 to stage 28 in blebbistatin and subsequently analyzed by HCR RNA-FISH against *cndp1* mRNA on cryosections (Figure 3.11). In the control embryos *cndp1* labels retinal periphery (Figure 3.11B). Similarly, in blebbistatin-treated embryos the *cndp1* signal was registered at the dorsal retinal periphery adjacent to the lens, which hints to the conclusion that RSCs are not strictly predefined at the optic vesicle stage. Interestingly, the *cndp1* signal in the retinal periphery of the blebbistatin-treated group was much brighter than in the

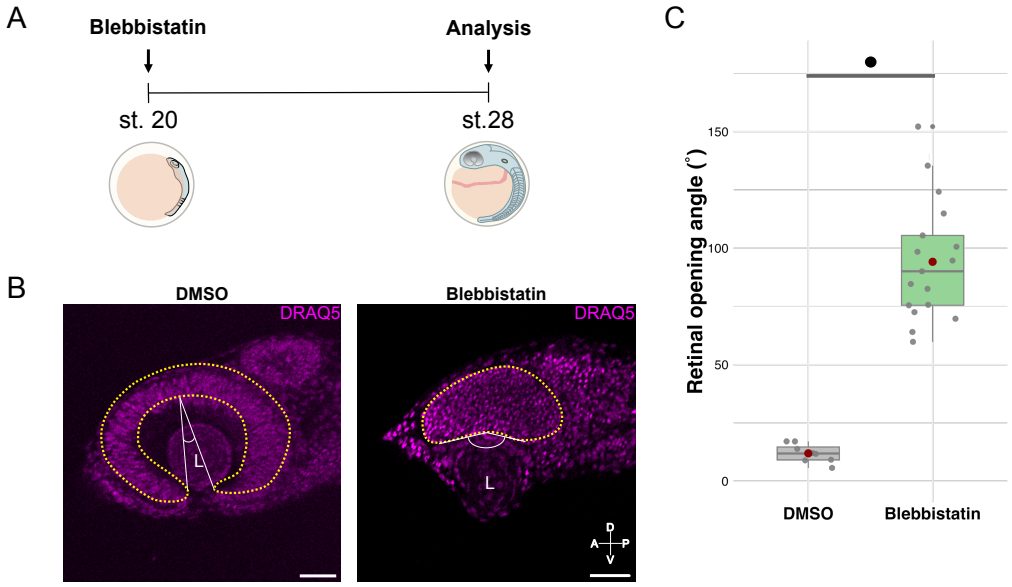

Figure 3.10. Blebbistatin treatment disrupts optic cup morphogenesis in medaka embryos.

(A) Dechorionated medaka embryos were subjected to 100 μM blebbistatin from st. 20 to 28. 90% Dimethylsulfoxid (DMSO) was used as vehicle control. **(B)** Blebbistatin treatment leads to a misshaped optic cup with an absent ventral part of the retina, while DMSO-treated embryos develop complete optic cups. DRAQ5 (magenta) was used for nuclei visualization. The retinal contour is indicated with yellow dashed lines. The retinal opening angle is marked with white arcs. L, lens; A, anterior; D, dorsal; P, posterior; V, ventral. Scale bars are 50 μm. **(C)** Analysis of retinal opening angles reveals blebbistatin interference with the process of optic cup invagination. The Welch two-sample t-test confirmed the significant difference in the retinal opening angle measurements between the two groups ($n_{\text{blebbistatin}} = 17$ retinas from 9 embryos; $n_{\text{DMSO}} = 8$ retinas from 4 embryos, $\bullet p = 2.448e^{-10}$). The bold lines indicate the median values, the red dots – the mean.

control group. Another remarkable difference is the presence of a high amount of pyknotic nuclei, visualized by DAPI in the blebbistatin-treated embryos (Figure 3.11B, yellow arrowheads).

3.2.3 Retinal stem cell marker is present in the rx3-null mutants

Since the blebbistatin treatment affects medaka embryo development quite extensively, I additionally employed the *eyeless* (*el*) rx3-null mutants, exhibiting eye morphogenetic phenotypes with different severity of defects from smaller-sized eyes (Figure 3.13), absence of ventral part of the retina to complete lack of the optic cup (Figure 3.13). Such phenotype is caused by the failed migration of retinal precursors from the ventral diencephalon to form the optic vesicles (Rembold et al., 2006). To date there has been described two lines of the mutants – the classical *el* mutants as well as recently established *rx3*-mutant fish carrying a GFP-tagged allele containing a terminator sequence, $Rx3^{saGFP}$ (Loosli et al., 2001; Rembold et al., 2006; Winkler et al., 2000; Zilova et al., 2021). I took advantage of partial penetrance of the phenotype in both lines and checked the *cndp1* mRNA presence by performing RNA whole-mount *in situ* hybridization at stage 28 and one day post-hatch (1 dph) in the variety of the phenotypes.

I found that the *cndp1* mRNA in the rx3-null mutants is located exclusively at the retinal periphery regardless of the stage and penetrance of the phenotype (Figure 3.13, white arrowheads), indicating that this very position might be instructive for the acquisition of RSC fate. In $Rx3^{saGFP+/+}$ embryos with the complete phenotype (complete loss of eyes), *cndp1* mRNA labeled the lateral wall of the forebrain dorsally from the lens (Figure 3.13F-G), suggesting that not only RSCs were potent of expressing *cndp1*.

Taken together, the presence of *cndp1* mRNA in the retinal periphery of the embryos with disrupted eye morphogenesis shows that the formation of the retinal periphery does not strictly depend on the proper optic cup morphogenesis.

3.2.4 Quantitative analysis of marker gene expression and tissue morphology reveals phenotypic variations in rx3 knockdown embryos

As I confirmed the presence of the retinal stem cell marker *cndp1* in the CMZ in conditions of perturbed eye morphogenesis, I then asked how the retinal ar-

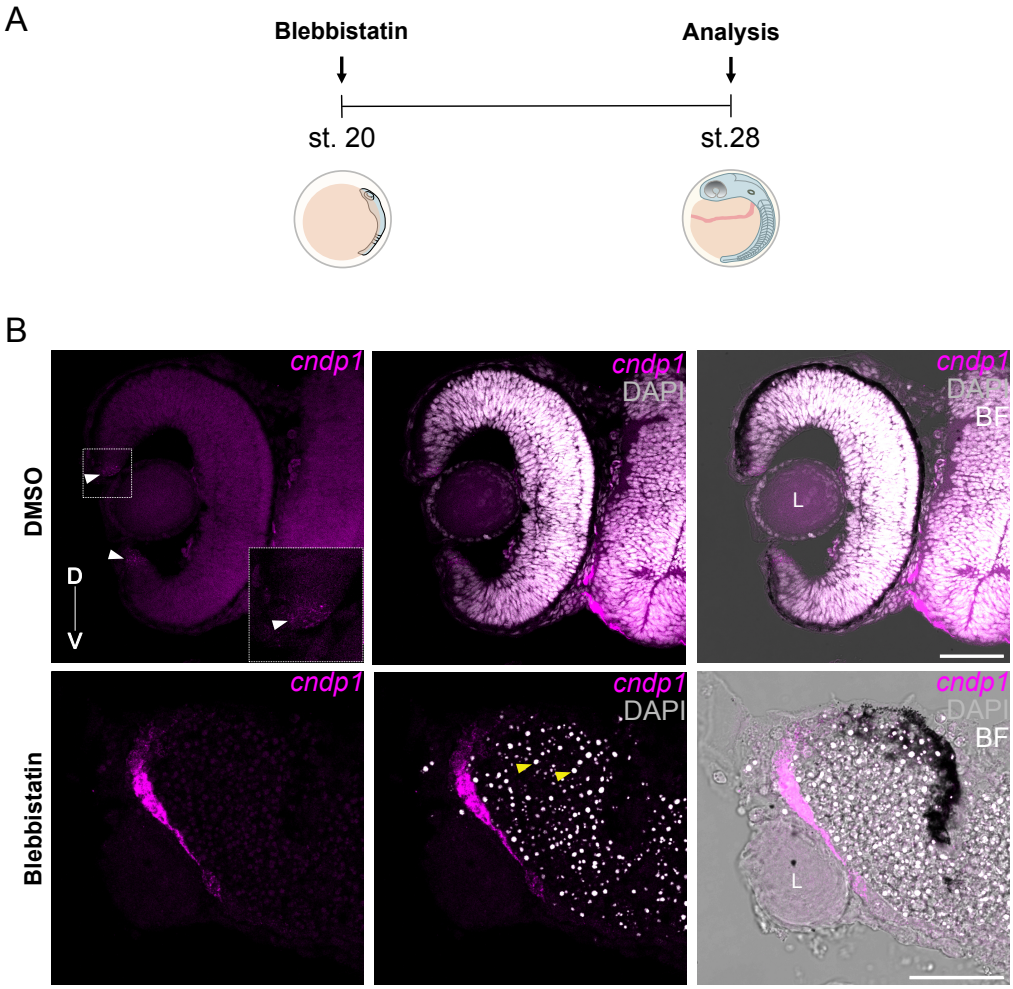

Figure 3.11. *cndp1* is present in the retinal periphery in the blebbistatin treated embryos upon optic cup morphogenesis.

(A) Dechorionated medaka embryos were subjected to 100 μM blebbistatin from stage 20 (st. 20) to stage 28 (st. 28). 90% DMSO was used as vehicle control.

(B) *cndp1* mRNA (magenta) was detected via HCR RNA-FISH in the retinal periphery of the embryos (white arrowheads), treated with blebbistatin from *st.20* to *st.28* ($n_{\text{blebbistatin}} = 12$ retinas from 6 embryos; $n_{\text{DMSO}} = 17$ retinas from 9 embryos). DAPI was used for nuclei visualization. Blebbistatin-treated embryos exhibited pyknotic nuclei (yellow arrowheads). All images in panel **(B)** represent single optical sections of transverse cryosections (16 μm) of the medaka retina acquired with a laser-scanning confocal microscope. D, dorsal; V, ventral; BF, bright-field; L, lens. Scale bars are 50 μm.

Figure 3.12. Impaired morphogenesis leads to absence of coherent eye structures.
(A)-(B) Comparative schematic representation of eye structures, depicting differences between wild-type and el mutant embryos; green, optic stalk; black, RPE; violet, NR; yellow, lens; D, dorsal; V, ventral. The panels adapted from Winkler et al. (2000). **(A')-(A")** Heterozygous *el* embryos have fully developed optic cups, while homozygous mutants **(B')-(B")** lack eyes (asterisks) in the most severe phenotype (the lens is outlined with dashed line in B'). Scale bars are 200 μm. Panels **(A')**, **(A")**, **(B')**, **(B")** are images from a bright-field binocular.

chitecture is changed in such phenotypes. To answer this, I joined my colleagues (see Contributions) in establishing the technique that combined light-sheet fluorescence microscopy and x-ray computed tomography. This multimodal approach enabled the alignment of gene expression patterns obtained through antibody staining with the anatomical details revealed by x-ray tomography. As mentioned above, $Rx3^{saGFP+/+}$ homozygous mutants expressed variable phenotypes, such as smaller optic cups and complete absence of those (Figure 1.14 A). To assess the alterations in retinal architecture within such variable phenotypes, we focused on genes marking main retinal compartments – Rx2 (CMZ, MG , and PhCs), Otx2 (RPE, BCs, PhCs), and HuC/D (RGCs and ACs) (Kim et al., 1996; Reinhardt et al., 2015; Zilova et al., 2021). Venera Weinhardt subjected wild-type medaka embryos of stage 34 to the whole-mount antibody staining and consequentially to x-ray tomography. I registered the resulting volumes onto each other using the Fijiyama plugin in Fiji software (Fernandez and Moisy, 2021; Schindelin et al., 2012) (Figure 3.14A). Retinas, brain, and lenses were segmented based on the x-ray tomography data (Figure 3.14B). The embryos were separated into 3 groups based on the severity of the phenotype: wild-type sibling (normal eye development), incomplete phenotype (altered optic vesicle evagination/optic cup formation), and complete phenotype (complete absence of the optic vesicle/optic cup) (Figure 3.14B). Using the segmentation data, I conducted a comparative analysis of tissue volumes across different phenotypes (Figure 3.14C-C"). The retina of the embryos with incomplete phenotype was notably smaller than the retina of a wild-type sibling (Figure 3.14C). The segmentation of x-ray tomography data revealed the retinal tissue to be stretched between two lenses while creating a small optic cup on the right side (Figure 3.14B, central panel, in green). This distinct phenotype could be attributed to the altered migration of RPCs from the developing forebrain. In contrast, the

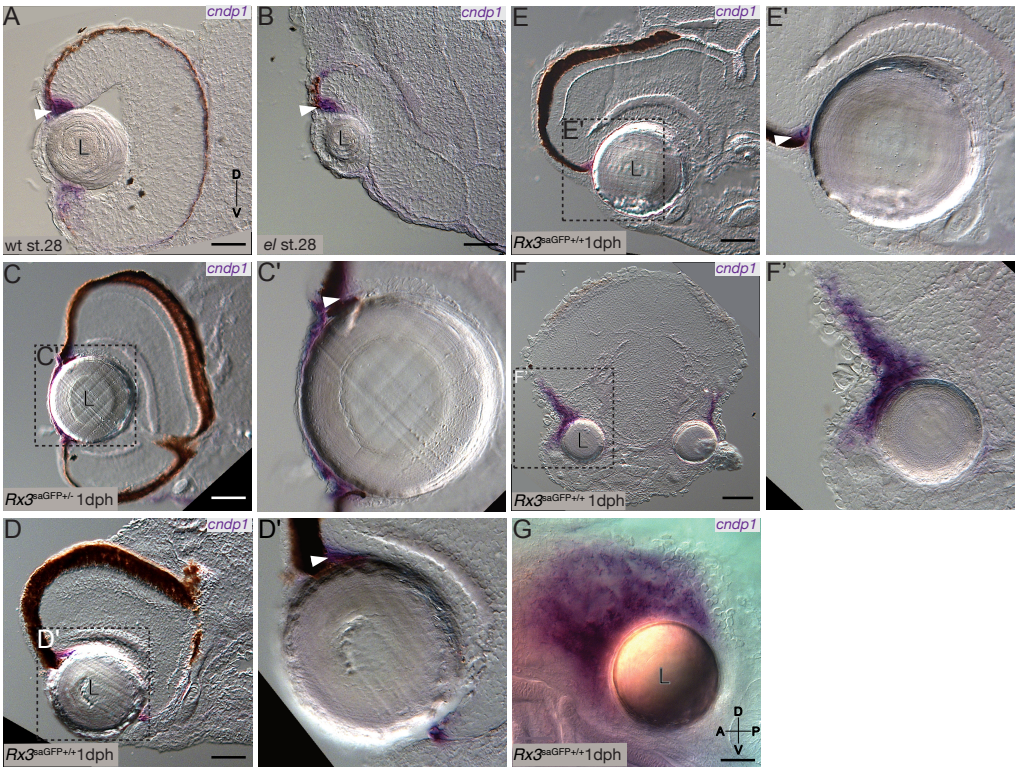

Figure 3.13. *cndp1* mRNA is present in the rx3-null mutants even in severe (eye-less) phenotype.

RNA *in situ* hybridisation showing *cndp1* expression. **(A)** *cndp1* mRNA labels RSCs in the peripheral retina at stage 28 (white arrowhead) (**?**). **(B)** Even within the deformed optic cup of the *el* mutant with incomplete phenotype, *cndp1* mRNA is present in the retinal periphery (white arrowhead). **(C)** *cndp1* mRNA in heterozygous rx3saGFP$^{+/-}$ heterozygous siblings is localized at the retina periphery (partially masked by RPE in **C'**). The penetrance of the phenotype is increasing from **(D)** to **(F)** in one day post hatch (1 dph) rx3saGFP$^{+/+}$ embryos. *cndp1* mRNA is always present at the retinal periphery (white arrowheads). **(F)-(F'')** *cndp1* mRNA is present only dorsally from the lens. **(G)** The whole-mount in situ hybridization against *cndp1* mRNA in a 1 dph rx3-deficient larvae. All panels represent single optical sections of transverse cryosections (16 μm) of the medaka retina acquired with DIC microscope. L, lens; D, dorsal; V, ventral; A, anterior; P, posterior. Scale bars are 30 μm.

complete phenotype demonstrated a scenario where this migration was entirely arrested, leading to the absence of optic vesicles/ optic cups (Figure 3.14B, right panel) (Rembold et al., 2006). Comparison of the brain volumes (segmented up to the otic vesicle in all embryos) helped to reveal a reduction in volume in the incomplete phenotype embryo in contrast to either the wild-type sibling or the complete phenotype embryo (Figure 3.14C'). Interestingly, the lens volume decreased with the increasing severity of the phenotype (Figure 3.14C"). To address how different cell types are represented among embryos with diverse phenotypes, I employed automatic Otsu thresholding across all channels within the combined retina and brain labels. This allowed me to obtain the voxel size occupied by each marker within the retina or brain. Subsequently, these values were normalized based on the corresponding tissue size derived from x-ray tomography (Figure 3.14D-D'). In the brain the relative ratio for all three markers was elevated (Figure 3.14D'), suggesting that, despite a migration arrest of retinal progenitor cells in the $Rx3^{saGFP+/+}$ homozygous mutants, these cells were still able to obtain the retinal identity while located within the developing forebrain (Zilova et al., 2021). Notably, in the retina of the embryos with incomplete phenotype, there was an elevation in Otx2 and HuC/D expression compared to the wild-type sibling, while Rx2 expression was diminished. This data suggests that even when retinal progenitor cell migration was arrested, these cells retained their retinal identity within the developing forebrain. These findings emphasize the robustness of cellular differentiation and identity processes despite disrupted eye morphogenesis.

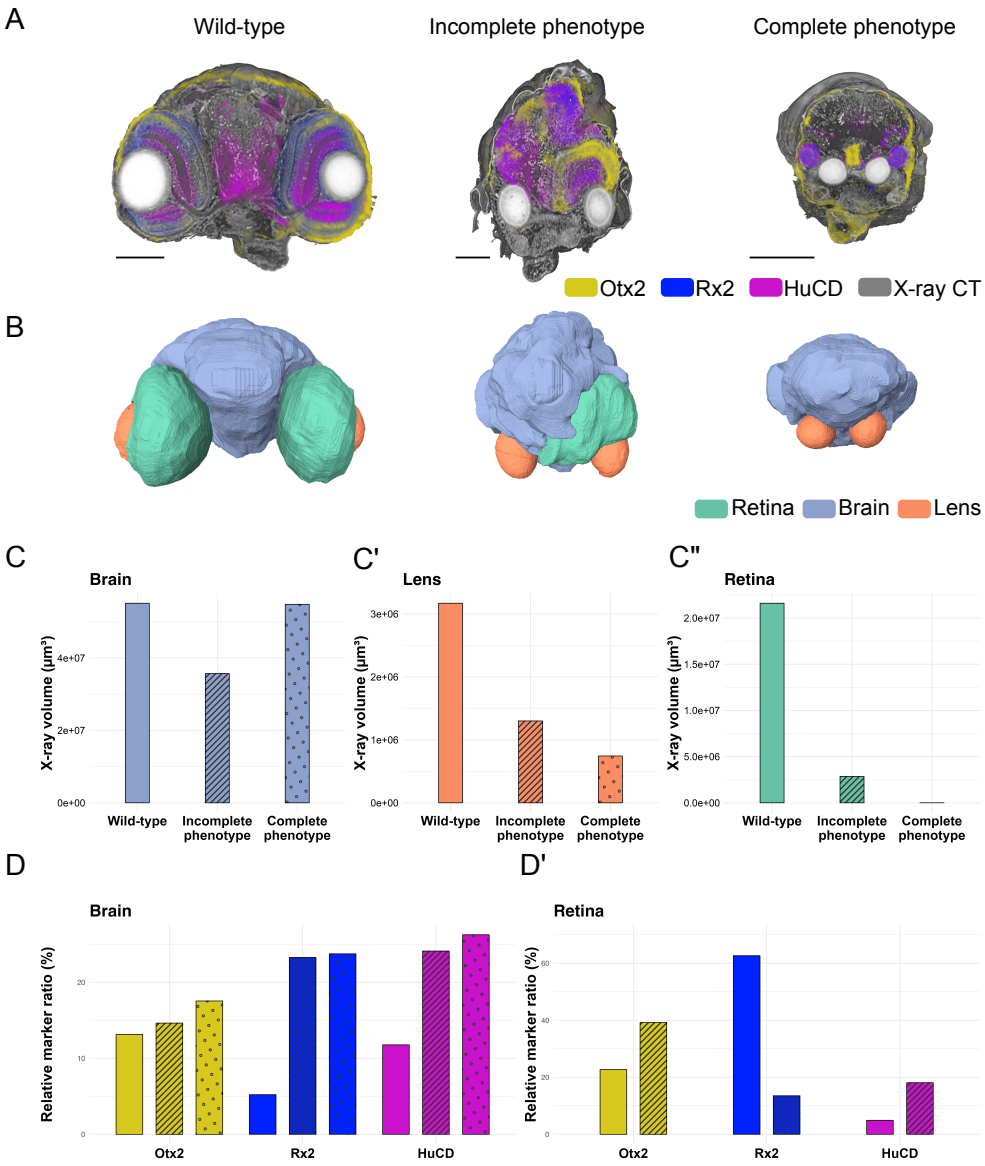

Figure 3.14. Alignment of retinal markers and x-ray tomography-derived tissue morphology reveals phenotypic differences in *Rx3*$^{saGFP+/+}$ homozygous mutants.

(A) Virtual slices through 3D rendering of stage 34 medaka embryos labeled by whole-mount immunohistochemistry with antibodies against Otx2 (yellow), rx2 (blue), and HuC/D (magenta) proteins. The x-ray tomography (grey) was registered onto the light-sheet dataset. Scale bars are 100 μm. **(B)** 3D surface renderings of segmented based on x-ray tomography 607 tissues, that is retina (green), brain (blue), and lens (orange). **(C)** Brain volumes along the severity of the phenotypes. **(C')** Lens volumes comparison across phenotypes. **(C")** Retinal volumes along the severity of the phenotypes. **(D)**-**(D')** Quantitative analysis of Otx2, Rx2 and HuC/D expression in brain **(D)** and retina **(D')**. The relative marker ratio was calculated by assessing the voxel size normalized based on the corresponding tissue (retina or brain) size.

Figure 3.14. Venera Weinhardt generated all the raw data used in the figure. Kristaps Kairišs created panels (A) and (B). I performed the quantitative analysis and assembled the figure. The figure is adapted from the submitted manuscript Kairiss et al. (2023).

3.3 Cell dynamics in the retinal periphery during embryonic development

As my previous results showed that the retinal periphery establishment does not rely on the proper optic cup morphogenesis (Figures 3.11-3.13), I focused on my second scenario (Figure 1.3) and tested how the behavior of the cells at the retinal periphery changed upon optic cup formation is completed. To track down features underlying the establishment and changes in and behavior of RSCs, it was crucial to understand when precisely they happen in the medaka embryonic development. RSCs in lower vertebrates can be characterized by two main characteristics: slow proliferation and the ability to contribute to growth by giving rise to ArCoS (Centanin et al., 2011; Ohnuma et al., 2001).

3.3.1 Retinal progenitors within the retinal periphery slow down their proliferation during embryonic development

To understand the changes in proliferative behavior, I employed two strategies. The first one involved short-pulse EdU incorporation in the span of embryonic development. After 2 h of the EdU pulse, the embryos were fixed, and the number of EdU-positive cells was assessed according to SHInE protocol (Figure 3.14A), which combines HCR RNA-FISH with EdU staining (Ćorić et al., 2023). This combination allowed me to simultaneously detect cells that actively proliferate and express *cndp1* (*cndp1*/EdU double-positive cells). As a result, I could observe a decrease in the proliferation rate of *cndp1*-positive cells during embryonic development (Figure 3.14B-C). At stage 24, *cndp1* mRNA is present in the retinal periphery, but only at later stages, its expression forms an evident rim around the lens (Figure 3.14B). Quantification of the ratio of double *cndp1*/EdU-positive cells per retina revealed a decrease in the proliferation of the retinal periphery cells between stages 24 and 28 (Figure 1.15 C). At st. 24, $51.7\% \pm 3.06\%$ of the *cndp1*-positive cells underwent S-phase in the 2 hours of the EdU incubation, while at st. 28 this number dropped

down to $0.4\% \pm 0.89\%$. At later stages these cells preserved their proliferation rate similar to stage 28 with $0\% \pm 0\%$ for stage 36 and $0.2\% \pm 0.45\%$ for stage 40 (Figure 1.15 C).

The second approach involved short-term Cre/loxP-mediated clonal analysis. This experiment was initially conceived by Lucie Zilova, the data presented was acquired by me. Embryos of the *ccl25b::Cre*$^{selectively tamoxifen-sensitive estrogen receptor (ERT2)}$, *Gaudí*^{RSG} line were recombined at different stages throughout embryonic development, grown for the same period of 4 days post recombination (dpr), and then fixed and analyzed for the presence and position of recombined (H2B-GFP-positive) cells (Figure 3.16A). As I performed whole-mount staining against GFP, I observed a difference in the number of GFP-positive cells populating the retina after 4 dpr (Figure 3.16B). When recombined at earlier stages (st. 24 and st.28), the *ccl25b::Cre*^{ERT2}-expressing cells located at the rim of the retina proliferated extensively and gave rise to multiple GFP-positive cells further located in more regions of the retina. When recombined at st. 30, after 4 dpr the *ccl25b::Cre*^{ERT2}-expressing cells seized their proliferation, as the recombined GFP-positive cells mainly stayed confined in the retinal periphery. The same pattern was observed when the recombination was performed at st. 40. Besides, at later stages, progeny of *ccl25b::Cre*^{ERT2}-expressing cells can also be detected in the choroid (Figure 3.16B, yellow arrowheads). Overall, both experiments consistently show that cells of the retinal periphery slow down the proliferation rate around st. 28-30 (Iwamatsu, 2004).

3.3.2 Initiation of iArCoS in development reveals retinal peripheral cell contribution to lifelong growth

The ultimate definition of a functioning RSC is its ability to generate lineages of differentiated cells. Since I focused on the emergence of such cells, elucidating the timing of their clonal initiation was essential. To address this question, I again used the previously established lineage analysis method, which utilizes an inducible Cre system under a stem cell promoter (Centanin et al., 2014; Eggeler, 2017). I recombined embryos of the previously mentioned *ccl25b::Cre*^{ERT2}, *Gaudí*^{RSG} line at stage 28 (Iwamatsu, 2004) with 4-OH tamoxifen, and treated them with short BrdU pulses at various stages in separate batches (Figure 3.17A). At 6 wph, I stained whole-mount retinas against GFP and BrdU. As the fish grows, BrdU, being incorporated by dividing progenitors of the CMZ, would be retained in more centrally located cells that exited the cell cycle to differentiate into retinal neurons, creating a ring-like pattern (here referred to as “BrdU ring”) when observed from the

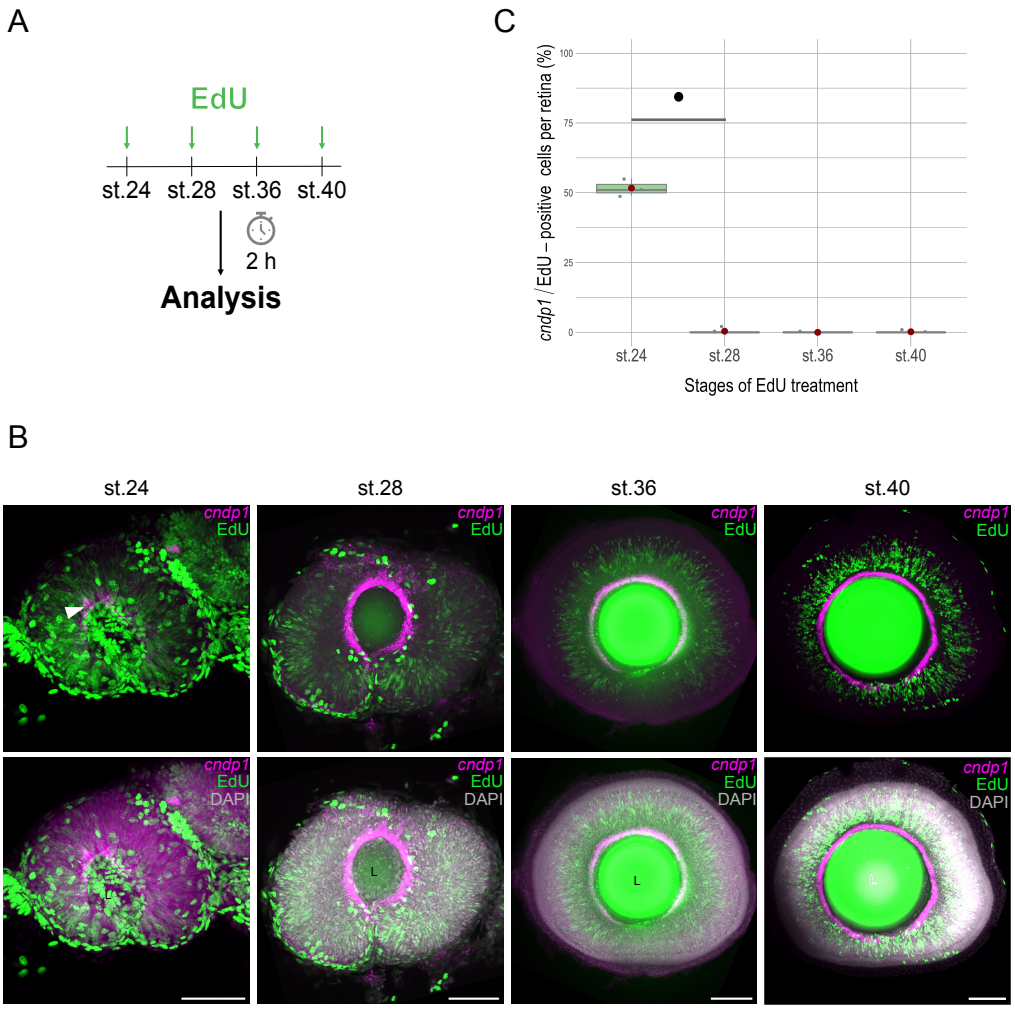

Figure 3.15. Short EdU pulses along embryonic development revealed the slowing of proliferation in retinal periphery in medaka.
(A) Schematic representation of the experimental setup. Dechorionated medaka embryos of st. 24, 28, 36, and 40 (Iwamatsu, 2004) were incubated in EdU for 2 hours, immediately sacrificed, and analyzed. **(B)** Representative images of retinas of different stages stained against cndp1 mRNA (magenta) and EdU-positive cells (green). DAPI (grey) was used for nuclei visualization. At st. 24, *cndp1* already marks the retinal periphery (white arrowhead), and in later stages, it labels the most distal part of the CMZ more intensively. All panels are maximum projections of the volumes obtained with a laser-scanning confocal microscope. D, dorsal; V, ventral; L, lens. Scale bars are 50 μm. **(C)** Quantitative analysis of double *cndp1*/EdU-positive cell ratio per retina across developmental stages. The ratios were estimated by dividing the number of double *cndp1*/EdU-positive cells by the number of EdU-positive cells. The Welch two-sample t-test between st. 24 and 28 confirmed the significant difference in the numbers of *cndp1*$^+$/EdU$^+$ cells between the two groups ($n_{\text{st.24}} = 3$ retinas from 2 embryos; $n_{\text{st.28}} = 5$ retinas from 3 embryos; $n_{\text{st.36}} = 3$ retinas from 2 embryos; $n_{\text{st.40}} = 5$ retinas from 3 embryos, $\bullet p = 0.0007141$). The bold lines indicate the median values, the red dots – the mean.

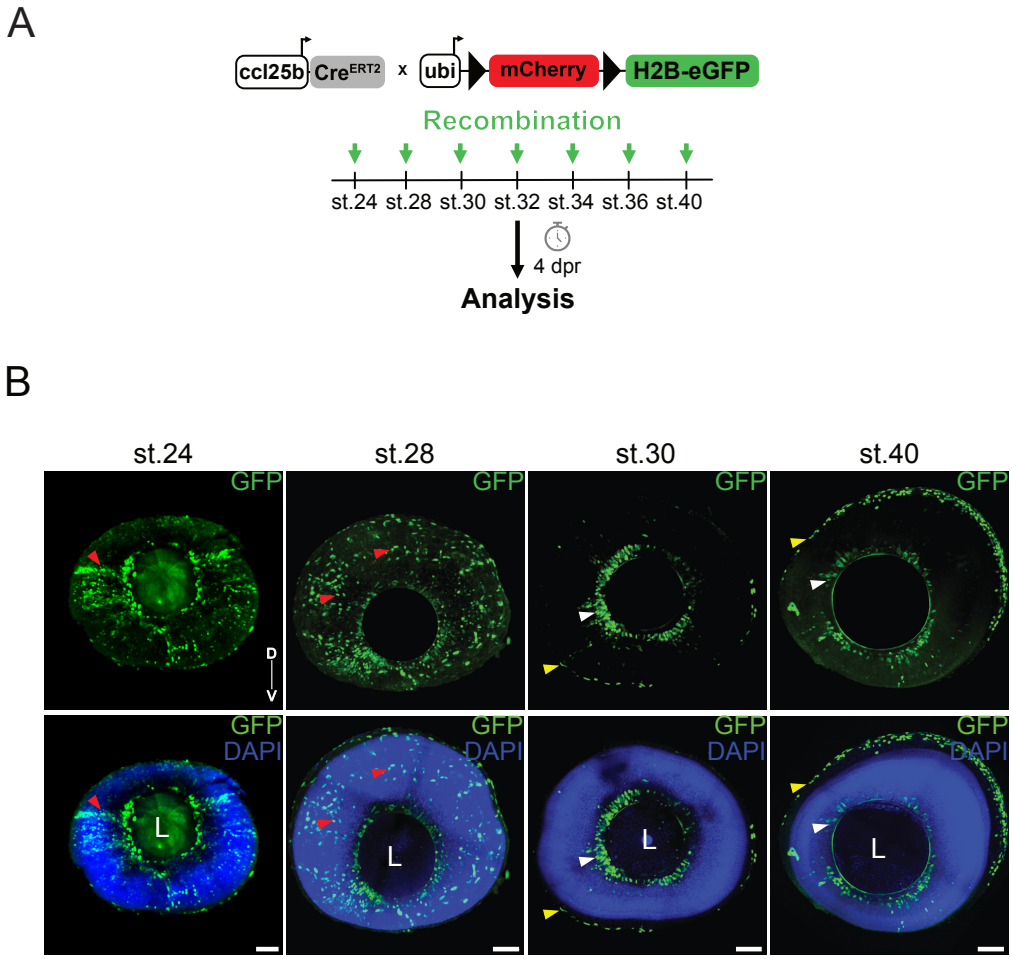

Figure 3.16. Short-term recombination mediated by *ccl25b::Cre*^{ERT2} revealed different proliferative behavior through the development.
(A) Schematic illustration of the experiment. *ccl25b::Cre*^{ERT2}, *Gaudi*^{RSG} line embryos were recombined with 4-OH tamoxifen at different stages and were analyzed 4 dpr. **(B)** At st. 24-28 ccl25b-positive cells were rather proliferative as indicated by the presence of their progeny outside of the CMZ (red arrowheads). However the proliferation at st.30 was already similar to the slow proliferation of these cells at the hatchling stage (white arrowheads). Besides expression in the CMZ, ccl25b-recombined cells can also be detected in the choroid (yellow arrowheads). Images in panel (B) are maximum projections of whole-mount medaka retinas acquired with a laser-scanning confocal microscope. D, dorsal; V, ventral; L, lens. Scale bars mark 30 μm.

back of the eye (Centanin et al., 2011) (Figures 1.1C, 3.17B). In such an experiment the iArCoS , which had started before the BrdU pulse crossed the BrdU ring, and the iArCoS which had begun after the pulse did not (Figure 3.17B). The time for recombination and BrdU pulse had to be titrated down: initial attempts yielded half-recombined retinas and a rather thick BrdU ring signal. The final protocol included recombination for 1 h with 2.5 mM 4-OH tamoxifen and the 1.5-hour BrdU pulse. With such, I was able to obtain sparse clones (Figure 3.17C-C").

Interestingly, there was a notable trend in the BrdU signal intensity across different stages: while the BrdU signal for stages 38 and older was notably bright, the signal for earlier stages was more elusive and at times impossible to obtain (Figure 3.17C-C). Additionally, besides continuous iArCoS (Figure 3.17D, D), I could also observe clonal footprints (7.9%±12%), disconnected from the CMZ (Figure 3.17D, F). Such footprints originate from RPCs being recombined (Centanin et al., 2014). This observation indicates that ccl25b marks not only RSCs but also a few RPCs.

The quantification of the ratio of the iArCoS that cross the BrdU ring to the total number of the iArCoS per retina revealed an intriguing distribution of the iArCoS initiation (Figure 3.17E). While some iArCoS crossed the BrdU ring already at stage 32, their peak appeared to be on stage 40 with 20%±28.3% for stage 32, 10.8%±9.57% for stage 34, 30.7%±29.7% for stage 36, 46.6%±15.4% for stage 38, 76.6%±14.3% for stage 40 and 100%±0% for 2 wph group of clones crossing the BrdU ring at corresponding stages (Figure 3.17E). By 2 wph, all iArCoS have already been initiated (Figure 3.17C, E). This data demonstrates the temporal initiation of iArCoS, reflecting the acquisition by the retinal peripheral cells ability to contribute to the retina life-long growth.

In summary, I conclude that retinal progenitors located at the retinal periphery of medaka retina undergo changes with respect to their proliferation rate and ability to produce ArCoS. By the time the optic cup completes the essential parts of its morphogenesis at stage 24, they are fast proliferating and slow down their proliferate rate by stage 28-30. Soon after that they start exhibiting another RSCs characteristic by producing continuous clones of differentiated cells. Just before the embryo hatches at stage 40, this activity peaks and reaches 100%±0% by 2 wph.

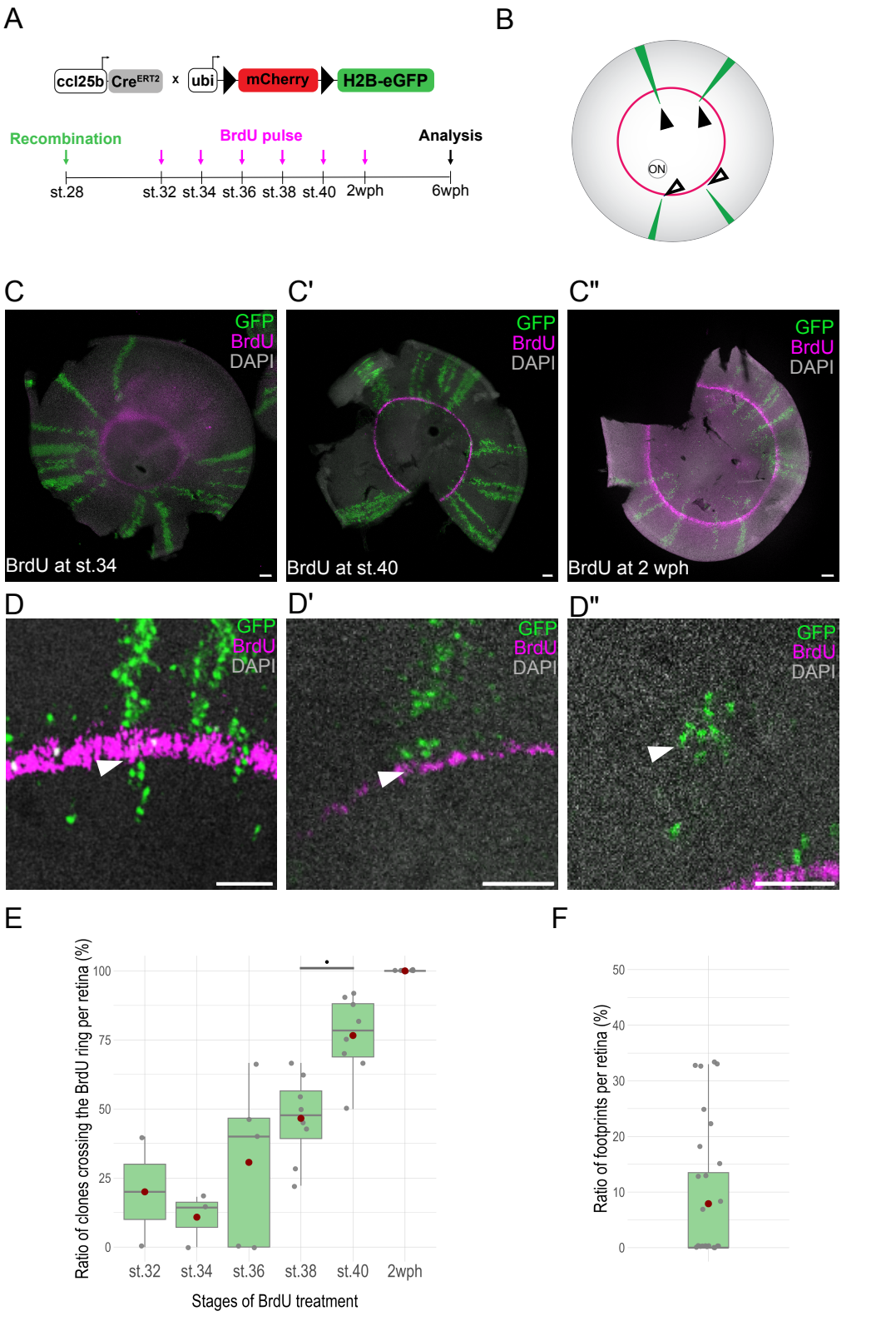

Figure 3.17. The distribution of iArCoS initiation during embryonic development.

(A) Schematic representation of the experimental design. In the *ccl25b::Cre*^{ERT2}, *Gaudí*^{RSG} reporter line, upon induction, mCherry is floxed out, leading to H2B-eGFP inheritance by daughter cells and forming iArCoS.

Figure 3.17. *ccl25b::Cre*^{ERT2}, *Gaudí*^{RSG} line embryos were recombined with 4-OH tamoxifen at stage 28. Individual groups were then subjected to 1.5 h BrdU pulses at stages 32, 34, 36, 38, and 40 (Iwamatsu, 2004). The fish were grown until 6 wph for analysis. **(B)** Due to the outward growth mode of the fish retina, iArCoS (green) which initiated before the BrdU treatment crossed the BrdU ring (magenta) (filled arrowheads). If they started post the BrdU treatment, they did not cross the ring (empty arrowheads). ON, optic nerve. **(C)-(C")** Representative images of retinas treated with BrdU at stages 34 (C), 40 (C'), and 2 wph (C"). **(D)** Representative image of an iArCoS crossing the BrdU ring (white arrowhead). **(D')** Representative image of an iArCoS in proximity but not crossing the BrdU ring (white arrowhead). **(D")** An example of a clonal footprint created by an RPC (white arrowhead). **(E)** Quantification of clones crossing the BrdU ring at stages 32, 34, 36, 38, 40, and 2 wph. Each data point signifies one retina, where the ratio of clones crossing the BrdU ring to total clones is quantified ($n_{\text{st.32}} = 2$, $n_{\text{st.34}} = 3$, $n_{\text{st.36}} = 5$, $n_{\text{st.38}} = 8$, $n_{\text{st.40}} = 8$, $n_{2wph} = 8$). In total, 301 clones from 34 retinas were quantified. Pairwise comparisons using the t-test unveiled the subsequent p-values: $p_{\text{st.32/34}} = 0.54$, $p_{\text{st.34/36}} = 0.11$, $p_{\text{st.36/38}} = 0.1$, $p_{\text{st.38/40}} = 0.001$, $p_{\text{st.40/2 wph}} = 0.008$. The $\bullet p_{\text{st.38/40}} = 0.001$ indicates that at stage 40 a notably larger number of iArCoS had begun than at stage 38. Bold line indicates median, red dot – mean. **(F)** Quantification of the clonal footprints from all the retinas. Each data point is a single retina, showing the ratio of footprints to the total number of clones in the retina ($n_{\text{footprints}} = 20$ footprints from 34 retinas). Bold lines signify median values, red dots – mean. Panels **(C)-(D")** represent single optical planes of flat-mounted retinas captured with a laser-scanning confocal microscope. Scale bars are 100μm for **(C)-(C")** and 50μm for **(D)-(D")**.

3.4 Exploration of the changes in gene expression along the temporal axis of RSC emergence by RNA bulk and single-cell sequencing

3.4.1 Bulk RNA sequencing of the sorted cells at different stages revealed discrepancies in the fluorescent signal of a reporter line

Having highlighted the distinct behaviors of retinal periphery cells throughout their developmental trajectory, I then asked what molecular mechanisms might drive these changes. I addressed this question in a collaborative effort with colleagues (see Contributions) through two different approaches (Figure 3.18A). The first approach included bulk RNA sequencing of the cells at the retinal periphery at different stages of development. For that, we used the *cndp1::mCherry-2A-oNTR*, *rx2::H2B-GFP* reporter line. The eyes of stages 24, 36, and 40 were dissected and dissociated. The resulting single-cell suspension was submitted for FACS to the Flow Cytometry & FACS Core Facility (FFCF). GFP-positive cells, representing RPCs, were sorted from the samples of stage 24 (Figure 3.18B, C). Cell suspensions of stages 36 and 40 were sorted for double fluorescence of green fluorescent protein (GFP) and mCherry in order to acquire RSCs positive for both cndp1 and Rx2 (Figure 3.18B, C). Stage 7 technical replicates containing 500 cells each were submitted to the Deep Sequencing Core Facility. The cDNA preparation, quality controls and sequencing were performed according to the Smart-seq2 protocol by David Ibberson (Picelli et al., 2014). Miguel Angel Delgado Toscano performed the analysis described below of the sequencing results. The initial quality of the reads was optimal, and the mean number within replicates turned out to be between 20 and 30 million reads. As the reads were aligned to the reference genome and annotated, differential gene expression (DGE) analysis was performed. Following the establishment of the counts matrix, the evaluation of correlation coefficients revealed a robust degree of correlation among the seven replicates for each stage (Figure 3.19A).

Upon the construction of a DESeq2 object from the counts matrix and the subsequent removal of genes with fewer than 10 counts across the diverse samples, a principal component analysis (PCA) was performed (Figure 3.19B). While generally, the clustering of the replicates per stage was good, there was evident variability among replicates of stage 40 (Figure 3.19A, B). As the next step, the heatmap of

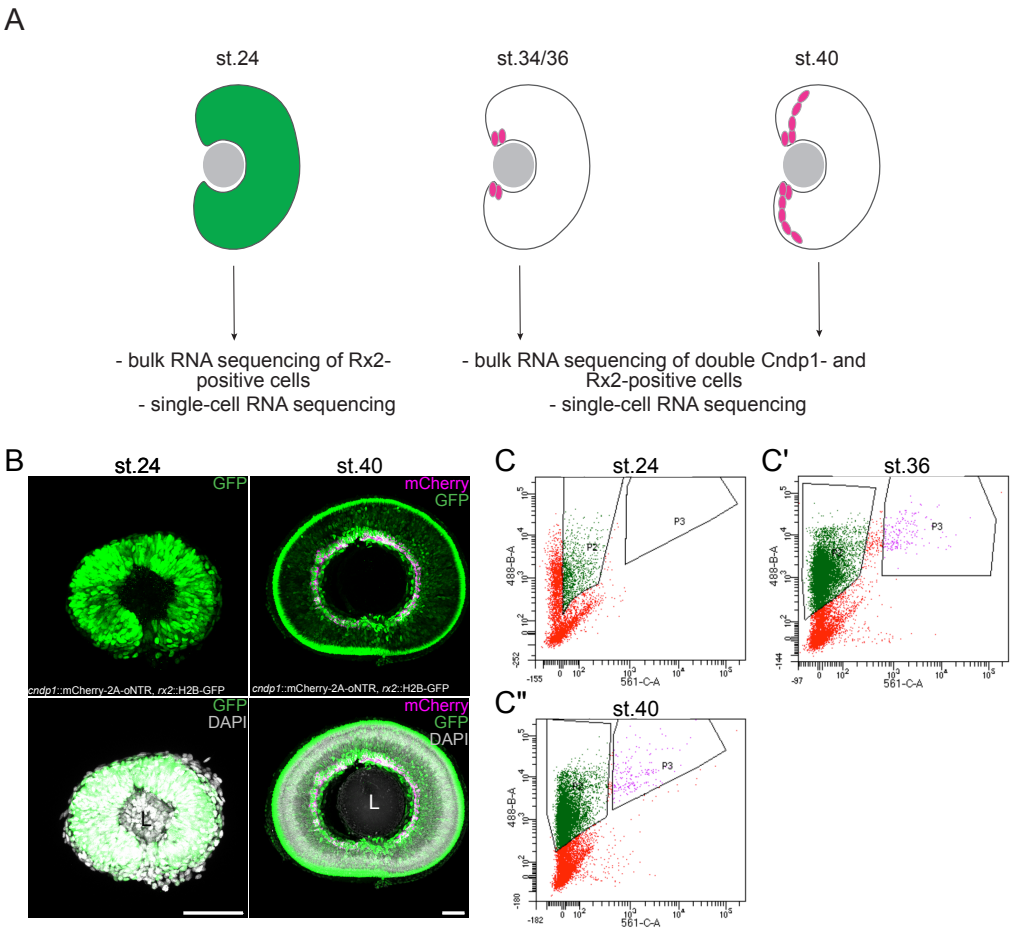

Figure 3.18. Elucidation of the transcriptional differences along temporal axis of RSCs emergence.

(A) Schematic representation of the experimental design. The retinas of st. 24, 36 and 40 of the *cndp1::mCherry-2A-oNTR*, *rx2::H2B-GFP* were dissociated and subjected to the FACS sorting based on the fluorescent profile. In addition, dissociated retinas of st. 24 and 40 were subjected for the scRNA sequencing and combined in the analysis with already available dataset of st.34. (B) At st. 24 nearly all early RPCs are marked by GFP (green) in the *cndp1::mCherry-2A-oNTR*, *rx2::H2B-GFP* reporter line. At later stages, RSCs are labeled by mCherry (magenta) and GFP (green) expression. All panels represent maximum projections of the medaka retinas at st. 24 and 40, captured from the front view with a laser-scanning confocal microscope. L, lens. Scale bars are 50 µm. (C)-(C") Fluorescence dot plots of the submitted dissociated retinas of st. 24 (C), 36 (C') and 40 (C"). Every event (cell) is expressed as a single dot. Fluorescent intensity for 561 laser is represented along X-axis, while y-axis illustrates the intensity of the 488 laser. P2 gating specifies the GFP-positive cells (only RPCs), the P3 gating identifies cells that positive for both GFP and mCherry (RSCs). Panels (C)-(C") were acquired by Monika Langlotz of the FFCF.

the fold change of the 10 most differentially expressed genes between stages was generated, with them being *ENSORLG00000025548*, *tob1a*, *pde6ha*, *mak*, *dusp5*, *ckba*, *si:ch211-251b21.1*, *rho*, *abcg1*, and *mark3a* (Figure 3.19C). A closer look at these genes and comparison to the scRNA data revealed that most of them are genes enriched in photoreceptor cells. Given such unexpected results and that the *cndp1* mRNA had never been detected in photoreceptors, we went back and assessed the expression pattern of mCherry in the retinas of *cndp1::mCherry-2A-oNTR*, *rx2::H2B-GFP* reporter line (Figure 3.19, D). Indeed, the fluorescent signal of mCherry was detected sparsely in photoreceptors, as indicated by the overlap with the GFP expression marking this layer (Figure 3.19, D). The fluorescent intensity of the mCherry in the RSCs was still much brighter than in photoreceptors, however, the DGE analysis results indicated contamination in the sorted cell population and, consequentially, the distortion of the sequencing results.

3.4.2 Combined scRNA sequencing revealed DEG in the stem cell cluster between stages

In parallel to the bulk RNA sequencing, I also performed scRNA sequencing of medaka retinas at stages 24 and 40 (Figure 3.20). For that, in a collaborative effort (see Contributions), I submitted single-cell suspensions of retinas of the aforementioned stages. 10 right optic cups of stage 24 and two right optic cups of stage 40 **?** were dissected and pooled together stage-wise. The single-cell suspension was prepared using a mix of trypsin and dispase enzymes. The viability of the cells was assessed via Trypan Blue staining followed by quantification in the Neubauer chamber. The single-cell suspensions with 88% (for stage 24) and 82% (for stage 40) of viable cells were submitted for sequencing with 10x Genomics. In the downstream pipeline, 1699 (st. 24), 4176 (st. 40), and 6397 (st. 34) with 100–20000 features and less than 20% mitochondrial transcripts were identified. These three datasets were then combined into one, containing a total of 12272 cells (Figure 3.20). The top 3000 features were used for clustering, with cell cycle or mitochondrial transcripts being regressed out. As a result, we obtained 20 clusters (Figure 3.20). Having obtained DEGs for all clusters, I compared the top markers with previously annotated datasets and identified the cluster containing RSCs as cluster 16. It was the only one containing *ccl25b* transcripts, as well as *aldh1a2* and *col2a1a*. Next, I performed preliminary DGE analysis and identified the DEGs in this cluster between samples of st. 34 and 40 (Figure 3.20C). The volcano plot illustrates the vast number of genes that differ in fold expression (logfc.threshold=0.5) between these two stages

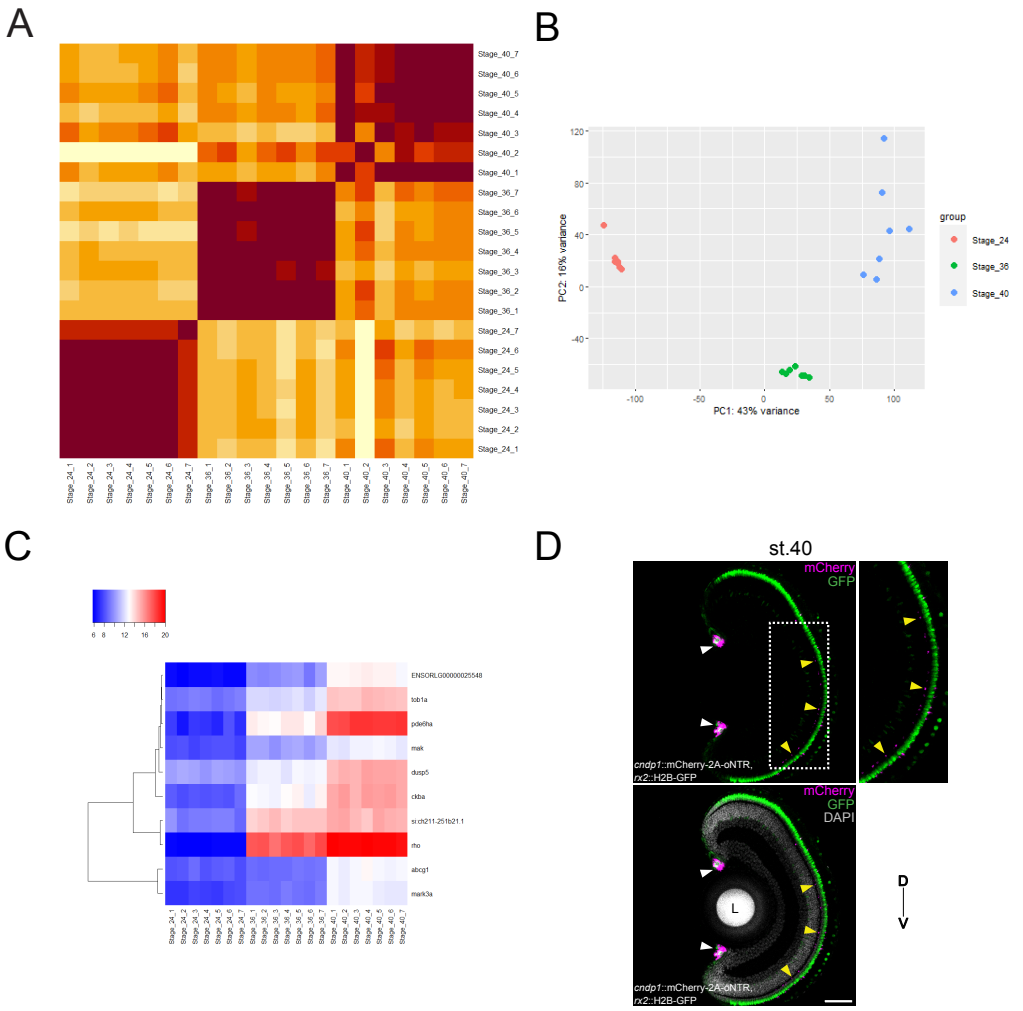

Figure 3.19. Photoreceptor markers were found among top 10 DEGs in the bulk RNA sequencing results.

(A) Assessment of correlation coefficients within the counts matrix. White color represents a weak correlation, and deeper hues of red reflect a stronger correlation. **(B)** PCA analysis of the DESeq2 object. **(C)** Heatmap of the fold change of the 10 most differentially expressed genes among different stages. **(D)** Besides labeling the RSCs (white arrowheads), mCherry expression turned out to be also evident in the photoreceptors (yellow arrowheads) of the cndp1::mCherry-2A-oNTR, rx2::H2B-GFP reporter line retina at st. 40 (as well as at st. 36). Panel **(D)** illustrates a single optical section of the transversely bisected in the medaka retina at st. 40, captured with a laser-scanning confocal microscope. Scale bar is 50 µm. L, lens; D, dorsal; V, ventral. Miguel Angel Delgado Toscano acquired panels (A)-(C), I acquired panel (D) and assembled the figure.

(Figure 3.20C). The analysis to validate these genes will be performed to identify a potential role in launching the retinal periphery cells to the RSCs fate.

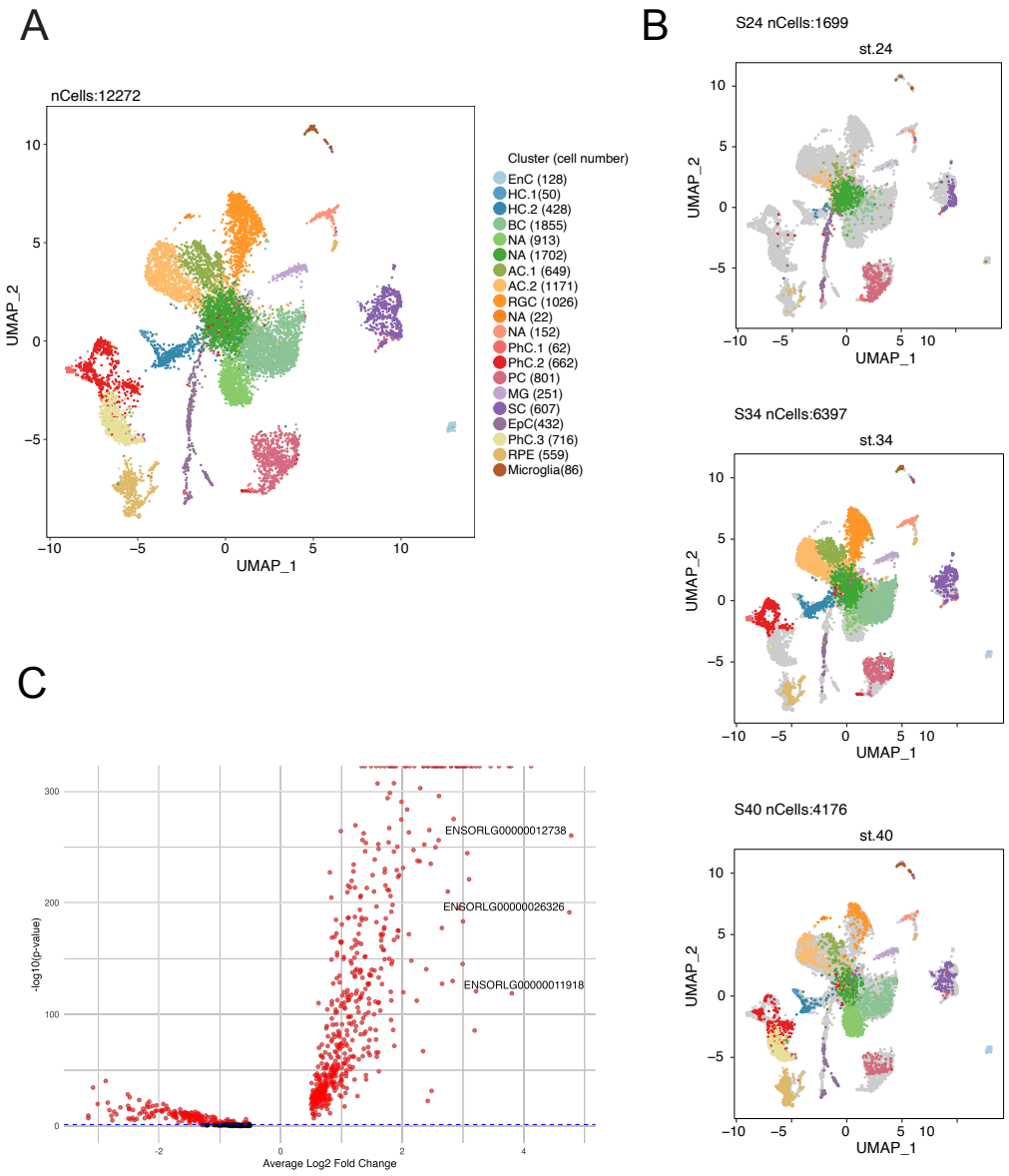

Figure 3.20. Combined datasets of scRNA sequencing of medaka retina at different stages.

(A) UMAP plot illustrating 20 clusters corresponding to primary cell types in the medaka retina. Integration of data from 3 datasets of st. 24, 34, and 40 using Seurat yielded a single dataset consisting of 12,272 cells.

(B) Workflow analysis accounting for features ranging from 100 to 20,000 with under 20% mitochondrial transcripts identified 1,699 cells from the st. 24 sample, 6,397 cells from the st. 34 sample, and 4,176 cells from the st. 40 sample. AC, amacrine cells; BC, bipolar cells; RGC, retinal ganglion cells; MG , Müller glia; HC, horizontal cells; PC, progenitor cells; PhC, photoreceptors; SC, stem cells; RPE , retinal pigmented epithelium; EpC, epithelial cells; NA, not identified; EnC, endothelium cells. **(C)** Volcano plot displaying the preliminary DGE analysis results in cluster 16 between st. 40 and st. 34 cells. Sebastian Gornik generated panels (A) and (B). I identified clusters in (A), crafted panel (C), and compiled the figure.

4

Discussion

The primary goal of this thesis centered on the characterization and exploration of the mechanisms governing the emergence of adult retinal stem cells in teleost fish. To achieve this, I utilized the following objectives:

1. Through scRNA sequencing of the medaka retina, I discovered novel markers for RSCs and RPCs and assessed their expression pattern in development.

2. I inspected the pattern of retinal stem cell marker expression in the conditions of interrupted eye morphogenesis via either pharmacological or genetic intervention.

3. I tracked the changes in the behaviour of the cells at the retinal periphery concerning their proliferation rates and ability to give rise to ArCoS during medaka embryonic development.

4. By performing bulk and single-cell RNA sequencing of different stages of development, I obtained the preliminary list of candidate genes potentially involved in the emergence of RSCs.

In the following, I discuss and offer future perspectives based on the selected findings of this thesis.

4.1 Molecular profiling of CMZ revealed novel markers for the retinal stem cell niche

The scRNA sequencing of the medaka retina yielded a comprehensive set of data and analysis identified a cluster presumably containing RSCs. During its validation, I identified novel markers for the medaka CMZ. While some have already been recognized in the retinal periphery of other species, others have not been reported to label the CMZ. The *aldh1* family has been widely known to mark stem cells in various tissues, including adult stem cells in the mammalian brain (Corti et al., 2006; Moreb, 2008; Obermair et al., 2010; Tomita et al., 2016). Notably, in *Xenopus*, chick, and mouse, *aldh1* has been reported to label the most distal part of the dorsal retina (Ang and Duester, 1999; Mic et al., 2000; Peters and Cepko, 2002). While this aligns with the observed expression pattern in medaka CMZ (Figure 3.3, 3.6), a strong signal was also evident in the ventral part of the CMZ. However, when whole-mount retinas were imaged from the lens, the signal was absent in the anterior and posterior domains of CMZ (data not shown). While this family is essential for retinoic acid (RA) biosynthesis, the deficiency of *Aldh1a1* did not alter the Aldh activity and neural stem cell (NSC) or hematopoietic stem cell (HSC) functions (Levi et al., 2009). Interestingly, the inhibition of RA synthesis was reported to inhibit the formation of the ventral retina in zebrafish (Marsh-Armstrong et al., 1994), potentially suggesting a link between RA signaling and rim involution.

Another family, collagens, have also been widely acknowledged to mark the retinal periphery cells in chick and mouse CMZ (Spence et al., 2004). In zebrafish, *col15a1b* mRNA labels the most distal part in CMZ, presumably containing only RSCs (Angileri and Gross, 2020). In addition, multiple members of this family have been attributed to be crucial members of stem cell niches across various systems (Kirkland, 2009; Liu et al., 2022; Motegi et al., 2014). Besides playing an essential part in stem cell functioning, they are also widely present in other ECM-rich tissues, such as cartilage, skin, and cornea (Alcaide-Ruggiero et al., 2021; Bruckner, 2010; Wu et al., 2010). Interestingly, while in medaka *col2a1a* mRNA was detected in the RSCs (Figures 3.6), its ortholog in zebrafish was reported as a marker for chondrocytes later contributing to osteoblasts and marrow adipocytes (Giovannone et al., 2019). Notably, the *col2a1a* expression in cartilages was revealed to be positively regulated by another gene identified in the medaka RSCs, *sparc*. Morpholino-mediated knockdown of *sparc* resulted in the inner ear and cartilage defect and rEdUced expression of *col2a1a* (Rotllant et al., 2008). In addition,

the characterization of *sparc* expression in medaka suggested further roles in chondrogenesis, as well as in the development of other tissues such as pronephri and epidermal cells, and further confirmed the co-expression of *sparc* and *col2a1* in the same tissue (Renn et al., 2006). As it is well established that ECM is an important component of stem cells niches and regulation of stem cells (Pardo-Saganta et al., 2019), these genes may contribute to the formation of the RSC niche in medaka.

The presence of *TGFß3*-like (Ensembl ID: ENSORLG00000009111) mRNA in the RSCs seems to be conserved in teleost fish: previously, *TGFß3* has been reported to mark retinal periphery and MG in zebrafish (Lee et al., 2020). Interestingly, this study also reported on the role of this gene in maintaining the quiescence of MG cells during retina regeneration (Lee et al., 2020). In addition, *TGFß* signaling was also shown to be required for (HSCs) emergence in zebrafish embryos (Monteiro et al., 2016). The potential role of *TGFß* signaling in the maintenance of RSC of the teleost retina remains to be established.

The discovery of *CD34*-like molecule (Ensembl ID: ENSORLG00000007619) marking the whole domain of CMZ was quite surprising. *CD34* has typically been considered a marker for HSCs (Sidney et al., 2014). However, in mammals, studies have shown that it is also present in other cell types, such as mesenchymal stromal cells, keratocytes, interstitial cells, and epithelial progenitors (Dupas et al., 2011; Hatou et al., 2013; Huss, 2000; Kuçi et al., 2010; Zheng et al., 2007). In many of these cases, the *CD34*-positive population is considered to be of stem or progenitor identity. Nevertheless, the knowledge of the function of this gene in neural stem cells is quite limited.

Notably, the expression of a number of genes from the identified RSC cluster could not be validated by chromogenic RNA *in situ* hybridization (Figure 3.4). While the regulatory element of *ccl25b* driving Cre expression was characterized as RSC-specific, based on the ability recombined cells to give rise to iArCoS in the medaka retina (Eggeler, 2017), multiple attempts of chromogenic *in situ* hybridization against its mRNA did not provide a discernible pattern in RSCs (Figure 3.3B). Only a more sensitive method of HCR RNA-FISH later confirmed the expression of ccl25b in RSCs. It is possible that the same problem might have occurred for other genes upregulated in the RSCs-containing cluster (Figure 3.4) where chromogenic RNA *in situ* hybridization failed to detect their expression. At the same time, mRNA of the majority of the genes, which were not detected in the CMZ, has been detected in the neighboring tissues, such as MG, lens epithelium, and cornea (Figure 3.4). Overall, these observations suggest that the RSC cluster might not contain exclusively RSCs. Before *in situ* cluster validation, this cluster was subclus-

tered with some of the chosen markers to be present only in one of the subclusters (data not shown). However, the performed *in situ* screen failed to indicate that RSCs were contained in either subcluster.

The data and newly discovered markers provide insight into the complex nature of the RSCs niche in medaka. Further investigation into the potential functions of these genes in establishing and maintaining RSCs is required. However, careful planning of experiments and potential outcomes of altered RSC function is necessary. Studying the ability of RSCs to produce ArCoS when specific genes are mutated could be insightful. Additionally, investigating the connection between RSC function and eye size is crucial. While it may be suggested that if RSCs are not established, then they cannot give rise to progenitors, and therefore lifelong growth cannot be supported, further investigation is necessary to confirm this. Previous studies have shown that activating (insulin-like growth factor (IGF) signaling in the postembryonic retina results in an increased number of RPCs but not RSCs, leading to increased eye size (Becker et al., 2021). Furthermore, the combination of injury and clonal analysis has indicated that external stimuli do not affect the preference for asymmetric division in RSCs (Centanin et al., 2014).

4.2 Mechanisms of RSCs specification

To gain insights into the mechanisms of RSCs specification, I followed the expression of RSC-specific marker over the course of retinal development. I performed a series of RNA in situ hybridizations against *cndp1* (Figure 3.8). The obtained results indicated that while absent in the optic vesicle stage, the *cndp1* mRNA appears at first in the differentiating RPE and later becomes more prominent in the RSCs in the most peripheral part of the retina (Figure 3.8). The gradual appearance of *cndp1* mRNA suggests that RSC specification in the retina is not fixed from early developmental stages but emerges in response to signaling cues. While arguing against Scenario I, in which the fate of RSCs is predetermined at the optic stage (Figure 1.3), such plasticity might reflect an adaptive strategy ensuring the specification of RSCs to establish and maintain robust growth of one of the most important sensory organs. These findings interestingly complement the specification of RSCs in the retina of another lower vertebrate, *Xenopus*, where the RSCs marker *Hes4* was found at the NR/ RPE border of the optic vesicle and with development moved to the retinal periphery (El Yakoubi et al., 2012). While on the one side, the *Xenopus* specification of RSCs may be considered as “predefinition”, more experiments, such as cell ablations, are necessary to make this point in both species. On the other

side, in the same paper, authors discuss the positive regulation of *Hes4* by canonical Wnt signaling (El Yakoubi et al., 2012). The presence and roles of canonical Wnt signaling in the retinal periphery are well-established in lower vertebrates as well as in mammals (Denayer et al., 2008; Kubo and Nakagawa, 2008; Kubo et al., 2003; Meyers et al., 2012; Van Raay and Vetter, 2004). At the same time, ligands of canonical Wnt signaling are known to be present in RPE and activation of canonical Wnt signaling to be crucial for RPE differentiation (Veien et al., 2008; Zilova et al., 2021). Consequently, it is possible that the initial presence of *cndp1* mRNA in the RPE of the developing optic cup is due to its upregulation by canonical Wnt signaling. While certain Wnt target genes, such as *axin2*, *lef1* or *myc* were shown to be expressed in the developing retinal periphery in medaka (Heilig, 2016), at stage 24 there are only two identified Wnt ligands, *wnt2ba*, has been located in the lens epithelium and *wnt2* in the RPE (data not shown). Further studies on the function of and the source of Wnt activation are required to draw conclusions on the Wnt signaling in the establishment of RSCs domain in medaka. Upon validation of the markers for RSCs and RPCs, I was then intrigued by whether newly identified makers of RSCs and *cndp1* are co-expressed by the same population of cells during early retinal development (Figure 3.9). While RNA *in situ* hybridizations against *sparc*, *col2a1a*, and *TGFß3-like* mRNA did not reveal a discernible pattern at stages 20-25 (data not shown), *aldh1a2* mRNA was evident in medaka retina at stage 24. In addition, I also performed RNA *in situ* hybridizations against *id1*, labeling both RSCs and RPCs in the mature retina, and hes6 *marking* exclusively RPCs. Interestingly, at stage 24 the *aldh1a2* mRNA labels the distal part of the optic cup, broader than *cndp1* domain at the same stage (Figures 3.8, 3.9). Later its expression becomes restricted to RSCs and early RPCs in the mature retina (Figure 3.6, 3.9). While members of *aldh* family have been reported to be present in the retinal periphery of the murine eye (Mccaffery et al., 1992; Sakai et al., 2004), in vitro studies in murine embryonic stem cells indicated that RA signaling inhibits canonical Wnt signaling while promoting non-canonical one (Osei-Sarfo and Gudas, 2014). This raises a question of how the RA and Wnt signaling pathways are crosstalking in the RSCs of medaka. Besides, my observations confirmed that *id1* mRNA predominantly labels embryonic RPCs at stage 24 and later targets undifferentiated cells. This aligns with the accepted view on *id1*, as the marker for undifferentiated, highly proliferative cells across various species and organs (Katagiri et al., 2002; Ling et al., 2014; Tzeng and Vellis, 1998; Yip et al., 2004). In turn, *hes6* mRNA was detected in the proximal domain of the optic cup at stage 24, later getting restricted in the progenitor zone of CMZ (Figure 3.9). In mouse and zebrafish, *hes6* (also known as

human epidermal growth factor receptor (her)13) has been recognized for promoting neural differentiation as well as involved in somitogenesis (Hu and Zou, 2022; Jhas et al., 2006; Kawamura et al., 2005; Pissarra et al., 2000; Schröter et al., 2012; Vasiliauskas and Stern, 2000). Besides, during somitogenesis, the expression pattern of this gene is known to be positively regulated by FGF signaling (Kawamura et al., 2005). Given that the blocking of FGF signaling has been found to hinder retinal differentiation in zebrafish (Martinez-Morales et al., 2005), the expression of *hes6* in the proximal layer of early medaka OC provides evidence supporting the role of FGF signaling in medaka retina as well. In addition, the inhibition of RA synthesis has been shown to result in expanded *hes6* expression during zebrafish somitogenesis (Kawamura et al., 2005) which explains the mutually exclusive expression patterns for *hes6* and *aldh1a2* (Figure 3.9). The growing evidence of the Wnt target genes being present in the distal region of medaka CMZ and *hes6* mRNA marking proximal RPCs domain of mature CMZ suggests a Wnt /FGF crosstalk involved in the establishment of this zone in development as well in the functioning of the mature CMZ. Recently, the concept that the interaction between FGF and Wnt signaling is essential for the formation of the ciliary marginal zone (CMZ) has also been explored in the context of the mammalian retina (Balasubramanian et al., 2021). While further for FGF and Wnt crosstalk in the fish retina is necessary, assuming such a conserved mechanism for CMZ establishment across vertebrates is possible.

4.3 RSCs are specified independently of eye morphogenesis

The intricate process of rim involution has been shown to contribute to optic cup morphogenesis in teleost fish (Heermann et al., 2015; Sidhaye and Norden, 2017; Sokolova, 2019). In the context of this phenomenon, cell tracking experiments conducted in zebrafish have suggested the emergence of a specific subset of retinal progenitor cells (RPCs) within the optic vesicle that subsequently contribute to the population of retinal stem cells (RSCs) (Heermann et al., 2015; Tang et al., 2017). An inherent limitation of these investigations has been the absence of distinct and exclusive marker for RSCs. While my original intention was to replicate these experiments utilizing the *cndp1* reporter line in medaka fish, this approach posed considerable challenges due to the elevated mortality rate observed in medaka embryos subjected to prolonged imaging sessions (data not shown).

Consequently, I opted to explore the hypothesis by assessing the presence of a RSC marker under conditions of perturbed eye morphogenesis (Figures 3.10-3.13). While the outcomes indicated the presence of *cndp1* mRNA in the peripheral retina of embryos treated with blebbistatin or in morphogenetic mutants (Figures 3.11, 3.13), it is essential to acknowledge certain constraints in the interpretation of these results.

The observation that blebbistatin treatment resulted in the absence of the ventral retina corroborates earlier observations in zebrafish studies (Moreno-Mármol et al., 2021; Nicolás-Pérez et al., 2016). However, in contrast to zebrafish, the slower developmental speed of medaka necessitated a longer drug exposure period which resulted in broad developmental aberrations as evidenced by high mortality (data now shown) and the presence of pyknotic nuclei (Figure 3.11). Thereby, it is crucial to further enhance the experimental protocol by optimizing various aspects, including the timing of the treatments and concentrations of blebbistatin. Besides, to establish a direct correlation between the observed phenotype and the disruption of myosin dynamic, an additional approach could involve visualizing the myosin distribution via live imaging of the developing optic cup using a corresponding reporter line.

The RNA in situ hybridization against *cndp1* in the retina of *el* or $Rx3^{saGFP+/+}$ mutant embryos as well suggested the independence of the RSCs specification from the proper eye morphogenesis (Figure 3.12-3.13). While *cndp1* expression marked the lateral brain wall dorsally from the lens, this expression might also be attributed to the RPE domain of *cndp1* expression in wild-type situation. Besides, both lines represent morphogenetic mutants, where the migration of individual retinal precursors from developing forebrain was reported to be blocked (Rembold et al., 2006), the process being prior to the rim involution. While the initial assumptions were that this process when interrupted would also lead to the interruption of rim involution, a more direct approach involving eye morphogenetic mutants where the optic cup morphogenesis is disrupted would be more beneficial.

Moreover, to further argue for RSCs specification independently of eye morphogenesis, relying solely on a single marker's expression is not sufficient. It would be beneficial to assess the functional potential of the *cndp1*-positive cells. One way to ascertain this would be to check if *cndp1*-positive cells are able to give rise to ArCoS. To this end, embryos of the *ccl25b::CreERT2; ubi::GaudíRSG* line could be exposed to blebbistatin, followed by recombination to see if the cells at the retinal periphery still produce multipotent cell lineages. Similarly, we could further assess their multipotent nature by crossing this line with the eye morphogenetic mutants.

Additionally, shifting to an in vitro environment could allow for the assessment of *cndp1*-positive cells' neurosphere formation capability. A comparative analysis of the transcriptomes of *cndp1*-positive cells in the wild-type and altered conditions would offer further insights.

While my results require further exploration, they find support in existing literature. The interplay between RSCs and disrupted morphogenesis has not been extensively addressed, but parallels can be drawn from studies on the origin of mammalian adult intestinal stem cells (Guiu et al., 2019). Guiu et al. (2019) used lineage-tracking, biophysical techniques, and transplantation to illustrate that all cells in the mouse fetal intestinal epithelium contribute to the adult intestinal stem cell pool, irrespective of their position and expression patterns during fetal development. Their data further reveals that the stem cell identity is an induced rather than predefined property. It is possible that a similar mechanism operates in the establishment of RSCs in medaka fish speaking in support of my Scenario II, which implements that the stem cell fate is not determined until after the eye morphogenesis is complete (Figure 1.3).

4.4 Marker gene expression and tissue morphology are altered in Rx3 knockdown embryos

Having verified the presence of the RSCs marker in the CMZ under disrupted eye morphogenesis conditions, I next explored how the retinal structure is altered in these phenotypes (Figure 3.14). For that, I used morphogenetic mutants $Rx3^{saGFP+/+}$ in combination with x-ray microtomography.

The histology-like information obtained from the x-ray microtomography helped reveal changes in the volumes of the retina, brain, and lens across phenotypes with different penetrance (Figure 3.14 C-C"). The retinal volume was reduced in the retina of the incomplete phenotype $Rx3^{saGFP+/+}$ mutant embryos and absent in the embryo with the complete phenotype (Figure 3.14 C). While such morphometric analysis has never been performed before on the retinal tissue, these findings align with previously reported phenotypes occurring upon loss of the *rx3*. As *rx3* controls the migration of RPCs from the developing forebrain, its loss results in localization of the RPCs within the neural tube (Rembold et al., 2006). Moreover, a recent study on retinal organoids further confirmed the individual migration of RPCs under the control of *rx3* to drive the optic vesicle formation *in vitro* (Zilova et al., 2021). This explains why, in the incomplete phenotype, when the migration was

not fully blocked, some RPCs were able to migrate laterally to shape a small optic vesicle, which then gave rise to an optic cup of a smaller volume (Figure 3.14 B, C). Interestingly, while the brain volumes of wild-types and embryos with complete phenotype lacking retina were comparable, the brain in the embryo with incomplete phenotype was smaller than the other two (Figure 3.14 C'). This suggests a presence of the mechanisms defining proper scaling between the retina and brain in embryonic development. Moreover, the concurrent decline in lens volume with the increasing severity of the phenotype offers evidence of the interplay between retina and lens surface ectoderm which gives rise to lens during embryogenesis.

Furthermore, the relative ratios of Otx2, HuC/D, and Rx2 provided additional insights into the differentiation process of retinal cells. In the brain, an increase in the relative ratio was observed for all three analyzed markers (Figure 3.14 D). Despite interrupted migration of RPCs in the $Rx3^{saGFP+/+}$ mutants, these cells were still able to obtain the retinal identity while located within the developing forebrain. This observation invites further speculation about the resilience and plasticity of embryonic cells. While Otx2 and HuC/D domains were larger in the retina of the embryos with incomplete phenotype when compared to the wild-type sibling, Rx2 expression drastically decreased (Figure 3.14 D'). It suggests that proper differentiation of retinal cell types is affected in the embryos with incomplete phenotype due to the initially altered architecture of the developing optic cup. In the incomplete phenotype retina, the compartments marked uniquely by Rx2 (CMZ and MG) may be less pronounced than in the wild-type sibling (as shown in Figure 3.14 D'). This could result in a relative increase in volume for the other two markers. To gain more insights, it would be useful to further investigate the CMZ in the embryos with incomplete phenotype by BrdU incorporation to test for the presence of proliferating cells.

4.5 Retinal peripheral cells acquire RSC identity upon eye morphogenesis

At the beginning of this work, pinpointing the exact nature of emerging adult RSCs in the medaka retina posed a challenge. However, a more defined description of emerging adult RSCs in the medaka retina was eventually established. Given that multipotency stands as a fundamental trait of all stem cells, it became evident that the emerging RSCs needed to generate multipotent ArCoS. Moreover, prior research indicated that cells at the distal rim of CMZ in lower vertebrates tend

to proliferate slowly, while the more proximal RPCs proliferate at a higher rate (Ohnuma et al., 2002; Perron et al., 1998; Wan et al., 2016). Thereby, I aimed to focus on these two characteristics and figure out the time when the cells at the retinal periphery become slow-proliferating and start giving rise to ArCoS. The proliferation assay revealed that the slowing down of the proliferation within *cndp1*-positive domain at the retinal periphery happens rather soon after optic cup has been formed and retinal differentiation has been initiated at stage 28 (Figure 3.15). The short-term clonal analysis corroborated this timeline. Further determination of the changes in the cell cycle length of this region in developmental timeline could enhance this finding. Potential methods for this include a dual-pulse S-phase-labeling technique using BrdU and EdU or deploying PCNA reporter (Becker et al., 2021; Klimova and Kozmik, 2014; Seleit et al., 2021). Although the proliferation rate difference between RSCs and RPCs is obvious, the nature for such difference remains very intriguing. While quiescence attributed to the adult neural stem cells in mammalian brain is suggested to be an actively maintained state (Cheung and Rando, 2013), investigating mechanisms that govern proliferation rates within the CMZ domain offers an exciting avenue. However, efforts to alter the cell cycle of RSCs by overexpressing mitogens, such as oncogene kras or IGF receptors, under cndp1 regulatory element did not lead to a larger eye size (Becker et al., 2021). This evidence hints at a complex regulatory system in place that ensures a consistent cell cycle length for RSCs.

Using long-term clonal analysis, I was able to determine when the retinal periphery cells initiate the formation of iArCoS (Figure 3.17). While some clones already started before stage 32, the peak of the clonal initiation within medaka embryonic development was detected at stage 40 (Figure 3.17 E). This indicated a gradual shift in the identity of the retinal periphery cells towards RSCs one. As it takes the retinal periphery cells 6 days (Iwamatsu, 2004) to acquire the identity of RSCs, it is rather unlikely that these cells contribute to the retinal growth in embryonic development. Additionally, the detection of clonal footprints suggests that the *ccl25b* domain comprises not only RSCs but also a few RPCs, which was confirmed by the presence of a few clones starting outside the cndp1-positive domain during the validation of the Cndp1 and Ccl25b expression correlation within RSCs (Figure 3.1). To obtain a more reliable confirmation of the clonal initiation timeline, one could repeat this experiment by changing the time for recombination. Although my evaluation revealed that the retinal periphery cells were marked by GFP before the BrdU incubation at stage 32 (data not shown), the speed of recombination may affect the distribution of iArCoS initiation.

Studies in mammalian brain have shown that a subset of progenitors that decelerated their cell cycle served as a pivotal source for the emerging adult NSCs (Furutachi et al., 2013, 2015). It is noteworthy that the deletion of the cyclin-dependent kinase inhibitor *p57* resulted in fewer slowly dividing progenitor cells, which consequently impaired the emergence of adult NSCs (Furutachi et al., 2015). In light of this evidence and my own findings, I propose that the slow cell cycle is a crucial prerequisite for the acquisition of RSCs identity by retinal peripheral cells. Overexpression of mitogens under the control of cndp1 regulatory element could potentially modify the deceleration rate of retinal periphery cells and, consequently, influence the onset of iArCoS. To identify other players essential for iArCoS initiation, I performed bulk and single-cell RNA sequencing at stages 24, 34-36, and 40 (Figures 3.19-3.21). For the bulk sequencing, the dissociated optic cups of *cndp1::mCherry-2A-oNTR*, *rx2::H2B-GFP* reporter line were subjected to FACS sorting. At stages 36 and 40, cell suspensions were sorted based on double fluorescence to enrich for the RSCs population co-expressing cndp1 and Rx2. However, RNA sequencing analysis revealed the presence of photoreceptor markers among the most DEGs (Figure 3.19 C). Upon closer examination of the reporter line, I confirmed the presence of mCherry in photoreceptor cells (Figure 3.19 D). Although the mCherry signal was not visible when imaging these retinas from the front view (Figure 3.18 B), this fluorescent signal led to the contamination of the targeted population, rendering the dataset unusable. If this pitfall had been avoided, the identified genes might have shed light on the molecular differences governing the changes in proliferation (stage 24 compared with stage 36) and driving the iArCoS initiation (stage 36 compared with stage 40). Thereby, I attempted another approach, aiming decipher these genes in the scRNA dataset (Figure 3.20). As I obtained the preliminary list of DEGs within the cluster, containing markers of RSCs, further validation is required to eventually specify the list of candidate genes.

Conclusion

In this thesis, I have focused on understanding the intricate processes involved in the emergence of retinal stem cells (RSCs) and the governing mechanisms in the medaka retina. I approached four goals to achieve this.

Firstly, I used scRNA sequencing to expand the markers associated with RSCs and RPCs. I elucidated their unique molecular identities and mapped their dynamic expression patterns throughout development. This work established a foundation for further investigations of the mechanisms controlling the CMZ.

Secondly, I examined the expression of retinal stem cell markers under conditions of disrupted eye morphogenesis. My data suggests that all retinal progenitors have the potential to acquire RSCs identity, and this process is independent of optic cup morphogenesis.

Thirdly, I investigated the changing behaviors of cells at the retinal periphery. Upon optic cup formation, the retinal periphery cells slow down their proliferation at 3 dpf. Later, they acquire the ability to produce ArCoS, with the peak of this activity at 10 dpf.

Finally, I performed scRNA sequencing across varied developmental stages to derive a preliminary list of candidate genes that might play a role in the emergence of RSCs. This list should be seen as an initial step, providing a foundation for further exploration into the molecular dynamics of RSC emergence and the associated pathways.

The further studies on the studies for RSCs emergence will be crucial for understanding the variations in growth modes across vertebrates.

5

Materials and Methods

5.1 Materials

5.1.1 Fish lines

Table 5.1. Fish lines used in this thesis.

Fish line	Internal stock number	Source
wildtype Cab	8617, 8813, 9698, 10052, 10346	Wittbrodt et al. (2002)
Heino mutant line	9238, 9842, 10317	Loosli et al. (2000)
el mutant line	9559, 9560, 10140	Winkler et al. (2000)
$Rx3^{saGFP}$ mutant line	9662, 9915	Zilova et al. (2021)
ccl25b::Cre^{ERT2}, $Gaudi^{RSG}$	9229, 9956, 10310, 10597	Lab stock
cndp1::mCherry-2A-oNTR; *ccl25b::Cre*^{ERT2}, $Gaudi^{RSG}$	9998	Lab stock
cndp1::mCherry-2A-oNTR, *rx2::H2B-GFP*; *Oca2* mutant	10057, 10448	Lab stock

5.1.2 cDNA templates from consolidated 20k library

The following clones were picked from the consolidated 20k library (Souren et al., 2009) and used as templates for antisense mRNA in situ probes.

Table 5.2. Gene Names/Ensemble IDs and Clone IDs

Gene name or Ensemble ID	Clone ID
sparc	cons_P02_D_05

Table 5.2. Gene Names/Ensemble IDs and Clone IDs

Gene name or Ensemble ID	**Clone ID**
TPM1	cons_P02_P_06
gadd45gb.1	cons_P08_H_02
pcolcea	cons_P10_K_21
serpinh1b	cons_P11_A_10
fgfr3	cons_P12_I_07
ENS9111	cons_P12_N_21
igf2b	cons_P13_I_24
tnn	cons_P14_I_15
ENSORLG00000024891	cons_P15_D_15
id3	cons_P16_M_18
ndnf	cons_P18_C_21
cnmd	cons_P19_F_04
dcn	cons_P20_O_14
pcdh18b	cons_P22_C_11
col2a1a	cons_P22_J_11
CKM.1	cons_P24_A_06
si:ch211-156l18.7	cons_P24_L_08
osr2	cons_P25_F_11
aldh1a2	cons_P28_O_176
nexn	cons_P30_N_21
pitx1	cons_P31_M_08
TGF-βi	cons_P36_F_18
ENSORLG00000007619	cons_P39_J_12
prrx1b	cons_P40_K_02
alx4b	cons_P45_O_18
id1	cons_P01_J_03
krt8	cons_P01_B_15
cndp1	cons_P36_G_16

5.1.3 Oligo pools

Oligo pools used as mRNA probes in the in situ HCR are summarized in Tables 5.3-5.9. They were ordered as oPools Oligo Pools from IDT.

Table 5.3. Oligo pool for *ccl25b* HCR RNA-FISH probe

Pool name	Sequence
B2_ccl25b	CCTCGTAAATCCTCATCAaaAAAATGAATCGTCCAGTTTTATCTT
B2_ccl25b	GTTATGCTTTGAGTAAAACACGTTTaaATCATCCAGTAAACCGCC
B2_ccl25b	CCTCGTAAATCCTCATCAaaTCCCGAAGAAAACTGAAGACGGTAA
B2_ccl25b	TCAAATCTAACCAAGACTTTTGTTTaaATCATCCAGTAAACCGCC
B2_ccl25b	CCTCGTAAATCCTCATCAaaAAACCCTGAACTGACCTGGACTGGA
B2_ccl25b	CTGCATGCTCATCATTTCCTCTGAAaaATCATCCAGTAAACCGCC
B2_ccl25b	CCTCGTAAATCCTCATCAaaAAATAAGCAGTTAAAGTGTTTATGA
B2_ccl25b	GGTCGTTTATGGGCTGTTAGTGATGaaATCATCCAGTAAACCGCC
B2_ccl25b	CCTCGTAAATCCTCATCAaaACACGTTTAGAAAGGCGGCATTGGC
B2_ccl25b	GACAGACTCTGCCAACTGAGGCAAAaaATCATCCAGTAAACCGCC
B2_ccl25b	CCTCGTAAATCCTCATCAaaAAACGTTGAAGGCACACATGCAGTT
B2_ccl25b	TATATCAGTTTCACTCCTCCAACACaaATCATCCAGTAAACCGCC
B2_ccl25b	CCTCGTAAATCCTCATCAaaGTCCCAGGAGGCCACTGTGCTCATT
B2_ccl25b	TCTTCAGAAATGCAACTCGATCACTaaATCATCCAGTAAACCGCC
B2_ccl25b	CCTCGTAAATCCTCATCAaaCTCCTCCAGCGTCAAAACTGTTGCA
B2_ccl25b	TACCCTGCACAGGCTTTCCCACACCaaATCATCCAGTAAACCGCC
B2_ccl25b	CCTCGTAAATCCTCATCAaaGGTGCCCTCCCCATGCCTCCTATCC
B2_ccl25b	TGCCTGCAGGGGCTCCTGTGGTTTTaaATCATCCAGTAAACCGCC
B2_ccl25b	CCTCGTAAATCCTCATCAaaCTGAAGGAAAAGCCTGCTGTTCTGT
B2_ccl25b	TCACATCCAGACTTTCACCACGCGTaaATCATCCAGTAAACCGCC
B2_ccl25b	CCTCGTAAATCCTCATCAaaTGCTGCTGATGATGATGGTCACACT
B2_ccl25b	GGTGTGAAACTTCATGGCTGCTGCTaaATCATCCAGTAAACCGCC
B2_ccl25b	CCTCGTAAATCCTCATCAaaGCAGGTGAAGAACAGAAGCAAGACG
B2_ccl25b	GGATCCTTGTGCCAAACTCAGATACaaATCATCCAGTAAACCGCC
B2_ccl25b	CCTCGTAAATCCTCATCAaaCACGTAGCCAAGGCAGCAGTTATCA
B2_ccl25b	GTTCCTCTTTCTTGGACCGAGTTCTaaATCATCCAGTAAACCGCC
B2_ccl25b	CCTCGTAAATCCTCATCAaaTTCCTGAATCCTGTAGCTCACAATG
B2_ccl25b	AGCTCTGATGTTGCAATCTCCATCTaaATCATCCAGTAAACCGCC
B2_ccl25b	CCTCGTAAATCCTCATCAaaCTGCTTTGCAAGTCCACGCCTCTTT
B2_ccl25b	GTCCTCTGGATTGGCGCAGACGGTCaaATCATCCAGTAAACCGCC

Table 5.4. Oligo pool for *rx2* HCR RNA-FISH probe

Pool name	Sequence
B1_rx2	GAGGAGGGCAGCAAACGGaaGAGGTTTATTAATTGGAATCCTTCC
B1_rx2	GAATGGTAGTAAAACCTGAGGGTTTtaGAAGAGTCTTCCTTTACG
B1_rx2	GAGGAGGGCAGCAAACGGaaCACAAGAGACACCAGAGCAGGCTGC
B1_rx2	TCCTCTGCCGACAAAACTCCTCTTAtaGAAGAGTCTTCCTTTACG
B1_rx2	GAGGAGGGCAGCAAACGGaaTCGTTGCAACCAGAACATGCAATGT
B1_rx2	GCTCCTTTCAAATAACTGAGCAAAAtaGAAGAGTCTTCCTTTACG
B1_rx2	GAGGAGGGCAGCAAACGGaaCTTGTTGCTCGCCGTGAAATCCTTA
B1_rx2	AACCAACTGCAGTGTCTACTCTGAAtaGAAGAGTCTTCCTTTACG
B1_rx2	GAGGAGGGCAGCAAACGGaaTCTACTCCTCACATCGTCCATAAGT
B1_rx2	TTTCTCTTCGTTCAGGTTTCTTGACtaGAAGAGTCTTCCTTTACG
B1_rx2	GAGGAGGGCAGCAAACGGaaAACAGAAGAGCAGACCTCAGCAGGG
B1_rx2	ATCAACAAATAGTTCTTGTGCCTCTtaGAAGAGTCTTCCTTTACG
B1_rx2	GAGGAGGGCAGCAAACGGaaAAAAGTCAAAGTCTACCAACTGAGA
B1_rx2	GGACTCACTTTCTGATTCTTGTCAAtaGAAGAGTCTTCCTTTACG
B1_rx2	GAGGAGGGCAGCAAACGGaaAATGCATTTGGCTGTGGACTTGCCT
B1_rx2	CCACCATCCCCAGGGTATCCATTGAtaGAAGAGTCTTCCTTTACG
B1_rx2	GAGGAGGGCAGCAAACGGaaTGTCAACGATTCCATGTCCGCTATC
B1_rx2	AGCCAGCGCCTTTCGCCATGTCATAtaGAAGAGTCTTCCTTTACG
B1_rx2	GAGGAGGGCAGCAAACGGaaATCTCCCACTGAATGCAGCAAGGGC
B1_rx2	GGCTCCGTTAACTTTGGGGCTGCCAtaGAAGAGTCTTCCTTTACG
B1_rx2	GAGGAGGGCAGCAAACGGaaGAAGGGACCGGCTTGGCGGGGTCCT
B1_rx2	AGTTCCGGAAGGTTTCCATAGGGTTtaGAAGAGTCTTCCTTTACG
B1_rx2	AGGAGGGCAGCAAACGGaaTAGGAATGATGCTGTGAGCTGTCCC
B1_rx2	TCACTCGAGAAAAGACTGGAGTCGTtaGAAGAGTCTTCCTTTACG
B1_rx2	GAGGAGGGCAGCAAACGGaaGTGAGATTGCTCATTTCTTCACACT
B1_rx2	GAGCCGTCAGCGATGTCCACTTCCTtaGAAGAGTCTTCCTTTACG
B1_rx2	GAGGAGGGCAGCAAACGGaaGGAGAGTCATGGAGCTTCATGGTAC
B1_rx2	ATCGGAGGACGATTGAAGGATAACAtaGAAGAGTCTTCCTTTACG
B1_rx2	GAGGAGGGCAGCAAACGGaaTTGGCCACCTGCCCCACACTAGGGG
B1_rx2	GTGAGCCAAGGATCCAGTGGCATCGtaGAAGAGTCTTCCTTTACG
B1_rx2	GAGGAGGGCAGCAAACGGaaATGGGTGTGGCACTGGAAATAGGTG
B1_rx2	GAGCTCATGAACCCCGGAATGGTGTtaGAAGAGTCTTCCTTTACG
B1_rx2	GAGGAGGGCAGCAAACGGaaGAGTAGGTGGGCTGCAGGGTCTGCG

Table 5.4. Oligo pool for *rx2* HCR RNA-FISH probe

Pool name	Sequence
B1_rx2	GGTGGGCTGTTGAGGAAGCTGTGGC

Table 5.5. Oligo pool for *cndp1* HCR RNA-FISH probe

Pool name	**Sequence**
B2_cndp1	CCTCGTAAATCCTCATCAaaCTAACCTTGTTAACCTCTTCTGGAA
B2_cndp1	TTTAATGTGGATAGTCAGATTGGGAaaATCATCCAGTAAACCGCC
B2_cndp1	CCTCGTAAATCCTCATCAaaCCCACACACCCAAACACATTCATTT
B2_cndp1	GTAGTATTAACCATGTACACGTCTAaaATCATCCAGTAAACCGCC
B2_cndp1	CCTCGTAAATCCTCATCAaaCATTTGAAGAGGCCACATCATCACG
B2_cndp1	ACTCCTCCTGAGGTGGATGTCCCTTaaATCATCCAGTAAACCGCC
B2_cndp1	CCTCGTAAATCCTCATCAaaAACCCAATTAGCAAAGCGCTTGTTA
B2_cndp1	TTCATCAGTGTTATCCGATCTCCAGaaATCATCCAGTAAACCGCC
B2_cndp1	CCTCGTAAATCCTCATCAaaAAGGAAAACGGCAGCATTCAAAAGC
B2_cndp1	CGAAGAATGTGGAGGTATGAAAGGTaaATCATCCAGTAAACCGCC
B2_cndp1	CCTCGTAAATCCTCATCAaaGAATAACACTAATCTGCCCAGCATG
B2_cndp1	GTACACTTTTCTTGCTGACATAATTaaATCATCCAGTAAACCGCC
B2_cndp1	CCTCGTAAATCCTCATCAaaCCCAGGGTCACATGACCAAAAGTTT
B2_cndp1	TTTTCTATGTCACGTGTCTACTTAAaaATCATCCAGTAAACCGCC
B2_cndp1	CCTCGTAAATCCTCATCAaaCTCAGCTGGGCACAAGATTTATAGC
B2_cndp1	CTTGTTGGGGTTGAGTGTGGTGATGaaATCATCCAGTAAACCGCC
B2_cndp1	CCTCGTAAATCCTCATCAaaGATTATCTCTGCTGTCTTACCTTTT
B2_cndp1	TTATCTGCAACATAAAACAAAATCCaaATCATCCAGTAAACCGCC
B2_cndp1	CCTCGTAAATCCTCATCAaaTTACAGAAAGACTCAATTGTCCTGG
B2_cndp1	TTGTTGTTTTAAAATGTGGCATACAaaATCATCCAGTAAACCGCC
B2_cndp1	CCTCGTAAATCCTCATCAaaACCACAGTAAGACTATGACAAAGTA
B2_cndp1	GGTCCTCATTGCAGATGCCAAAATCaaATCATCCAGTAAACCGCC
B2_cndp1	CCTCGTAAATCCTCATCAaaAAGCTCCGATGTTCATCTATGAAAA
B2_cndp1	TTGAAAGGACCAACAGGATTGAAAGaaATCATCCAGTAAACCGCC
B2_cndp1	CCTCGTAAATCCTCATCAaaGCTGGTTGTACTGGAAAGCATGGAC
B2_cndp1	CTTGATGCTCATCAACATACTGGGCaaATCATCCAGTAAACCGCC
B2_cndp1	CCTCGTAAATCCTCATCAaaAGTCCCTGAGAGCCTCCACATATTC
B2_cndp1	TGCTGGAGTCACTTTCAACTGCAACaaATCATCCAGTAAACCGCC

Table 5.5. Oligo pool for *cndp1* HCR RNA-FISH probe

Pool name	**Sequence**
B2_cndp1	CCTCGTAAATCCTCATCAaaGGTGAAGCTCAGGCCTTCGTAGAAC
B2_cndp1	GCTTCTGAGCCACCATCTCCATCATaaATCATCCAGTAAACCGCC
B2_cndp1	CCTCGTAAATCCTCATCAaaACTCTACAGCGCCTCCCATCTGTTG
B2_cndp1	GGAGCTCTTGGTCTCCAACGTCCACaaATCATCCAGTAAACCGCC
B2_cndp1	CCTCGTAAATCCTCATCAaaTAGGCAACGCCAGCGTCTGCCTGTC
B2_cndp1	CACTGCCAAAGCGAGCGGTCACCACaaATCATCCAGTAAACCGCC
B2_cndp1	CCTCGTAAATCCTCATCAaaAGACACACAGTGTGTGCTTATTGGG
B2_cndp1	TTGATTTCTGTCAGGTTACGTGACCaaATCATCCAGTAAACCGCC
B2_cndp1	CCTCGTAAATCCTCATCAaaGAGGCTCCCCGTCCGTAAAGATTTC
B2_cndp1	CAGGCTAAAACAGGAGCCTTGTTGTaaATCATCCAGTAAACCGCC
B2_cndp1	CCTCGTAAATCCTCATCAaaTTCTGGTAAGCCTCCACAGCGTGCA
B2_cndp1	ACATTTACTGGCAGCGCCATACTCAaaATCATCCAGTAAACCGCC
B2_cndp1	CCTCGTAAATCCTCATCAaaTCCTCCATGCCCTCGATGATAAACT
B2_cndp1	ATGGCCTCCAGCCCATTTGAGCCGGaaATCATCCAGTAAACCGCC
B2_cndp1	CCTCGTAAATCCTCATCAaaAAGAAAGTGTCTTTCTGGGCCAGGA
B2_cndp1	GAGACCACGATGTAGTCCACATCCGaaATCATCCAGTAAACCGCC
B2_cndp1	CCTCGTAAATCCTCATCAaaGGTCGTCTACTCAGCCAGCCACAGT
B2_cndp1	TTGCCTCTAGTCCCATATGTGATGGaaATCATCCAGTAAACCGCC
B2_cndp1	CCTCGTAAATCCTCATCAaaCCATGAACCTCTGCTAAGAAGTAGC
B2_cndp1	ACCCCAGAATGCAGGTCCTGTTTAGaaATCATCCAGTAAACCGCC
B2_cndp1	CCTCGTAAATCCTCATCAaaATAGGTTCAATCACAGTCCCTCCAT
B2_cndp1	GTGTCGAGAATGCCAATAAGGTCAGaaATCATCCAGTAAACCGCC
B2_cndp1	CCTCGTAAATCCTCATCAaaTCATCGTCAGAACTGGGGCTGATGA
B2_cndp1	AACTCTATGTCCTGGTACATCCTCCaaATCATCCAGTAAACCGCC
B2_cndp1	CCTCGTAAATCCTCATCAaaATCTTGTTCTTGTAGTCGTCCACAT
B2_cndp1	TTGCTGTACATGAGCTTGCTGACCCaaATCATCCAGTAAACCGCC
B2_cndp1	CCTCGTAAATCCTCATCAaaCATTTGTGGGCCAACAAGTCCACCT
B2_cndp1	CCGTGGATGGAGACGGTGGGGTAGCaaATCATCCAGTAAACCGCC
B2_cndp1	CCTCGTAAATCCTCATCAaaTAGTACCGGGGTCAGAGAAAGCCCC
B2_cndp1	CACAAACTTTGGAGGGGATGACGGTaaATCATCCAGTAAACCGCC
B2_cndp1	CCTCGTAAATCCTCATCAaaTGGGAACTTGTCTTATTGAGAACTT
B2_cndp1	TTTTCTCAACCACAGTGGGGTCCATaaATCATCCAGTAAACCGCC
B2_cndp1	CCTCGTAAATCCTCATCAaaACACTGAATGAAGGTGGTCTGACAC
B2_cndp1	AGGTATTGGGGCTTTGTCTTTTGGAaaATCATCCAGTAAACCGCC

Table 5.5. Oligo pool for *cndp1* HCR RNA-FISH probe

Pool name	**Sequence**
B2_cndp1	CCTCGTAAATCCTCATCAaaTGGCCCCAATCACCATCGAAACTTT
B2_cndp1	GATGATGAATGTCGGCCAGCCACGGaaATCATCCAGTAAACCGCC
B2_cndp1	CCTCGTAAATCCTCATCAaaTTTGATGGCTGCTTTTCCGGCCTCA
B2_cndp1	AAGATCAGGATCGACGCTGAAAACTaaATCATCCAGTAAACCGCC
B2_cndp1	CCTCGTAAATCCTCATCAaaAATAGGGATTGTCCCACCCTCACGG
B2_cndp1	CCCCGTCACATCCTGGAAAGTTCTGaaATCATCCAGTAAACCGCC
B2_cndp1	CCTCGTAAATCCTCATCAaaTCCAATGGGCATCATAATAATGCTT
B2_cndp1	CTGAGAGTGTAGTCCATCATCGAAGaaATCATCCAGTAAACCGCC
B2_cndp1	CCTCGTAAATCCTCATCAaaATAGTTGTACCTGCTCATTTTCTCA
B2_cndp1	GGCAATGAATAATTTGGTTCCCTCAaaATCATCCAGTAAACCGCC

Table 5.6. Oligo pool for *sparc* HCR RNA-FISH probe

Pool name	Sequence
B1_sparc	GAGGAGGGCAGCAAACGGaaCGCAGAGAAGTCAGGCGTGTGCGGG
B1_sparc	CATCTTCAAAGTCTTCAGCTTTGGCtaGAAGAGTCTTCCTTTACG
B1_sparc	GAGGAGGGCAGCAAACGGaaGCACAGGAGGAAGACGATCCACACC
B1_sparc	AGGAGCAGCCATGGCGTGGCCAGCCtaGAAGAGTCTTCCTTTACG
B1_sparc	GAGGAGGGCAGCAAACGGaaCTCTTCCAGCGCTGGCTCCTCTTCA
B1_sparc	CTCCTCAGCTGGTTCCTCTGTGACCtaGAAGAGTCTTCCTTTACG
B1_sparc	GAGGAGGGCAGCAAACGGaaCGACCTCCACCTGCACGGGGTTGGC
B1_sparc	CAACCTCAATGGCTTCGTCAAACTCtaGAAGAGTCTTCCTTTACG
B1_sparc	GAGGAGGGCAGCAAACGGaaGGCAGGGATTCTCAGCGGCATCCTC
B1_sparc	CTTTGCCCTTCTTGCAGCGGTGGTTtaGAAGAGTCTTCCTTTACG
B1_sparc	GAGGAGGGCAGCAAACGGaaGGGTGTTGGTGTCATCCACCTCACA
B1_sparc	TGGAGGGGTCCTGGCACACGCACATtaGAAGAGTCTTCCTTTACG
B1_sparc	GAGGAGGGCAGCAAACGGaaTGCCGCAGATGTGCTCAAACTCCCC
B1_sparc	AGGATGAGTCATAGGTCTTGTTGTCtaGAAGAGTCTTCCTTTACG
B1_sparc	GAGGAGGGCAGCAAACGGaaGGGCGCACTTGGTGGCGAAGAAGTG
B1_sparc	GCTTGTGGCCCTTCTTGGTTCCCTCtaGAAGAGTCTTCCTTTACG
B1_sparc	GAGGAGGGCAGCAAACGGaaTGCAGGAGCCGATGTAGTCGAGGTG
B1_sparc	CGTTGTCCAGGCAGGGCTCGATGAGtaGAAGAGTCTTCCTTTACG
B1_sparc	GAGGAGGGCAGCAAACGGaaTCATGCGCAGCGGGAACTCCGTCAG

Table 5.6. Oligo pool for *sparc* HCR RNA-FISH probe

Pool name	Sequence
B1_sparc	TCACCAGGACGTTCTTCAGCCAGTCtaGAAGAGTCTTCCTTTACG
B1_sparc	GAGGAGGGCAGCAAACGGaaTGTTGTCCTCGTCGCGCGCGTACAG
B1_sparc	TGAGCTTCTGCTTCTCGGTGAGCAGtaGAAGAGTCTTCCTTTACG
B1_sparc	GAGGAGGGCAGCAAACGGaaTCTCATTCTCGTAGATCTTCTTTAC
B1_sparc	AAGAGTGGTCGCCCGCCTCCAGGCGtaGAAGAGTCTTCCTTTACG
B1_sparc	GAGGAGGGCAGCAAACGGaaGCGGGAAATCCCGAGCCAACAGGTC
B1_sparc	AGCTCCGAGTGTGTCAGGTATCCGTtaGAAGAGTCTTCCTTTACG
B1_sparc	GAGGAGGGCAGCAAACGGaaGGGCGATGTACTTGGGGAATGAGGG
B1_sparc	TGCCAAAGCAGGCGGCCCACTCCTCtaGAAGAGTCTTCCTTTACG
B1_sparc	GAGGAGGGCAGCAAACGGaaGATCTTTGTCCACGTCCTGCTCTTT
B1_sparc	CGCTGGTCAGAGGAGTTTAGATGACtaGAAGAGTCTTCCTTTACG
B1_sparc	GAGGAGGGCAGCAAACGGaaGTAGCAACTAGTTGGTCCTCAAACT
B1_sparc	CTTAGGGATCAGCACCATTTCTGGTtaGAAGAGTCTTCCTTTACG
B1_sparc	GAGGAGGGCAGCAAACGGaaACAAAGAAAAGGATTTGCAATTAGC
B1_sparc	AAGCAAATATCATTATTAAAGAAAAtaGAAGAGTCTTCCTTTACG
B1_sparc	GAGGAGGGCAGCAAACGGaaTGCAGATTTCTCTTTTAGTGGTATA
B1_sparc	ACTGCTCATGATGGTTAGTACAGACtaGAAGAGTCTTCCTTTACG
B1_sparc	GAGGAGGGCAGCAAACGGaaGGTTTTCTTTACTGGGTCTTTAGTT
B1_sparc	TGGTCAGCGACTCAAATTTACATCCtaGAAGAGTCTTCCTTTACG
B1_sparc	GAGGAGGGCAGCAAACGGaaGAAACGCAGCATCAACAACAGAGAA
B1_sparc	AATGCGATGCGTTCAAAGGCCCTGAtaGAAGAGTCTTCCTTTACG

Table 5.7. Oligo pool for *col2a1a* HCR RNA-FISH probe

Pool name	Sequence
B1_col2a1a	GAGGAGGGCAGCAAACGGaaAGCAGTACAGTCCTGGATTCCAAAA
B1_col2a1a	AATAAACAAAGTTGGGTTGCTACAAtaGAAGAGTCTTCCTTTACG
B1_col2a1a	GAGGAGGGCAGCAAACGGaaTCATCCAGCTGACATCTCACAACGG
B1_col2a1a	ACACAGCTAAATTCATCTTCCAGGTtaGAAGAGTCTTCCTTTACG
B1_col2a1a	GAGGAGGGCAGCAAACGGaaAGGTCATTGTAACGCTGTCCATCTT
B1_col2a1a	GTACTCCAGGGCTTGTAGGCTCATCtaGAAGAGTCTTCCTTTACG
B1_col2a1a	GAGGAGGGCAGCAAACGGaaGCTCACCCTTCTGGCCCTTAATTCC
B1_col2a1a	CTCTCCTCTTGGCAGTAATGTCACCtaGAAGAGTCTTCCTTTACG

Table 5.7. Oligo pool for *col2a1a* HCR RNA-FISH probe

Pool name	Sequence
B1_col2a1a	GAGGAGGGCAGCAAACGGaaAGGTGGTCCTCTGGGTTTCTCTCCT
B1_col2a1a	CTGTGGGCCAGGTGATCCTGTGGGGtaGAAGAGTCTTCCTTTACG
B1_col2a1a	GAGGAGGGCAGCAAACGGaaTGGTTCTCCTGGGTTGCCTTGGAAA
B1_col2a1a	CATGGGGCCAGATTGTCCGGGTTCTtaGAAGAGTCTTCCTTTACG
B1_col2a1a	GAGGAGGGCAGCAAACGGaaTTTCCGGGTGGTCCAGGAGGGCCAC
B1_col2a1a	TTCCCAGCTTCACCGTCATCACCGGtaGAAGAGTCTTCCTTTACG
B1_col2a1a	GAGGAGGGCAGCAAACGGaaCAGGACGGCTCTCCTGATTTACCTG
B1_col2a1a	CCTGGTCTCCAGCTTGACCTGTGGAtaGAAGAGTCTTCCTTTACG
B1_col2a1a	GAGGAGGGCAGCAAACGGaaCAGCAGGCCCAGCAGGTCCAGTTGC
B1_col2a1a	CCACAGGTCCAGGTGGTCCTCTTTGtaGAAGAGTCTTCCTTTACG
B1_col2a1a	GAGGAGGGCAGCAAACGGaaCATTTGCGCCATCTCTACCAGAGGG
B1_col2a1a	GCTGGAGGGGTTGTGGTCCTGGTAGtaGAAGAGTCTTCCTTTACG
B1_col2a1a	GAGGAGGGCAGCAAACGGaaGCTTGACCACCAGTTCTTGCGAGGA
B1_col2a1a	AAACCAGACATGTTTGTTTCTGCTCtaGAAGAGTCTTCCTTTACG
B1_col2a1a	GAGGAGGGCAGCAAACGGaaGTGGAATCCTCCATTCATCGTCTCT
B1_col2a1a	TGCCAAGCTGTCATCGCCATAGTTGtaGAAGAGTCTTCCTTTACG

Table 5.8. Oligo pool for *aldh1a2* HCR RNA-FISH probe

Pool name	Sequence
B1_aldh1a2	GAGGAGGGCAGCAAACGGaaTACACAAATGTGCAGGCCGAACTGT
B1_aldh1a2	TTTTACATACTTATTCATAGTTTTAtaGAAGAGTCTTCCTTTACG
B1_aldh1a2	GAGGAGGGCAGCAAACGGaaCTTCTCCCCGACTCCAACAGTTGAG
B1_aldh1a2	ACCCACCTCACAGTCCCGGTACACTtaGAAGAGTCTTCCTTTACG
B1_aldh1a2	GAGGAGGGCAGCAAACGGaaGCTAGGGAGGAGGAACACATCCACC
B1_aldh1a2	TTACATAAAACGAGCCCAGCCGTGCtaGAAGAGTCTTCCTTTACG
B1_aldh1a2	GAGGAGGGCAGCAAACGGaaGTCCTTTTGAAAATTAAATTCGAGC
B1_aldh1a2	CCCTTTCATTGGGCAAAGCAAAGGGtaGAAGAGTCTTCCTTTACG
B1_aldh1a2	GAGGAGGGCAGCAAACGGaaGTTTATAGCCAGGTGTCGGTCGCCG
B1_aldh1a2	GATTCGGGCTTCTAGGTTCCTTCCTtaGAAGAGTCTTCCTTTACG
B1_aldh1a2	GAGGAGGGCAGCAAACGGaaGTCTCTAGGTTCCCTCGGCAGATTT
B1_aldh1a2	CTGCGCTGCTGTGCTTGCGTGCTGCtaGAAGAGTCTTCCTTTACG
B1_aldh1a2	GAGGAGGGCAGCAAACGGaaTCTTACTGGAAGTCATGACTGCCGT

Table 5.8. Oligo pool for *aldh1a2* HCR RNA-FISH probe

Pool name	Sequence
B1_aldh1a2	CGCTCTTCACCTCTCCGGGGATCTCtaGAAGAGTCTTCCTTTACG
B1_aldh1a2	GAGGAGGGCAGCAAACGGaaGGAGGGATGCCATGAGGGCAGCCGG
B1_aldh1a2	GGTTGGGTACCGGTGAGGGCATCAGtaGAAGAGTCTTCCTTTACG
B1_aldh1a2	GAGGAGGGCAGCAAACGGaaTGAAAATCTTTGTGTACTTGAGCTC
B1_aldh1a2	TCACAGAGACATGCCACTCATTGTTtaGAAGAGTCTTCCTTTACG
B1_aldh1a2	GAGGAGGGCAGCAAACGGaaGGTTGTAGACAGGGAAGACCTTCCC
B1_aldh1a2	CTTCACAGATCTGCTCTCCAGTTGCtaGAAGAGTCTTCCTTTACG
B1_aldh1a2	GAGGAGGGCAGCAAACGGaaCAACATCAGCCTTATCAGCCTCCTG
B1_aldh1a2	CCAGGCGAGCTGCCTGCACTGCTTTtaGAAGAGTCTTCCTTTACG
B1_aldh1a2	GAGGAGGGCAGCAAACGGaaTTCGCCAAACTGAGCCCAAAGAGAA
B1_aldh1a2	GTTTTCCTCTTTCAGAGGCATCCATtaGAAGAGTCTTCCTTTACG
B1_aldh1a2	GAGGAGGGCAGCAAACGGaaCCACCAGGTCAGCCAGTTTGGCCAG
B1_aldh1a2	TTGTTGCTAGGTAGACGCTGTCCCTtaGAAGAGTCTTCCTTTACG
B1_aldh1a2	GAGGAGGGCAGCAAACGGaaACGGTTTCCCGCTGTTCAGAGACTC
B1_aldh1a2	GGAGGTCAACAAACAGCGTTGGCAGtaGAAGAGTCTTCCTTTACG
B1_aldh1a2	GAGGAGGGCAGCAAACGGaaAGTATCTGAGAGTCTTTATAGTTCC
B1_aldh1a2	CATGGATTTTGTCTGCATATCCAGCtaGAAGAGTCTTCCTTTACG
B1_aldh1a2	GAGGAGGGCAGCAAACGGaaACTCTCCATCCATTGGAATAGAAGT
B1_aldh1a2	ACGCAGCCATCATCAGGAATGTCAGtaGAAGAGTCTTCCTTTACG
B1_aldh1a2	GAGGAGGGCAGCAAACGGaaCACATGCCAGTGCAGGGGCCAGCTT
B1_aldh1a2	CAGATGGTTTGAGGACCACAGTGTTtaGAAGAGTCTTCCTTTACG
B1_aldh1a2	GAGGAGGGCAGCAAACGGaaCATAGAGACAGGTGAGCGGCGTCTC
B1_aldh1a2	ACCCAGCCTCCTTCACGAGAGCTGCtaGAAGAGTCTTCCTTTACG
B1_aldh1a2	GAGGAGGGCAGCAAACGGaaGCAAAATATTGACAACTCCTGGTGG
B1_aldh1a2	CAGCTCCTGCTGTTGGCCCAAATCCtaGAAGAGTCTTCCTTTACG
B1_aldh1a2	GAGGAGGGCAGCAAACGGaaTATCGATGCCCATGTGCGAAGCAAT
B1_aldh1a2	CCTCAGTTGATCCTGTGAAAGCAACtaGAAGAGTCTTCCTTTACG
B1_aldh1a2	GAGGAGGGCAGCAAACGGaaCTGCCGCCTCTTGGATAAGCTTGCC
B1_aldh1a2	GCGTCACTCTCTTCAGGTTACTCCTtaGAAGAGTCTTCCTTTACG
B1_aldh1a2	GAGGAGGGCAGCAAACGGaaCATCTGCAAATATGATGTTGGGGTT
B1_aldh1a2	CCTGTTCCACTGCCAGATCCAAATCtaGAAGAGTCTTCCTTTACG
B1_aldh1a2	GAGGAGGGCAGCAAACGGaaCAGTGCAACACTGGCCCGCATTGAA
B1_aldh1a2	GCTCCTCCACATAGATGCGAGAGCCtaGAAGAGTCTTCCTTTACG
B1_aldh1a2	GAGGAGGGCAGCAAACGGaaTCCGGCGAACAAACTCATCATAAAT

Table 5.8. Oligo pool for *aldh1a2* HCR RNA-FISH probe

Pool name	Sequence
B1_aldh1a2	CTATCCTCCTCTTTGCTCGCTCCACtaGAAGAGTCTTCCTTTACG
B1_aldh1a2	GAGGAGGGCAGCAAACGGaaCAGTTGTGGGGTCAAAAGGACTGCC
B1_aldh1a2	GCTCCCGGCTGATCTGAGGACCCTGtaGAAGAGTCTTCCTTTACG
B1_aldh1a2	GAGGAGGGCAGCAAACGGaaGGATATATTCTAGCACACGATTCTG
B1_aldh1a2	GCTTGGCTCCTTCCTGGATTCCACTtaGAAGAGTCTTCCTTTACG
B1_aldh1a2	GAGGAGGGCAGCAAACGGaaAGCCCAGAGCTTTGCCTCCACACTC
B1_aldh1a2	CTGTGGGTTCAATGAAGAACCCTTTtaGAAGAGTCTTCCTTTACG
B1_aldh1a2	GAGGAGGGCAGCAAACGGaaCGCTTCTTCAACTCACGTCAGAGAA
B1_aldh1a2	GTAATCAGAGTTGTTGGCTCTTTCAtaGAAGAGTCTTCCTTTACG
B1_aldh1a2	GAGGAGGGCAGCAAACGGaaAGTGGTGAACACAGCAGCAGTCAAA
B1_aldh1a2	GGAGACGGTCATGGCTTTGTTGATGtaGAAGAGTCTTCCTTTACG
B1_aldh1a2	GAGGAGGGCAGCAAACGGaaCCAGACAGTGCCGGCCTGCATGGCT
B1_aldh1a2	TGTGCTGAGAGCATTGAAGCAGTTTtaGAAGAGTCTTCCTTTACG
B1_aldh1a2	GAGGAGGGCAGCAAACGGaaCATTTTGTATCCTCCAAAAGGACAC
B1_aldh1a2	TTCTCCTAATTCACGTCCATTCCCAtaGAAGAGTCTTCCTTTACG
B1_aldh1a2	GAGGAGGGCAGCAAACGGaaTATTTCTAAGTACTCCTTCAAGCCG
B1_aldh1a2	GGTGACTGTTTTCATGGTGATGGTCtaGAAGAGTCTTCCTTTACG
B1_aldh1a2	GAGGAGGGCAGCAAACGGaaAGAAATGTGCTGGCCTTAAGAGTTC
B1_aldh1a2	GGATGAGGAAGAGCGTCTTCTCCCAtaGAAGAGTCTTCCTTTACG
B1_aldh1a2	GAGGAGGGCAGCAAACGGaaGTAACTAATTCTGATGACTGCCGGG
B1_aldh1a2	AAGGTAGCTTGAACAGCTTGTTAAGtaGAAGAGTCTTCCTTTACG
B1_aldh1a2	GAGGAGGGCAGCAAACGGaaTGACAAGTTTAATGAAGAGTCTTGC
B1_aldh1a2	CGTACAGAAGTTGATATAGCTGAAAtaGAAGAGTCTTCCTTTACG
B1_aldh1a2	GAGGAGGGCAGCAAACGGaaTTTCTTCGATGTAGTTAACGGAGGG
B1_aldh1a2	GCGGTGTAGTGGTCAGACAGTTGTTtaGAAGAGTCTTCCTTTACG
B1_aldh1a2	GAGGAGGGCAGCAAACGGaaAGGGGATTGAGCGTGTGGGAGGGAA
B1_aldh1a2	TACCAAGAAAGGAGCTTATTTTAAGtaGAAGAGTCTTCCTTTACG
B1_aldh1a2	GAGGAGGGCAGCAAACGGaaGCAAACGTCCTCTCAGCACATGAGT
B1_aldh1a2	AAGGATTAGAGCACACACAGTACAAtaGAAGAGTCTTCCTTTACG
B1_aldh1a2	GAGGAGGGCAGCAAACGGaaTACCAAGGCAATGACACATGAGGTT
B1_aldh1a2	CTAAGGCGCAAATGCTTCCATAAGTtaGAAGAGTCTTCCTTTACG
B1_aldh1a2	GAGGAGGGCAGCAAACGGaaAAGGCTGAGGACGTCAGTGGTCTCA
B1_aldh1a2	GCATTAACGTTTCATCCATTACTGTtaGAAGAGTCTTCCTTTACG
B1_aldh1a2	GAGGAGGGCAGCAAACGGaaAAAATATAAACAAAGGCAATTACAA

Table 5.8. Oligo pool for *aldh1a2* HCR RNA-FISH probe

Pool name	Sequence
B1_aldh1a2	ATAGTACAGTGTTAGATCATACAAGtaGAAGAGTCTTCCTTTACG
B1_aldh1a2	GAGGAGGGCAGCAAACGGaaAGAGTTTAAATTCGGTCAATGGTTT
B1_aldh1a2	TTCAGCAGATGACAGTAACATGCTAtaGAAGAGTCTTCCTTTACG
B1_aldh1a2	GAGGAGGGCAGCAAACGGaaTAATGTTTAAAATAAATCTACTCCT
B1_aldh1a2	GATGGACATCAAAGAAAATCAGTTAtaGAAGAGTCTTCCTTTACG
B1_aldh1a2	GAGGAGGGCAGCAAACGGaaGCATATAATTGTATAAACTTAAACA
B1_aldh1a2	AAACTACAATCATTTTATCATTTTAtaGAAGAGTCTTCCTTTACG
B1_aldh1a2	GAGGAGGGCAGCAAACGGaaATTGTTATCCACACAAAAGATTACT
B1_aldh1a2	TTGCTCTAACAATGTAATGAACACTtaGAAGAGTCTTCCTTTACG
B1_aldh1a2	GAGGAGGGCAGCAAACGGaaAGAAAAGACAAGTGGACGGTGGAAT
B1_aldh1a2	AAGTGTTTGGTGGTGAAGAAAGGGAtaGAAGAGTCTTCCTTTACG
B1_aldh1a2	GAGGAGGGCAGCAAACGGaaTACTTTGTTCCGGTTTAGAAGGTCC
B1_aldh1a2	TTACTTACTAAATGTTGTGATTGGTtaGAAGAGTCTTCCTTTACG
B1_aldh1a2	GAGGAGGGCAGCAAACGGaaCCTGAAAAGTGCTACATAGATAAAA
B1_aldh1a2	TTTGTAAAACACTTTGATATTTTATtaGAAGAGTCTTCCTTTACG
B1_aldh1a2	GAGGAGGGCAGCAAACGGaaTTATCTGTCTGTGTCTTGAGGTCTG
B1_aldh1a2	GCTGGTCCTTCTCAGTATTGGATGTtaGAAGAGTCTTCCTTTACG
B1_aldh1a2	GAGGAGGGCAGCAAACGGaaTTTTAGTTGATTTAAATCTAATGGT
B1_aldh1a2	GGTTAAGACATTTGTATTCAGAAAAtaGAAGAGTCTTCCTTTACG
B1_aldh1a2	GAGGAGGGCAGCAAACGGaaGCTACATCAGATAAACTCTCAAATG
B1_aldh1a2	TTATCTTTGGAATTCCCTTCCTTTGtaGAAGAGTCTTCCTTTACG
B1_aldh1a2	GAGGAGGGCAGCAAACGGaaGGATCTCGCCTTTCAAACTGATGCT
B1_aldh1a2	AAAGTTCTTCAATTATCTCTCATAAtaGAAGAGTCTTCCTTTACG
B1_aldh1a2	GAGGAGGGCAGCAAACGGaaATTTGTTTTATTTCTTAAAAGAATA
B1_aldh1a2	AAAGCATTGAATCTTGAATTGGAAAtaGAAGAGTCTTCCTTTACG

Table 5.9. Oligo pool for *ENSORLG00000009111* HCR RNA-FISH probe

Pool name	Sequence
B1_ENS9111	GAGGAGGGCAGCAAACGGaaCCACTAAAGCTTTAGCCAAATGCAT
B1_ENS9111	AAGTGGCGCAGTGGAGGACGAGAAGtaGAAGAGTCTTCCTTTACG
B1_ENS9111	GAGGAGGGCAGCAAACGGaaTGGCGCAGGTCGAGAGGGATGAGCT
B1_ENS9111	TCCGTTTCACGTGGTCAATGTCCACtaGAAGAGTCTTCCTTTACG

Table 5.9. Oligo pool for *ENSORLG00000009111* HCR RNA-FISH probe

Pool name	Sequence
B1_ENS9111	GAGGAGGGCAGCAAACGGaaTTTGACCTCGTATTGCTTCAACCCT
B1_ENS9111	GGCTCGTTAGTCGGAGTTTGCTGAGtaGAAGAGTCTTCCTTTACG
B1_ENS9111	GAGGAGGGCAGCAAACGGaaTCTTGCTGGGTCCCTGGGAGTGCGG
B1_ENS9111	CGTACAGCGCCTGGACCTGATAGGGtaGAAGAGTCTTCCTTTACG
B1_ENS9111	GAGGAGGGCAGCAAACGGaaGTTTTCATTGTCAATGATGTCCCCG
B1_ENS9111	CCCTTTGAACTTTACCTCCAGAACCtaGAAGAGTCTTCCTTTACG
B1_ENS9111	GAGGAGGGCAGCAAACGGaaGCGGCTGGGCTCCTCGTCTCCATCC
B1_ENS9111	CTTCCTCTTTAGTTGATCGAGATCCtaGAAGAGTCTTCCTTTACG
B1_ENS9111	GAGGAGGGCAGCAAACGGaaGGGGATCATCATGAGGATGAGGTGA
B1_ENS9111	CGTGGTTTGAGCGTCCAGGCGATGCtaGAAGAGTCTTCCTTTACG
B1_ENS9111	GAGGAGGGCAGCAAACGGaaTAGTTGGCGTCCAGCGCTCGCTTGC
B1_ENS9111	CAGCTCTCCTCAGCGTTTGAGAAGCtaGAAGAGTCTTCCTTTACG
B1_ENS9111	GAGGAGGGCAGCAAACGGaaAAGTCGATGTGAAGGCGGCGAACGC
B1_ENS9111	ATCCACTTCCAGTCCAGATCCCGCCtaGAAGAGTCTTCCTTTACG
B1_ENS9111	GAGGAGGGCAGCAAACGGaaTTGGCATCGTAACCGCTGGGCTCGT
B1_ENS9111	AGATAGGGACACGGCCCGGAGCAATtaGAAGAGTCTTCCTTTACG
B1_ENS9111	GAGGAGGGCAGCAAACGGaaAATCCCGCCGTGGACGCCGCCTCCA
B1_ENS9111	GGGTTCCAGTGGCTTCTGTACCTCAtaGAAGAGTCTTCCTTTACG
B1_ENS9111	GAGGAGGGCAGCAAACGGaaTTTGCTGCAGTTCCACCACCAGTCC
B1_ENS9111	TCAGACTCCTTCAGGTCTCCTTCAGtaGAAGAGTCTTCCTTTACG
B1_ENS9111	GAGGAGGGCAGCAAACGGaaGAAAAGCTCTGCGTCTCTGGGTTCA
B1_ENS9111	ATGGAAGACAGAAAGAAAGCGTCTCtaGAAGAGTCTTCCTTTACG
B1_ENS9111	GAGGAGGGCAGCAAACGGaaGCTGCTGTACATTTAGAACTAACTG
B1_ENS9111	CAGTGAAGGAACCTGAAAGTGGTCAtaGAAGAGTCTTCCTTTACG
B1_ENS9111	GAGGAGGGCAGCAAACGGaaGAGCCACGACTCTTTCTTGATCGAG
B1_ENS9111	GGATGAAGCAGGTTCTCCGTTCTTTtaGAAGAGTCTTCCTTTACG
B1_ENS9111	GAGGAGGGCAGCAAACGGaaGAGGTTCTGATCTTAAATAAGTCCT
B1_ENS9111	CAATTTATTGATCCACTTTTCACAAtaGAAGAGTCTTCCTTTACG
B1_ENS9111	GAGGAGGGCAGCAAACGGaaGCTGGATGAAAGACTTTCAACAAAA
B1_ENS9111	ATCTTTCAGGGAGAAAGGTTCTGCTtaGAAGAGTCTTCCTTTACG
B1_ENS9111	GAGGAGGGCAGCAAACGGaaCAAAGCGGATTCATGACGGAGATCC
B1_ENS9111	GCTGCACGGCGTGGACCACCGTGACtaGAAGAGTCTTCCTTTACG
B1_ENS9111	GAGGAGGGCAGCAAACGGaaTCAACAGTGAAAGGCTTTGAGTAAC
B1_ENS9111	TGACAATTTTATTATGATGGAGCTTtaGAAGAGTCTTCCTTTACG

Table 5.9. Oligo pool for *ENSORLG00000009111* HCR RNA-FISH probe

Pool name	Sequence
B1_ENS9111	GAGGAGGGCAGCAAACGGaaATTCACATCATCCACAGCTTCTTTT
B1_ENS9111	GCTCCGCCCACACTTCTTTTCTCCCtaGAAGAGTCTTCCTTTACG
B1_ENS9111	GAGGAGGGCAGCAAACGGaaCATGGGTTGGATTAGGCTTTCGTTG
B1_ENS9111	CTTATCGTTACCCTTTTATTTCCCCtaGAAGAGTCTTCCTTTACG
B1_ENS9111	GAGGAGGGCAGCAAACGGaaACGCTTTTAAGTTTCTCCTTGGCAG
B1_ENS9111	CTCAGTTCCATCCGGTTTCAGGCATtaGAAGAGTCTTCCTTTACG
B1_ENS9111	GAGGAGGGCAGCAAACGGaaTAAGAAGATTTGTTGCTTTTCTGGT
B1_ENS9111	GGGCACATAAAGCTTTAATGTTATTtaGAAGAGTCTTCCTTTACG
B1_ENS9111	GAGGAGGGCAGCAAACGGaaTGAGGGCAGGGGTAAGTAGTGCCTT
B1_ENS9111	TCGGGTGGCAGGGGCAGAAAGGGAGtaGAAGAGTCTTCCTTTACG
B1_ENS9111	GAGGAGGGCAGCAAACGGaaGCTGGACGGATTAATATGACAGCAG
B1_ENS9111	CCAGTGAAGATTCAATCACTGGCTCtaGAAGAGTCTTCCTTTACG
B1_ENS9111	GAGGAGGGCAGCAAACGGaaTGTCAACTCCTCTTAGAAATTTGGA
B1_ENS9111	GCCATCTTGAATTTTACCCTCTAAAtaGAAGAGTCTTCCTTTACG
B1_ENS9111	GAGGAGGGCAGCAAACGGaaTCGGCAGATTGACCTCAGGAAGAGG
B1_ENS9111	GGTTTGCTTATTTGTGAAATCTGAAtaGAAGAGTCTTCCTTTACG
B1_ENS9111	GAGGAGGGCAGCAAACGGaaTTGAAAAGAGGAATTTCAGGAGCCC
B1_ENS9111	CTGCTGCCGGAGAATCCCATTGTCCtaGAAGAGTCTTCCTTTACG
B1_ENS9111	GAGGAGGGCAGCAAACGGaaCTCCTCCTACTGAAGGTGGTGTTCG
B1_ENS9111	GTGACGTAAAAGGGAGACATGATCTtaGAAGAGTCTTCCTTTACG
B1_ENS9111	GAGGAGGGCAGCAAACGGaaCATTAGGAAAGCAAAATATTTACAA
B1_ENS9111	GCAGGTTTCTGCTTTCAGGCGCCGGtaGAAGAGTCTTCCTTTACG
B1_ENS9111	GAGGAGGGCAGCAAACGGaaCCTGAAGGTTTCTCCACGTAAAACC
B1_ENS9111	GGAAAATGTTTCCGCAGATCCGCTTtaGAAGAGTCTTCCTTTACG
B1_ENS9111	GAGGAGGGCAGCAAACGGaaCAAACGGAAATCTAGCTTCAGTGAC
B1_ENS9111	TGCAGCTCCAGAGATTCAGGCAAAAtaGAAGAGTCTTCCTTTACG
B1_ENS9111	GAGGAGGGCAGCAAACGGaaAGGGTTTGAATTTATTACACAGTTA
B1_ENS9111	CCATTCAGGCCTGGAAAAGAGGTTGtaGAAGAGTCTTCCTTTACG
B1_ENS9111	GAGGAGGGCAGCAAACGGaaAATAACATGCTCTGGGAACGGACGG
B1_ENS9111	ACAGACCAAACAACGAGACATCTGTtaGAAGAGTCTTCCTTTACG

5.1.4 Oligonucleotides

Table 5.10. Oligonucleotides used in this work.

Name	Sequence 5'-3'
ISPCR oligo	AAGCAGTGGTATCAACGCAGAGT
Template Switching Oligos (TSO)	AAGCAGTGGTATCAACGCAGAGT ACATrGrG+G
oligo-dT30VN (100 µM)	AAGCAGTGGTATCAACGCAGAGT ACT30VN

5.1.5 Antibodies

Table 5.11. Primary antibodies used in this work.

Primary antibody	Species	Concentration	Supplier
anti-BrdU	rat	1:100	Abcam, Cat# ab6326
anti-eGFP	chicken	1:200	Life Technologies, Cat# A10262
anti-HuC/HuD	mouse	1:200	Life Technologies, Cat# A21271
anti-Otx2	goat	1:200	R&D systems, Cat# AF1979
anti-Rx2	rabbit	1:200	In-house, Reinhardt et al. (2015)

Table 5.12. Secondary antibodies used in this work.

Secondary antibody	Species	Concentration	Supplier
anti-rat DyLight 549	goat	1:500	Jackson, Cat# 112-505-143
anti-chicken Alexa Fluor 488	donkey	1:500	Jackson, Cat# 703-545-155
anti-mouse Alexa Fluor 647	donkey	1:500	Jackson, Cat# 715-605-151
anti-goat Alexa Fluor 488	chicken	1:500	Invitrogen, Cat# A21467
anti-rabbit Alexa Fluor 594	donkey	1:500	Thermo Fisher Scientific, Cat# A2

5.1.6 Antibiotics

Table 5.13. Antibiotics used in this work.

Antibiotic	Stock concentration	work.ing concentration	Supplier
Ampicillin	100 mg/ml	100 µg/ml	Roth

5.1.7 Kits

Table 5.14. Kits used in this work.

Kit	Company
Agilent TapeStation D1000 assay	Agilent Technologies
Direct-zol DNA/RNA Miniprep Kit	Zymo Research
innuPREP PCRpure	Analytik Jena
Click-iT EdU Alexa Fluor 647 Imaging Kit	Thermo Fisher Scientific
Nextera XT DNA Library Preparation Kit	Illumina
NextSeq 500 High Output Reagent Kit	Illumina

5.1.8 Enzymes

Table 5.15. Enzymes used in this work.

Enzyme	Supplier
Restriction enzymes and buffers	NEB/Thermo Fisher Scientific
Proteinase K powder (stock solution 20 mg/ml)	Roche
Turbo DNase (2U/µl)	Thermo Fisher Scientific
DNase I 1U/µl	Thermo Fisher Scientific

5.1.9 Chemicals

Table 5.16. Chemicals used in this work.

Chemical/Reagent	Supplier
2-isopropanol	Sigma-Aldrich
Acetone	Sigma-Aldrich
Agar	Roth
Agarose	Sigma-Aldrich
Agarose, low melting	Roth
Ampicillin	Roth
Antipyrin	Sigma-Aldrich
Bacto-Trypton	Gibco

Chemical/Reagent	**Supplier**
BCIP	Roche
(±)-Blebbistatin	Calbiochem
Borax anhydrous	Fluka
bovine serum albumin (BSA)	Sigma-Aldr
Bromphenol Blue	Sigma-Aldr
BrdU (5-Bromo-2-deoxyuridine)	Sigma-Aldr
Calcium chloride dihydrate ($CaCl_2 \cdot 2\ H_2O$)	AppliChem
DAPI (4',6-Diamidino-2-Phenyindole, Dilactate)	Sigma-Aldr
Digoxigenin-11-UTP	Roche
DMSO	Roth
Disodium hydrogen phosphate (Na_2HPO_4)	Sigma-Aldr
Disodium hydrogen phosphate dihydrate ($Na_2HPO_4 \cdot 2\ H_2O$)	Sigma-Aldr
dNTPs (10 mM)	Sigma-Aldr
Draq5	Thermo Fis
DTT (dithiothreitol) (100 mM)	Thermo Fis
EdU	Thermo Fis
Ethanol 70% (denatured)	Roth
Ethanol 96% (denatured)	Roth
Ethanol 96%	Sigma-Aldr
ethidium bromide (EtBr)	Roth
Ethylenediamine tetraacetic acid (EDTA)	AppliChem
Ficoll Type 400	Amersham
Formamide	Sigma-Aldr
Glacial acetic acid	Merck
Glucose	Sigma-Aldr
Glycerol	Merck
Glycine	Sigma-Aldr
Heparin	Gibco
HEPES (4-(2-hydroxyethyl)-1- piperazineethanesulfonic acid)	Roth
Hydrochloric acid (HCl)	Merck
Hydrogen peroxide (H_2O_2)	Sigma-Aldr
Lithium chloride (LiCl)	Sigma-Aldr
Magnesium chloride ($MgCl_2$)	AppliChem
Magnesium sulfate heptahydrate ($MgSO_4 \cdot 7\ H_2O$)	AppliChem
Methanol (MeOH)	Roth

Chemical/Reagent	**Supplier**
Methylene blue trihydrate	Sigma-Aldrich
Nail polish	Essence
Nicotinamide	Sigma-Aldrich
nitro blue tetrazolium chloride (NBT)	Roche
N,N,N ,N -Tetrakis-(2-hydroxypropyl)-ethylendiamin	Sigma-Aldrich
N-Butyldiethanolamin	Sigma-Aldrich
Orange G	Sigma-Aldrich
paraformaldehyde (PFA)	Sigma-Aldrich
PBS (-$CaCl_2$, -$MgCl_2$), pH 7.4	Gibco
Penicillin-Streptomycin (Pen/Strep)	Sigma-Aldrich
Ponceau S solution 0.2% in 3% TCA	Serva
Potassium acetate (CH_3CO_2K)	AppliChem
Potassium chloride (KCl)	AppliChem
Potassium dihydrogen phosphate (KH_2PO_4)	Merck
Potassium hydrogen phosphate (K_2HPO_4)	Merck
Potassium hydroxide (KOH)	Merck
Proteinase K	Roche
RNase-free water	Sigma-Aldrich
ribonucleoside triphosphate (rNTP)s (, cytidine triphosphate (CTP), CTP, CTP)	Roche
Sheep Serum (SS)	Sigma-Aldrich
Sodium chloride (NaCl)	Sigma-Aldrich
Sodium dodecyl sulfate (SDS), 20%	Roth
Sodium hydrogen carbonate ($NaHCO_3$)	Merck
Sodium hydroxide (NaOH)	AppliChem
Sucrose	Roth
4-OH tamoxifen (4-hydroxytamoxifen)	Sigma-Aldrich
Tricaine (MS-222)	Sigma-Aldrich
Tris base	Roth
Tris-hydrochloride (Tris-HCl)	Sigma-Aldrich
Triton X-100	Sigma-Aldrich
Tween20	Sigma-Aldrich
Yeast Extract	Roth
Urea	Sigma-Aldrich

5.1.10 Molecular materials

Table 5.17. Molecular materials used in this work.

Material	Supplier
Anti-Digoxigenin-AP Fab fragments	Roche
DNA Loading Dye	homemade
GeneRuler DNA Ladder Mix	Thermo Fisher Sc
Mach1T1 T1 phage resistant chemically competent Escherichia coli (E.coli)	Thermo Fisher Sc
RiboLock RNase Inhibitor	Thermo Fisher Sc
RNA from torula yeast Type VI	Sigma-Aldrich
RNA Loading Dye 2x Rapid	Thermo Fisher Sc

5.1.11 Consumables

Table 5.18. Consumables used in this work.

Consumable	Supplier
96-well cell culture plate, V-bottom	Corning
Scalpel blades	Roth
Cell saver tips, 200/1000 µl	Roth
Cover slips	Roth
Cryosection Superfrost Plus slides	Thermo Fisher Scientific
FACS glass round-botton tubes, 5 ml	Corning
Filter Tips 10 µl, 20 µl, 200 µl, 1.25 ml	Starlab
Glass beads	Roth
Glass-bottom dishes	MatTek
Glass petri dishes STERIPLAN 4 cm, 9 cm	Roth
Glass vials	Roth
Glassware	Duran
Immersion liquid, Type G	Leica
Latex gloves	Semperguard
Lens cleaning tissue	Cytiva
Low protein binding microcentrifuge tubes 1.5 ml and 2.0 ml	Thermo Fisher Scientific
Microtome blades C35	Feather
Molding cups	Polysciences

Consumable	Supplier
Needles BD Microlance, 0.3 mm x 13 mm	BD
Nitrile gloves	Starlab
Parafilm M	Bernis
Pasteur pipettes	Biosigma
PCR stripes	Sarstedt
PCR tubes	Kisker
Petri dishes	Greiner
Pipette tips	Kisker
Plastic pipettes 2 ml, 5 ml, 10 ml, 25 ml	Sarstedt
Sandpaper 1000 grit	Bauhaus
SafeSeal SurPhob low-binding tips 10 µl, 20 µl, 200 µl, 1250 µl	Biozym
Strainers 40 µm	pluriSelect
Syringes, 1 ml	BD Plastipak
Tough-tags for tubes	Sigma Aldrich
Tissue Freezing Medium	Jung, Leica Microsystems
Tubes 10 ml, 15 ml, 50 ml	Sarstedt
Well plates 6-well, 12-well, 24-well	Böttger, Roth

5.1.12 Equipment

Table 5.19. Equipment used in this work.

Equipment	Supplier
Bacterial Shaker INNOVA 44	New Brunswick
BD FACSAria III Cell sorter	BD Biosciences
Bioanalyzer 2100	Agilent Technologies
Camera Nikon DS-Ri1	Nikon
Centrifuges 5417C, 5425, 5430R, 5810R	Eppendorf
Centrifuge for PCR tubes	Steinbrenner Laborsysteme
Cold light source for stereomicroscope KL 1500 LCD	Schott
Cryostat CM 3050S	Leica
DeNovix DS-11+ spectrophotometer	DeNovix
DM5000B DIC	Leica
Electrophoresis chambers and combs for agarose gels	homemade and Peqlab

Equipment	**Supplier**
Fish incubator	Heraeus instruments and RuMed
Forceps 5, 55 Inox stainless steel	Dumont
Forceps 110 mm, straight	NeoLab
Freezer -20°C	Liebherr
Freezer -80°C	Thermo Fisher Scientific
Fridge 4°C	
Liebherr Incubators 32°C, 37°C, 60°C	Binder
Leica TCS SP8	Leica
LockMailer microscope slide jar	Simport
MacBook Pro (2,4 GHz 8-Core Intel Core i9, Intel UHD Graphics 630 1536 MB, 32 GB 2400 MHz DDR4)	Apple
Microwave	Sharp
Microplate centrifuge	Roth
Milli-Q water filtration station	Millipore Corporation
Mini-centrifuge	Sarstedt
MuVi SPIM light-sheet microscope	Bruker Corporation
NextSeq 550, 2000	Illumina
Nikon SMZ18 stereomicroscope	Nikon
Olympus SZX7	Olympus
PCR C100 Touch Thermal Cycler	Bio-Rad
pH-Meter	Sartorius
Pipetboy	Integra biosciences
Pipettes 20 µl, 1 ml	Gilson
Pipettes 2.5 µl, 10 µl, 200 µl	Eppendorf
Power supply Power-PAC Basic	Bio-Rad
Qubit	Thermo Fisher Scientific
Rocking shaker DRS-12	neoLab
Rotating Arm	homemade
Scale	Sartorius
TapeStation	Agilent Technologies
Thermomixer Compact	Eppendorf
ThermoMixer F1.5	Eppendorf
UV -Gel Documentation System INTAS iX20 SmartViewer Imager	Intas

Equipment	Supplier
UV transilluminator ECX-F20.L	Vilber Lourmat
Vortex Genie 2	Scientific Industries
Water bath	GFL mbH

5.1.13 Solutions for fish husbandry

Table 5.20. Solutions for fish husbandry used in this thesis.

Solution	Ingredients
1x embryonic rearing medium (ERM)	17 mM NaCl, 0.4 mM KCl, 0.27 mM CaCl2 · 2 H2O, 0.66 mM MgSO4 · 7 H2O, 17 mM HEPES pH 7.3; pH 7.1
Hatch medium	2 mg/L Methylene blue in 1x ERM
1x PBS	137 mM NaCl, 2.7 mM KCl, 1.44 g/L Na2HPO4, 240 mg/L mM KH2PO4; pH 7.4
20x tricaine	4 g/L tricaine, 10 g/L Na2HPO4 · H2O in 1x ERM, pH 7-7.5
Blebbistatin solution	(±)-Blebbistatin powder reconstituted in 90% DMSO to stock concentration of 75mg/ml and to 100 µm of final concentration with 1x ERM
16% PFA	160 g/L PFA, pH 7.0
4% PFA	25% (v/v) 16% PFA in 1x , pH 7-7.5
Dissociation buffer (bulk RNA sequencing)	2.5% trypsin:dispase, 1:1
Cell lysis buffer	(Ribolock:0.2% Triton X100, 1:20), Oligo-dT30VN (10 mM), and dNTPs (10 mM), 2:1:1
FACS buffer	0.1% BSA, 25 mM HEPES in PBS, pH 7.4
Dissociation buffer (scRNA sequencing)	2.5% trypsin : dispase : 1U/µl DNase I, 25 : 25 : 1
Wash buffer	For 5 ml: 32.5 µl of 45% glucose, 25 µl of 1M HEPES, 250 µl of FBS and 4.69 µl of PBS (Xu et al., 2020)

5.1.14 Solutions for fish husbandry

Table 5.21. Solutions for bacterial work. used in this thesis.

Solution	Ingredients
lysogeny broth (LB) medium	10 g/L Bacto-Tryptone, 5 g/L Yeast Extract, 5 g/L NaCl
LB plates	15 g/L Agar, boil in LB medium containing 10 g/L NaCl
TB Medium	12 g/L Bacto-Tryptone, 24 g/L Yeast Extract, 0.4% (v/v) Glycerol, 2.13 g/L KH2PO4, 12.54 g/L K2HPO4

5.1.15 Solutions for DNA and RNA work.

Table 5.22. Solutions for DNA and RNA work. used in this thesis.

Solution	Ingredients
EtBr bath	0.02% (v/v) EtBr
6x DNA loading dye	15% (w/v) Ficoll, 0.05% (w/v) Xylene cyanol, 0.05% (w/v) Bromphenol Blue, 0.2% (w/v) Orange G, 0.2% (w/v) Ponceau S
P1 buffer	50 mM glucose, 25 mM Tris-HCl, 10 mM EDTA, 100 µg/ml RNaseA; pH 8.0; stored at 4°C
P2 buffer	0.2 N NaOH, 1% (v/v) SDS
P3 buffer	5 M Potassium acetate; pH 5.5
2x RNA loading dye	0.25% (w/v) Xylene cyanol, 0.25% (w/v) Bromphenol Blue, 0.025% (v/v) SDS, 5 mM EDTA [pH 8.0], 95% (v/v) Formamide
50x Tris-acetate-EDTA-buffer (TAE)	2 M Tris-base, 1 M glacial acetic acid, 500 mM EDTA; pH 8.5

5.1.16 Solutions for immunohistochemistry

Table 5.23. Solutions for immunohistochemistry used in this thesis.

Solution	Ingredients
Bleaching solution	30% H2O2, 10% KOH, 1x

Solution	Ingredients
Borax phosphate buffered saline plus Tween 20 (PTW)	4 ml saturated Borax solution, 6 ml 1x PTW
2 mg/ml DAPI solution	2 mg/ml DAPI in DMSO
Whole mount antibody blocking solution	1% (v/v) BSA, 1% (v/v) DMSO, 4% (v/v) Sheep Serum
30% sucrose	30% (w/v) sucrose in 1x PTW
Tissue-clearing media	20% urea, 30% D-sorbitol, and 5% glycerol in DMSO

5.1.17 Solutions for chromogenic *in situ* hybridization

Table 5.24. Solutions for chromogenic *in situ* hybridization used in this thesis.

Solution	Ingredients
Hybridisation Mix	50% (v/v) Formamide, 5X SSC, 150 µg/ml Heparin, 5 mg/ml Ribonucleic acid from Torula yeast Typ VI, 0.1% (v/v) Tween20
Pre-staining buffer	0.1 M Tris-HCl (pH 7.5), 0.1 M NaCl, 0.1% (v/v) Tween 20
Staining buffer	0.1 M Tris-HCl (pH 9.5), 0.1 M NaCl, 50 mM MgCl2, 0.1% (v/v) Tween 20
20x SSC (saline sodium citrate)	3 M NaCl, 300 mM Tri-sodium citrate dihydrate; pH 7.0
4x SSCT	4x SSC, 0.1% (v/v) Tween 20
2x SSCT	2x SSC, 0.1% (v/v) Tween 20
0.2x SSCT	0.2x SSC, 0.1% (v/v) Tween 20

5.1.18 Solutions for CUBIC delipidation

Table 5.25. Solutions for CUBIC delipidation used in this thesis.

Solution	Ingredients
CUBIC-L	10% Triton X-100, 10% N-butyldiethanolamine, dH2O
CUBIC-R1a	10% Urea, 5% N,N,N',N'-tetrakis, 10% Triton X-100, 5M NaCl, dH2O

Solution	Ingredients
RI matching solution CUBIC-R+(N)	45% Antipyrine, 30% Nicotinamide, dH2O; pH 9.6–9.8, RI 1.522

5.1.19 Solutions for HCR RNA-FISH

Table 5.26. Solutions for HCR RNA-FISH used in this thesis.

Solution	Ingredients/Supplier
20x SSC (saline sodium citrate)	3 M NaCl, 300 mM Tri-sodium citrate dihydrate; pH 7.0
5x SSCT	5x SSC, 0.1% (v/v) Tween 20
Probe hybridization buffer	Molecular Instruments
Probe wash buffer	Molecular Instruments
Amplification buffer	Molecular Instruments

5.1.20 Software

Table 5.27. Software used in this thesis.

Software	License
Affinity Designer 2	Affinity
BD FACSDiva 9.0.1	BD Biosciences
DragonFly	Dragonfly 2020.2 for Windows. Object Research Systems (ORS) Inc, Montreal, Canada, 2020; software available at `http://www.theobjects.com/dragonfly`
Ensemble	(Martin et al., 2023)
Fiji distribution of ImageJ2	(Schindelin et al., 2012)
Geneious	Biomatters Limited
LAS X	Leica, Inc.
Mendeley desktop	Mendeley, Ltd
Microsoft Office	Microsoft
Overleaf	AGPLv3
R	(R Core Team, 2022)

Software	**License**
RStudio	RStudio, PBS

5.2 Methods

5.2.1 Fish husbandry

Medaka fish (*Oryzias latipes*) stocks were raised and maintained in closed stocks as described previously (Loosli et al., 2000). Fish were kept in constant recirculating systems at 28°C on a 14 h light/10 h dark cycle at the Centre for Organismal Studies of Heidelberg University. Fish husbandry and experiments were performed according to German animal welfare standards (Tierschutzgesetz §11, Abs. 1, Nr. 1) and European Union welfare guidelines (Bert et al., 2016). The following permits are provided:

- fish husbandry permit (number 35–9185.64/BH Wittbrodt)
- experiments permit (numbers 35-9185.81/G-271/20 Wittbrodt)
- terminal experimentation (numbers T-71/17)

5.2.2 BrdU incorporation

Dechorionated embryos or hatchlings were incubated in freshly prepared 2.5 mM BrdU dissolved in 1x ERM at 26 ° C in dark for respective amounts of times. Upon incubation embryos were washed 3 times with 1x ERM.

5.2.3 Cre/LoxP recombination

Prior to the recombination induction, embryos were rolled on the sandpaper. Recombination in *ccl25b::Cre*^{ERT2}, *Gaudi*^{RSG} was induced by incubation of embryos or hatchlings in 2.5 µM 4-OH tamoxifen in 1x ERM at 26 °C for 1 hour in the dark. Upon induction embryos were washed 3 times with 1x ERM.

5.2.4 Blebbistatin treatment of medaka embryos

Medaka embryos of st. 20 (Iwamatsu 2004) were dechorionated at 28 °C with a home-made hatching enzyme. After being rinsed in a 10 cm glass Petri dish with 1x ERM, they were transferred to a 3 cm glass Petri dish containing 100 µm solution of blebbistatin in 1x ERM. 90 % DMSO served as a vehicle control. The embryos were incubated in the dark at 26 °C until they reached st. 28. Then they were washed several times with 1x ERM and fixed in 4 % PFA/2x PTW at 4 °C overnight.

5.2.5 Probe design for HCR RNA-FISH

HCR probe sets for *ccl25b* (ENSORLG00000028881), *rx2* (ENSORLG00000018007), *cndp1* (ENSORLG00000003701), *sparc* (ENSORLG00000011369), *col2a1a* (ENSORLG00000012738), *aldh1a2* (ENSORLG00000008319), and a novel gene ENSORLG00000009111 were designed against unique mRNA sequences, based on the Japanese medaka HdrR ASM223467v1 transcriptome. Probes (50 pmol) were ordered as IDT Oligo pools and reconstituted in 50 µL of RNAse-free water.

5.2.6 Probe synthesis for chromogenic *in situ* hybridization

Clones of template cDNA plasmids were obtained from a consolidated 20k mRNA medaka library. The DNA was extracted according to the QIAprep Miniprep protocol. The templates were linearized at the 5′-end and purified with the innuPREP PCRpure kit. The transcription of antisense probes was set up according to Table 5.28.

Table 5.28. Transcription reaction for the synthesis of antisense RNA probes.

Component	Amount
Linearized template	1 µg
100 mM DTT	2 µl
rNTPs	1.3 µl
10 mM digoxigenin-labelled CTP	0.7 µl
Ribolock	0.5 µl
10x transcription buffer	2 µl
RNAse-free H2O	up to 20 µl
T7 RNA polymerase	2 µl

5.2.7 Sample preparation for immunohistochemistry

Fish were euthanized with 20x tricaine dissolved in 1x ERM. Afterwards, they were rinsed with 1x PTW and fixed in 4% PFA/1x PTW (for subsequent antibody staining) or 4%PFA/2x PTW (for subsequent in situ hybridization) for at least overnight at 4°C. For long-tERM storage, the embryos were manually dechorionated and dehydrated with increasing concentrations of MeOH (25%, 50%, 75%, 100%) in 1x PTW. Samples then were stored in 100% MeOH at -20°C. Prior to further processing, the samples were rehydrated in a reverse MeOH series (100%, 75%, 50%, 25%) in 1x PTW.

5.2.8 Preparation of cryosections

Medaka embryos were fixed in 4% PFA/2x PTW overnight at 4°C. Subsequently, they were washed with 1x PTW and transferred to 30% sucrose/1x PTW for overnight at 4°C and then cryoprotected in the 1:1 30% sucrose:1x PTW and tissue freezing medium (TFM). For the cryosectioning, embryos were placed in the plastic molds with their heads down. The molds were filled with TFM, frozen in liquid nitrogen, and afterwards transferred to the cryostat chamber for 10 minutes to equilibrate. The cryosections (16 μm) were performed using Leica Cryostat. After drying overnight at RT, they were rehydrated with PBS for 15 minutes and processed further.

5.2.9 Whole-mount immunohistochemistry

All washes were performed in the 6-well plates on the orbital shaker. Samples were washed in 1x PTW at least twice for 5 minutes. Adult retinae were enucleated using fine forceps by removing conjunctiva, sclera, and choroid. If pigmented, samples were bleached in the bleaching solution (0.5% KOH, 0.3% H_2O_2 in 1x PTW) while shaking in the dark on the orbital shaker in the 6-well plates. Once pigmentation was gone, the samples were washed in 1x PTW 3 times for 5 minutes and optionally postfixed in 4% PFA/1x PTW for at least 30 minutes and sequentially washed with 1x PTW 3 times for 5 minutes. Afterwards, samples were permeabilized in 100% pre-cooled acetone for 15 minutes at -20°C in 1.5ml reaction tubes and rinsed with 1x PTW 2 times for 10 minutes. Blocking was performed in 2ml reaction tubes in the blocking solution (1% bovine serum albumin, 4% sheep serum, 1% DMSO) for 2 hours at RT or overnight at 4°C on a rotator. Incubation with primary antibodies (dilution 1:200 in the blocking buffer) was performed in PCR tubes at 4°C at least overnight on a rotator. Afterward, the samples were washed 5 times for 30 minutes with 1x PTW. Incubation with secondary antibodies (dilution 1:250 in the blocking buffer) was performed in PCR tubes in the dark at 4°C at least overnight on a rotator. DAPI (1:500 dilution) was added to the secondary antibody solution to label nuclei. Upon overnight incubation, the samples were washed 3 times for 15 minutes with 1x PTW covered with aluminum foil. For imaging storage, the samples were equilibrated in tissue-clearing media. The samples were stored in the TCM at 4°C in a carton box.

5.2.10 Whole-mount HCR RNA-FISH

If stored in MeOH, embryos were rehydrated in a reverse MeOH series (100%, 75%, 50%, 25%) in 1x PTW. CUBIC-based clearing method was used to allow for better penetration ((**?**) and `http://www.cubic.riken.jp`). Medaka embryos were incubated in 50% CUBIC-L/R1a (mixed 1:1 and then diluted to 50% in dH_2O) for 30 minutes at room temperature while shaking and moved to a 100% CUBIC-L/R1a solution for another 30-minute incubation at room temperature on a shaker. Afterward, the embryos were washed 4 times for 20 minutes with 1x PBS.

HCR was performed according to the Molecular Instruments instructions. All buffers and hairpins were acquired from Molecular Instruments. Embryos were prehybridized with 1 ml of probe hybridization buffer for 30 minutes at 37°C rotating. In the meantime, the probe solution was prepared by mixing 4 pmol of each probe with 500 μl of the probe hybridization buffer and prewarmed to 37°C. Samples were then incubated in the probe solution at 37°C overnight (for 12-16 hours) shaking. The next day, samples were washed 4 times for 15 minutes with the probe wash buffer at 37°C shaking and then with 5x SSCT twice for 5 minutes at RT. If the protocol was combined with EdU immunohistochemistry, the EdU staining was performed at this point. Samples were equilibrated in 1 ml of amplification buffer for 5 minutes at RT. In the meantime, 30 pmol of hairpin h1 and hairpin h2 were separately snap-cooled by heating to 95°C in a PCR cycler and cooling to RT for 30 minutes in the dark. The amplification solution was prepared by adding all hairpins to 500 μl of the amplification buffer. The samples were incubated in the amplification solution overnight (12-16 hours) at RT in the dark. The next day the excess of hairpins was removed by washing the samples 2-3 times with 5x SSCT. Embryos were incubated with DAPI (1:500 in 5X SSCT) for 10 minutes at room temperature. For imaging, embryos were transferred to a MatTek glass-bottom dish and equilibrated in CUBIC refractive index matching solution CUBIC R+(N) until transparent.

5.2.11 HCR RNA-FISH on cryosections

All incubation steps were performed using Parafilm to cover the samples to avoid drying out. The samples were prehybridized with 200 µL of Hybridization buffer (Molecular Instruments) in a prewarmed to 37 °C humidified chamber. Probe solution was prepared as following: 0.8 pmol of each probe (0.8 µL of 1 µmol L^{-1} stock) was added to 100 µL of Hybridization buffer prewarmed to 37 °C. As the prehybridization buffer was removed from the samples, they were incubated with the

probe solution (100 µL per glass slide) overnight at 37 °C in the humidified chamber.

The next day the slides were washed with probe wash buffer (prewarmed to 37 °C). Then the excess probes were removed by washing slides in a reverse series of the probe wash buffer (75%, 50%, 25%) in 5x SSCT for 15 minutes at 37 °C. Afterward, the slides were incubated in 5x SSCT for 5 minutes at RT and dried with a paper towel.

For amplification, the slides were incubated with 200 µL of amplification buffer (prewarmed to RT) in a humidified chamber for 30 minutes at RT. Meanwhile the hairpin solution was prepared by heating 6 pmol of hairpin h1 and 6 pmol h2 (2 µL of 3 µmol stock) individually for 90 seconds at 95 °C in a PCR cycler and cooling to RT in dark for 30 minutes. The hairpin solution was prepared by adding the h1 hairpins and h2 hairpins to 100 µL (per slide) of the amplification buffer at RT.

The pre-amplification solution was removed and 100 µL of the hairpin solution was added on top of the sample. The samples were incubated in a dark humidified chamber for overnight at RT. The next day the samples were washed with 5x SSCT at RT for 3x 5 minutes. For nuclear staining DAPI (1:500 dilution in SSCT) was applied in one of the washes. For mounting, 60 µL of 60% glycerol in PBS was added on each slide, the coverslip was lowered and sealed with transparent nail polish. The slides were stored at 4 °C in the dark.

5.2.12 Whole-mount BrdU immunohistochemistry

As BrdU staining always followed the previously described protocol for whole-mount immunohistochemistry, all steps in this paragraph were performed in the dark (samples were covered with aluminum foil). All washes and incubations were performed in the 6-well plates on the orbital shaker unless stated otherwise. The samples were washed several times in 1x PTW and postfixed in 4% PFA/1x PTW for 1h at RT on a rotator in 1.5 ml reaction tubes. DNA denaturation was performed by incubating samples in 1.7N HCl solution for 45 minutes. After that, the samples were rinsed and washed 3 times for 5 minutes with 1x PTW. The pH was recovered by incubating samples in 40% Borax solution in 1x PTW for 10 minutes. After pH recovery, the samples were rinsed and washed twice for 5 minutes with 1x PTW. Consequentially, the samples were transferred into 1.5 ml reaction tubes.

5.2.13 Whole-mount EdU immunohistochemistry

EdU immunohistochemistry was combined with whole-mount in situ HCR and performed on the second day of HCR protocol before the amplification step (Ćorić et al., 2023). The EdU staining was conducted with a Click-iT EdU Alexa Fluor 647 kit according to the protocol. Samples were washed 3 times for 10 minutes with 1x PTW. 75 μl of the detection mix per tube was prepared according to Table 5.29.

Table 5.29. Recipe for EdU detection mix.

Substance	**Amount (μl)**
H2O	56.82
10x Reaction buffer	7.5
CuSO4	3
Alexa Fluor 647	0.18
10x Buffer additive	7.5

Samples were incubated with the detection mix for 2-3 hours at RT in the dark. Afterwards, they were washed 3 times for 10 minutes with 1x PTW and processed further along the HCR protocol.

5.2.14 Whole-mount chromogenic *in situ* hybridization

Washing and Treatment of Embryos

All washes were performed in the 6-well plates on the orbital shaker. If stored in 100% MeOH, embryos were transferred to 6-well plates and rehydrated in a reverse MeOH series (100%, 75%, 50%, 25%) in 1x PTW. To improve the permeabilization, proteinase K (pK) treatment was performed by incubating embryos in 10 μg/ml of pK diluted in 1x PTW for respective amounts of time:

[label=–]st. 20 – 7 minutes st. 21-24 – 9 minutes st. 25-27 – 12 minutes st.28 – 15 minutes st.32-34 – 75 minutes st.40 – 120 minutes

The treatment was performed at RT without shaking. Afterward, the embryos were rinsed twice with 2 mg/ml glycine in 1x PTW, incubated in 4% PFA/1x PTW for 20 minutes, and washed in 1x PTW 5 times for 5 min.

Hybridization

Embryos of varying stages were transferred to separate 2 ml tubes (10-15 embryos per tube), and equilibrated in 1 ml of prewarmed Hybridization mix at room tem-

perature for 5 minutes until they settled at the bottom of the tube. Afterwards, the samples were prehybridized in 2 ml of Hybridization mix in a water bath at 65 ° C for 2 h. 10 μl of mRNA in situ probes were denatured in 200 μl of Hybridization mix by incubation for 10 minutes at 80 ° C. In the meantime, the hybridization mix was removed from the tubes with embryos, and the probe-containing Hybridization mix was added directly after denaturation on top of the embryos. Hybridization was performed in a water bath at 65 ° C overnight.

Post-Hybridization

After hybridization, embryos were washed via sequential incubation in the reverse series of SSCT: 50% formamide/2x SSCT – 2 times 30 minutes, 2x SSCT – 2 times 15 minutes, 0.2% SSCT – 2 times 30 minutes. Prior to washing, solutions were prewarmed for 30 minutes at 65 ° C. Then, blocking was performed by incubating embryos in 5% sheep serum/1x PTW for 1 h, rotating in 1.5 ml tubes at RT. Anti-Digoxigenin-AP Fab fragments were diluted in the ratio 1:2000 in 1 ml of 5% sheep serum/1x PTW. Embryos were incubated in this solution overnight at 4 ° C. The next day, embryos were transferred to 6-well Petri dishes and washed 6x for 10 min in PTW. Prestaining and staining buffers were freshly prepared. Embryos were equilibrated 2x for 5 min in the prestaining buffer. 4.5 μl NBT and 3.5 μl per 1 ml of staining buffer was added to the staining buffer. Embryos were incubated in this solution in the dark until obtaining a specific staining pattern. Afterward, they were washed 3x for 5 min with PTW. Stained embryos were fixed in 4% PFA/1x PTW overnight at 4 ° C, rotating. Then, they were washed 3x for 5 min in PTW and processed for cryosectioning.

5.2.15 Imaging Methods

Cryosections and immunohistochemistry

Cryosections of chromogenic *in situ* hybridizations were imaged using a Leica DIC DM5000 B Microscope with 20x (dry) and 40x (dry) objectives. All immunohistochemistry and HCR signals were captured using an inverted confocal laser scanning microscope Leica TCS SP8 (ACS APO objective lenses: 10x/0.3 dry, 20x/0.75 multi-immersion, 63x/1.3 glycerol; laser lines: 405 nm, 488 nm, 532 nm, 638 nm) with matching laser and PMT settings. Whole-mount retinas were mounted in the MatTek dishes in tissue-clearing media. Flat-mount retinas were positioned between two 60x24 mm cover slides with 24x24 mm slides on the sides.

Light-sheet microscopy

The following paragraph is adapted from the manuscript (Kairiss et al., 2023).

- "3D fluorescent imaging of all specimens was performed on the 16× detection MuVi SPIM Multiview light-sheet microscope (Luxendo Light-sheet, Bruker Corporation). To assure that the specimens can be used for further imaging with X-rays, instead of mounting specimens with 2% low melting agarose, they were rested on the 2% agarose as shown in Figure 1- figure supplement 1. After solidification of the agarose, the tube was further filled with 1x PBS and samples were pipetted inside the tube. The tube was placed vertically such that the specimen fell onto the solid support of agarose.

  Two volumes at 0 and 90 rotation each, with 1.6 μm z step size for three channels, that is, GFP 488 nm excitation laser at 80% intensity, 525/50 nm emission filter, 200 ms exposure time, RFP 561 nm excitation laser at 30% intensity, 607/70 nm emission filter, 100 ms exposure time, and far-red 642 nm excitation laser at 50% intensity, 579/41 nm emission filter, 250 ms exposure time, were acquired. The four volumes for each channel were then combined together with the Luxendo Light-Sheet microscopy software."

5.2.16 Synchrotron X-ray microtomography

The following paragraph is adapted from the manuscript (Kairiss et al., 2023).

"To improve X-ray absorption of soft tissues, samples were dehydrated in ethanol series of 10%, 30%, 50% and 70% for 1 hour each and stained with 0.3% phosphotungstic acid in 70% ethanol, respectively, for one day at room temperature. After the staining procEdUre, the samples were washed in 70% ethanol and sealed in polypropylene containers for X-ray tomography. All specimens were scanned at the IPS UFO 1 tomographic station at the Imaging Cluster of the KIT Light Source. A parallel polychromatic X-ray beam produced by a 1.5 T bending magnet was spectrally filtered by 0.5 mm aluminum to remove low energy components from the beam. The resulting spectrum had a peak at about 17 keV, and a full-width at half maximum bandwidth of about 10 keV. X-ray projections were detected by a CMOS camera (pco.dimax, 2016×2016 pixels, $11 \times 11\,\mu m^2$ pixel size) coupled with an optical light microscope (OPtique Peter; total magnification 10×). Photons were converted to the visible light spectrum by a LSO:Tb scintillator of 13 µm.

A complete optical system resulted in an effective pixel size of 1.22 µm. For each specimen, a set of 3000 projections with 70 ms exposure time each were recorded over a 180° tomographic rotation axis. The 3D volumes were reconstructed using the filtered back projection algorithm implemented in tofu (Faragó et al., 2022)."

5.2.17 Bulk RNA sequencing of the UV -sorted populations

Retina dissociation

Dechorionated embryos were transferred to a 10 cm glass Petri dish filled with ice-cold PBS. The eyes of the embryos were dissected using syringe needles and transferred to a 1.5 ml Eppendorf tube using low-binding tips, and kept on ice. Around 30 eyes were dissociated for each stage. Once this amount was reached, the PBS in the tube was replaced by 200 μl dissociation buffer, prewarmed to 30 ° C. Dissociation took place on a heating block at 30 ° C and 300 rpm, with the samples being mixed every 2 minutes by pipetting. The progression of cell dissociation was checked under a binocular microscope and after 10-20 min the dissociation reaction was stopped by adding 50 μl 100% FBS. The mix was applied onto a 40 μm strainer and spun down at 180 g at 8 ° C for 3 min. The resulting pellet was then resuspended in 500 μl PBS, centrifuged once again, and eventually resuspended in 200 μl UV buffer. Prior to UV sorting the suspension was transferred into 5 ml flow cytometry tubes.

UV

Monika Langlotz of the FFCF at Heidelberg University conducted the UV . Cells were sorted on a BD FACSAria III using BD FACSDiva 9.0.1 software, with the sorting gates adjusted by the fluorescent signal of events. Cells were sorted into a 96-well V-bottom plate containing a solution composed of cell lysis buffer (Picelli et al., 2014). The plates were centrifuged at 180 g and 7 ° C for 3 min, sealed with parafilm, and stored at -80 ° C until the cDNA amplification and preparation of the sequencing libraries.

Library preparation and sequencing

Library preparation of the cell lysates prepared from the UV -sorted populations was conducted by David Ibberson at the Deep Sequencing Core Facility of Heidelberg University. cDNA amplification was performed according to the SmartSeq2 protocol (Picelli et al., 2014). The quality of the cDNA was assessed by Agilent 2100

Bioanalyzer. The libraries were prepared using Nextera XT DNA sample preparation kit. The libraries were sequenced on the Illumina NextSeq 500 Hight Output Reagent Kit v2.5 (75 cycles) in a single-end mode. The resulting data was analyzed by Miguel Ángel Delgado Toscano.

5.2.18 Single-cell RNA sequencing of the medaka retina

Retina dissociation

Dechorionated embryos were transferred to a 10 cm glass Petri dish filled with ice-cold PBS. The eyes of the embryos were dissected using syringe needles and transferred to a 1.5 ml low-binding Eppendorf tube with RNase-free low-binding tips, and kept on ice. 10, 2 and 2 right eyes of st. 24, 34, and 40 were dissected correspondingly. As the eyes were transferred into the tube, the PBS in the tube was replaced by 200 μl dissociation buffer. The tubes were transferred to the heating block prewarmed to 30 $^\circ$C and incubated there at 300 rpm for 10-30 minutes depending on the stage. The progression of cell dissociation was checked under the binocular microscope and stopped when the suspension reached single-cell state with 800 μl of wash buffer. The mixture was pipetted up and down, loaded on a 40 μm strainer and spun down at 180 g at 8 $^\circ$C for 3 min. Then it was resuspended in 500 μl of PBS and centrifuged again. The final pellet was then resuspended in 40 μl of PBS. 6 μl of the cell suspension was mixed with 6 μl of Trypan Blue, 10 μl of this mixture was loaded on the Neubauer chamber. The viability of the cells was estimated by calculating the ratio of alive cells per total amount of cells in 4 main squares. The number of cells in 1 ml was calculated using the following formula:

$$\text{number\_of\_cells\_in\_1ml} = \text{average\_number\_of\_cells\_per\_square} \times 10^4 \times 2$$

Then the suspension volume containing 12000 cells with more than 80% viability was submitted on ice to the Deep Sequencing Core Facility.

Library preparation and sequencing

Library preparation of single-cell suspension was conducted by David Ibberson and Bianka Berki at the Deep Sequencing Core Facility of Heidelberg University and according to the protocols by 10x Genomics. The quality of the cDNA was assessed by Agilent 2100 Bioanalyzer. The libraries were sequenced on Illumina NextSeq 550 (in case of samples of stages 24 and 34) and NextSeq 2000 (in case of stage 40 sample). The resulting data was processed by Sebastian Gornik, and clusters identified by Jørgen Benjaminsen and myself.

5.2.19 Image and data analysis

Raw images were processed with Fiji, distribution of ImageJ2 software (Schindelin et al., 2012). Registration of x-ray and light-sheet volumes was performed using Fijiyama plugin (Fernandez and Moisy, 2021). Segmentation and analysis of marker gene expression in chapter 2.2.3 were performed using Dragonfly software, Version 2020.2 for Windows. Object Research Systems (ORS) Inc, Montreal, Canada, 2020; software available at `http://www.theobjects.com/dragonfly`. Statistical analysis and graphical data visualization was performed in R (version 4.3.0) (R Core Team, 2022) using RStudio (RStudio Team, 2020). The following packages were used: dplyr (Wickham et al., 2023), ggpattern (FC et al., 2022), ggplot2 (Wickham, 2016), tidyr (Wickham et al., 2023), tidyverse (Wickham et al., 2019), patchwork (Pedersen, 2023), SCP (Zhang, 2023), heatmap3 (Shilin et al., 2021). Sample size (n) and statistical tests are provided in the respective figure or figure legend. All figures were composed in Affinity Designer 2 (version 2.0.4).

5.2.20 Thesis writing

The current thesis was written in Microsoft Word for Mac (version 16.54) and assembled in the online LaTeX editor Overleaf using the modified template by Jeongbin Park (`https://github.com/pjb7687/uni-heidelberg-phd-thesis-latex-template`)

Bibliography

Ahmad, I., Tang, L., and Pham, H. (2000). Identification of neural progenitors in the adult mammalian eye. *Biochemical and biophysical research communications*, 270(2):517–21.

Alcaide-Ruggiero, L., Molina-Hernández, V., Granados, M. M., and Domínguez, J. M. (2021). Main and minor types of collagens in the articular cartilage: The role of collagens in repair tissue evaluation in chondral defects. *International Journal of Molecular Sciences*, 22(24).

Ang, H. L. and Duester, G. (1999). Retinoic acid biosynthetic enzyme ALDH1 localizes in a subset of retinoid-dependent tissues during Xenopus development. *Developmental Dynamics*, 215(3):264–272.

Angileri, K. M. and Gross, J. M. (2020). dnmt1 function is required to maintain retinal stem cells within the ciliary marginal zone of the zebrafish eye. *Scientific Reports*, 10(1):11293.

Baden, T., Euler, T., and Berens, P. (2019). Understanding the retinal basis of vision across species. *Nature Reviews Neuroscience 2019 21:1*, 21(1):5–20.

Balasubramanian, R., Min, X., Quinn, P. M., Giudice, Q. L., Tao, C., Polanco, K., Makrides, N., Peregrin, J., Bouaziz, M., Mao, Y., Wang, Q., da Costa, B. L., Buenaventura, D., Wang, F., Ma, L., Tsang, S. H., Fabre, P. J., and Zhang, X. (2021). Phase transition specified by a binary code patterns the vertebrate eye cup. *Science Advances*, 7(46):9846.

Barker, N., Van Es, J. H., Kuipers, J., Kujala, P., Van Den Born, M., Cozijnsen, M., Haegebarth, A., Korving, J., Begthel, H., Peters, P. J., and Clevers, H. (2007). Identification of stem cells in small intestine and colon by marker gene Lgr5. 449(7165):1003–1007.

Becker, C., Lust, K., and Wittbrodt, J. (2021). Igf signaling couples retina growth with body growth by modulating progenitor cell division. *Development*, 148(7):dev.199133.

Bélanger, M.-C., Robert, B., and Cayouette, M. (2017). Msx1-Positive Progenitors

in the Retinal Ciliary Margin Give Rise to Both Neural and Non-neural Progenies in Mammals. *Developmental Cell*, 40(2):137–150.

Bernardos, R. L., Barthel, L. K., Meyers, J. R., and Raymond, P. A. (2007). Late-Stage Neuronal Progenitors in the Retina Are Radial Müller Glia That Function as Retinal Stem Cells. *Journal of Neuroscience*, 27(26):7028–7040.

Bert, B., Chmielewska, J., Bergmann, S., Busch, M., Driever, W., Finger-Baier, K., Hößler, J., Köhler, A., Leich, N., Misgeld, T., Nöldner, T., Reiher, A., Schartl, M., Seebach-Sproedt, A., Thumberger, T., Schönfelder, G., and Grune, B. (2016). Considerations for a European animal welfare standard to evaluate adverse phenotypes in teleost fish. *The EMBO Journal*, 35(11):1151–1154.

Bond, A. M., Ming, G. L., and Song, H. (2015). Adult Mammalian Neural Stem Cells and Neurogenesis: Five Decades Later. *Cell Stem Cell*, 17(4):385–395.

Bruckner, P. (2010). Suprastructures of extracellular matrices: paradigms of functions controlled by aggregates rather than molecules. *Cell and tissue research*, 339(1):7–18.

Bryan, C. D., Chien, C. B., and Kwan, K. M. (2016). Loss of laminin alpha 1 results in multiple structural defects and divergent effects on adhesion during vertebrate optic cup morphogenesis. *Developmental Biology*, 416(2):324–337.

Cardozo, M. J., Sánchezsánchez-Bustamante, E., and Bovolenta, P. (2023). Optic cup morphogenesis across species and related inborn human eye defects. *Development*, 150(2).

Casey, M. A., Lusk, S., and Kwan, K. M. (2021). Build me up optic cup: Intrinsic and extrinsic mechanisms of vertebrate eye morphogenesis. *Developmental Biology*, 476:128–136.

Centanin, L., Ander, J.-J., Hoeckendorf, B., Lust, K., Kellner, T., Kraemer, I., Urbany, C., Hasel, E., Harris, W. A., Simons, B. D., and Wittbrodt, J. (2014). Exclusive multipotency and preferential asymmetric divisions in post-embryonic neural stem cells of the fish retina. *Development (Cambridge, England)*, 141(18):3472–82.

Centanin, L., Hoeckendorf, B., and Wittbrodt, J. (2011). Fate restriction and multipotency in retinal stem cells. *Cell Stem Cell*, 9(6):553–562.

Centanin, L. and Wittbrodt, J. (2014). Retinal neurogenesis. *Development (Cambridge, England)*, 141(2):241–4.

Cepero Malo, M., Duchemin, A.-L., Guglielmi, L., Patzel, E., Sel, S., Auffarth, G. U., Carl, M., and Poggi, L. (2017). The Zebrafish Anillin-eGFP Reporter Marks Late Dividing Retinal Precursors and Stem Cells Entering Neuronal Lineages.

Cheung, T. H. and Rando, T. A. (2013). Molecular regulation of stem cell quiescence. *Nature reviews. Molecular cell biology*, 14(6):329–340.

Chow, R. L. and Lang, R. A. (2001). Early eye development in vertebrates. *Annu. Rev. Cell Dev. Biol*, 17(1):255–96.

Coles, B. L., Angénieux, B., Inoue, T., Del Rio-Tsonis, K., Spence, J. R., McInnes, R. R., Arsenijevic, Y., and Van Der Kooy, D. (2004). Facile isolation and the characterization of human retinal stem cells. *Proceedings of the National Academy of Sciences of the United States of America*, 101(44):15772–15777.

Ćorić, A., Stockinger, A. W., Schaffer, P., Roković, D., Tessmar-Raible, K., and Raible, F. (2023). A fast and versatile method for simultaneous HCR, immunohistochemistry and EdU labeling (SHInE). *Integrative and comparative biology*.

Corti, S., Locatelli, F., Papadimitriou, D., Donadoni, C., Salani, S., Del Bo, R., Strazzer, S., Bresolin, N., and Comi, G. P. (2006). Identification of a primitive brain-derived neural stem cell population based on aldehyde dehydrogenase activity. *Stem cells (Dayton, Ohio)*, 24(4):975–985.

Denayer, T., Locker, M., Borday, C., Deroo, T., Janssens, S., Hecht, A., van Roy, F., Perron, M., and Vleminckx, K. (2008). Canonical Wnt Signaling Controls Proliferation of Retinal Stem/Progenitor Cells in Postembryonic Xenopus Eyes . *Stem Cells*, 26(8):2063–2074.

Diacou, R., Nandigrami, P., Fiser, A., Liu, W., Ashery-Padan, R., and Cvekl, A. (2022). Cell fate decisions, transcription factors and signaling during early retinal development. *Progress in Retinal and Eye Research*, 91:101093.

Diamond, J. S. (2017). Inhibitory Interneurons in the Retina: Types, Circuitry, and Function. *Annual Review of Vision Science*, 3:1–24.

Dupas, T., Rouaud, T., Rouger, K., Lieubeau, B., Cario-Toumaniantz, C., Fontaine-Pérus, J., Gardahaut, M. F., and Auda-Boucher, G. (2011). Fetal muscle contains

different CD34+ cell subsets that distinctly differentiate into adipogenic, angiogenic and myogenic lineages. *Stem cell research*, 7(3):230–243.

Eggeler, F. (2017). Ccl25 chemokines and Ccr9 receptors in the retinal stem cell niche of medaka.

Eiraku, M., Adachi, T., and Sasai, Y. (2012). Relaxation-expansion model for self-driven retinal morphogenesis. *BioEssays*, 34(1):17–25.

Eiraku, M., Takata, N., Ishibashi, H., Kawada, M., Sakakura, E., Okuda, S., Sekiguchi, K., Adachi, T., and Sasai, Y. (2011). Self-organizing optic-cup morphogenesis in three-dimensional culture. *Nature*, 472(7341).

El Yakoubi, W., Borday, C., Hamdache, J., Parain, K., Tran, H. T., Vleminckx, K., Perron, M., and Locker, M. (2012). Hes4 controls proliferative properties of neural stem cells during retinal ontogenesis. *Stem cells (Dayton, Ohio)*, 30(12):2784–2795.

Faragó, T., Gasilov, S., Emslie, I., Zuber, M., Helfen, L., Vogelgesang, M., and Baumbach, T. (2022). Tofu: a fast, versatile and user-friendly image processing toolkit for computed tomography. *urn:issn:1600-5775*, 29(3):916–927.

FC, M., Davis, T. L., and ggplot2 authors (2022). ggpattern: 'ggplot2' Pattern Geoms.

Fernandez, R. and Moisy, C. (2021). Fijiyama: a registration tool for 3D multimodal time-lapse imaging. *Bioinformatics (Oxford, England)*, 37(10):1482–1484.

Fernández-Nogales, M., Murcia-Belmonte, V., Chen, H. Y., and Herrera, E. (2019). The peripheral eye: A neurogenic area with potential to treat retinal pathologies? *Progress in retinal and eye research*, 68:110.

Ferraro, F., Lo Celso, C., and Scadden, D. (2010). ADULT STEM CELLS AND THEIR NICHES. *Advances in experimental medicine and biology*, 695:155.

Fischer, A. J. and Reh, T. A. (2000). Identification of a proliferating marginal zone of retinal progenitors in postnatal chickens. *Developmental biology*, 220(2):197–210.

Frøen, R., Johnsen, E. O., Nicolaissen, B., Facskó, A., Petrovski, G., and Moe, M. C. (2013). Does the Adult Human Ciliary Body Epithelium Contain "True" Retinal Stem Cells? *BioMed Research International*, 2013.

Fuentealba, L. C., Rompani, S. B., Parraguez, J. I., Obernier, K., Romero, R., Cepko, C. L., and Alvarez-Buylla, A. (2015). Embryonic Origin of Postnatal Neural Stem Cells. *Cell*, 161(7):1644–1655.

Fuhrmann, S. (2010). Eye Morphogenesis and Patterning of the Optic Vesicle. *Current Topics in Developmental Biology*, 93:61–84.

Furutachi, S., Matsumoto, A., Nakayama, K. I., and Gotoh, Y. (2013). p57 controls adult neural stem cell quiescence and modulates the pace of lifelong neurogenesis. *The EMBO journal*, 32(7):970–981.

Furutachi, S., Miya, H., Watanabe, T., Kawai, H., Yamasaki, N., Harada, Y., Imayoshi, I., Nelson, M., Nakayama, K. I., Hirabayashi, Y., and Gotoh, Y. (2015). Slowly dividing neural progenitors are an embryonic origin of adult neural stem cells. *Nature Neuroscience 2015 18:5*, 18(5):657–665.

Giovannone, D., Paul, S., Schindler, S., Arata, C., Farmer, D. T., Patel, P., Smeeton, J., and Gage Crump, J. (2019). Programmed conversion of hypertrophic chondrocytes into osteoblasts and marrow adipocytes within zebrafish bones. *eLife*, 8.

Grandel, H., Kaslin, J., Ganz, J., Wenzel, I., and Brand, M. (2006). Neural stem cells and neurogenesis in the adult zebrafish brain: Origin, proliferation dynamics, migration and cell fate.

Guiu, J., Hannezo, E., Yui, S., Demharter, S., Ulyanchenko, S., Maimets, M., Jørgensen, A., Perlman, S., Lundvall, L., Mamsen, L. S., Larsen, A., Olesen, R. H., Andersen, C. Y., Thuesen, L. L., Hare, K. J., Pers, T. H., Khodosevich, K., Simons, B. D., and Jensen, K. B. (2019). Tracing the origin of adult intestinal stem cells. *Nature*, 570(7759):107–111.

Harris, W. A. and Hartenstein, V. (1991). Neuronal determination without cell division in xenopus embryos. *Neuron*, 6(4):499–515.

Hatou, S., Yoshida, S., Higa, K., Miyashita, H., Inagaki, E., Okano, H., Tsubota, K., and Shimmura, S. (2013). Functional corneal endothelium derived from corneal stroma stem cells of neural crest origin by retinoic acid and Wnt/β-catenin signaling. *Stem cells and development*, 22(5):828–839.

Heavner, W. E., Andoniadou, C. L., and Pevny, L. H. (2014). Establishment of the neurogenic boundary of the mouse retina requires cooperation of SOX2 and WNT signaling. *Neural Development*, 9(1).

Heermann, S., Schütz, L., Lemke, S., Krieglstein, K., and Wittbrodt, J. (2015). Eye morphogenesis driven by epithelial flow into the optic cup facilitated by modulation of bone morphogenetic protein. *eLife*, 4.

Heilig, A. K. (2016). *Localisation of Wnt signalling in the CMZ*. PhD thesis.

Hilgers, L. and Schwarzer, J. (2019). The untapped potential of medaka and its wild relatives. *eLife*, 8.

Hollyfield, J. G. (1971). Differential growth of the neural retina inXenopus laevis larvae. *Developmental Biology*, 24(2):264–286.

Hu, N. and Zou, L. (2022). Multiple functions of Hes genes in the proliferation and differentiation of neural stem cells. *Annals of Anatomy - Anatomischer Anzeiger*, 239:151848.

Huss, R. (2000). Isolation of primary and immortalized CD34-hematopoietic and mesenchymal stem cells from various sources. *Stem cells (Dayton, Ohio)*, 18(1):1–9.

Iwamatsu, T. (2004). Stages of normal development in the medaka Oryzias latipes. *Mechanisms of Development*, 121(7-8):605–618.

Jhas, S., Ciura, S., Belanger-Jasmin, S., Dong, Z., Llamosas, E., Theriault, F. M., Joachim, K., Tang, Y., Liu, L., Liu, J., and Stifani, S. (2006). Hes6 Inhibits Astrocyte Differentiation and Promotes Neurogenesis through Different Mechanisms. *The Journal of Neuroscience*, 26(43):11061.

Johns, P. R. and Easter, S. S. (1977). Growth of the adult goldfish eye. II. Increase in retinal cell number. *Journal of Comparative Neurology*, 176(3):331–341.

Kairiss, K., Sokolova, N., Lucie, Z., Schlagheck, C., Baumbach, T., Faragó, T., van de Kamp, T., Wittbrodt, J., and Weinhardt, V. (2023). Visualisation of gene expression within the context of tissues: an X-ray computed tomography-based multimodal approach. *in preparation*.

Kaslin, J., Ganz, J., Geffarth, M., Grandel, H., Hans, S., and Brand, M. (2009). Stem Cells in the Adult Zebrafish Cerebellum: Initiation and Maintenance of a Novel Stem Cell Niche. *Journal of Neuroscience*, 29(19):6142–6153.

Katagiri, T., Imada, M., Yanai, T., Suda, T., Takahashi, N., and Kamijo, R. (2002). Identification of a BMP-responsive element in Id1, the gene for inhibition of myogenesis. *Genes to Cells*, 7(9):949–960.

Kawamura, A., Koshida, S., Hijikata, H., Sakaguchi, T., Kondoh, H., and Takada, S. (2005). Zebrafish Hairy/Enhancer of split protein links FGF signaling to cyclic gene expression in the periodic segmentation of somites. *Genes and Development*, 19(10):1156–1161.

Kim, C. H., Ueshima, E., Muraoka, O., Tanaka, H., Yeo, S. Y., Huh, T. L., and Miki, N. (1996). Zebrafish elav/HuC homologue as a very early neuronal marker. *Neuroscience Letters*, 216(2):109–112.

Kirkland, S. C. (2009). Type I collagen inhibits differentiation and promotes a stem cell-like phenotype in human colorectal carcinoma cells. *British Journal of Cancer 2009 101:2*, 101(2):320–326.

Klimova, L. and Kozmik, Z. (2014). Stage-dependent requirement of neuroretinal Pax6 for lens and retina development. *Development*, 141(6):1292–1302.

Kovács, M., Tóth, J., Hetényi, C., Málnási-Csizmadia, A., and Seller, J. R. (2004). Mechanism of blebbistatin inhibition of myosin II. *The Journal of biological chemistry*, 279(34):35557–35563.

Kubo, F. and Nakagawa, S. (2008). Wnt signaling in retinal stem cells and regeneration. *Development Growth and Differentiation*, 50(4):245–251.

Kubo, F., Takeichi, M., and Nakagawa, S. (2003). Wnt2b controls retinal cell differentiation at the ciliary marginal zone. *Development*, 130(3):587–598.

Kubota, R., Hokoc, J. N., Moshiri, A., McGuire, C., and Reh, T. A. (2002). A comparative study of neurogenesis in the retinal ciliary marginal zone of homeothermic vertebrates. *Developmental Brain Research*, 134(1-2):31–41.

Kuçi, S., Kuçi, Z., Kreyenberg, H., Deak, E., Pütsch, K., Huenecke, S., Amara, C., Koller, S., Rettinger, E., Grez, M., Koehl, U., Latifi-Pupovci, H., Henschler, R., Tonn, T., von Laer, D., Klingebiel, T., and Bader, P. (2010). CD271 antigen defines a subset of multipotent stromal cells with immunosuppressive and lymphohematopoietic engraftment-promoting properties. *Haematologica*, 95(4):651.

Kuwahara, A., Ozone, C., Nakano, T., Saito, K., Eiraku, M., and Sasai, Y. (2015). Generation of a ciliary margin-like stem cell niche from self-organizing human retinal tissue. *Nature Communications*, 6(May 2014):1–15.

Kwan, K. M., Otsuna, H., Kidokoro, H., Carney, K. R., Saijoh, Y., and Chien, C.-B. (2012). A complex choreography of cell movements shapes the vertebrate eye. *Development*, 139(2):359–372.

Lee, J. Y. and Hong, S. H. (2020). Hematopoietic Stem Cells and Their Roles in Tissue Regeneration. *International Journal of Stem Cells*, 13(1):1.

Lee, M.-S., Wan, J., and Goldman, D. (2020). Tgfb3 collaborates with PP2A and notch signaling pathways to inhibit retina regeneration. *eLife*, 9: e55137.

Levi, B. P., Yilmaz, H., Duester, G., and Morrison, S. J. (2009). Aldehyde dehydrogenase 1a1 is dispensable for stem cell function in the mouse hematopoietic and nervous systems. 113:1670–1680.

Li, L. and Xie, T. (2005). STEM CELL NICHE: Structure and Function. *https://doi.org/10.1146/annurev.cellbio.21.012704.131525*, 21:605–631.

Li, Z., Joseph, N. M., and Easter, S. S. (2000). The Morphogenesis of the Zebrafish Eye, Including a Fate Map of the Optic Vesicle.

Lim, D. A. and Alvarez-Buylla, A. (2016). The Adult Ventricular–Subventricular Zone (V-SVZ) and Olfactory Bulb (OB) Neurogenesis. *Cold Spring Harbor Perspectives in Biology*, 8(5):18820–18821.

Lin, C. Y., Chiang, C. Y., and Tsai, H. J. (2016). Zebrafish and Medaka: new model organisms for modern biomedical research. *Journal of Biomedical Science 2016 23:1*, 23(1):1–11.

Ling, F., Kang, B., and Sun, X. H. (2014). Id proteins: small molecules, mighty regulators. *Current topics in developmental biology*, 110:189–216.

Liu, H., Xu, S., Wang, Y., Mazerolle, C., Thurig, S., Coles, B. L., Ren, J. C., Taketo, M. M., van der Kooy, D., and Wallace, V. A. (2007). Ciliary margin transdifferentiation from neural retina is controlled by canonical Wnt signaling. *Developmental Biology*, 308(1):54–67.

Liu, Y., Ho, C., Wen, D., Sun, J., Huang, L., Gao, Y., Li, Q., and Zhang, Y. (2022). Targeting the stem cell niche: role of collagen XVII in skin aging and wound repair. *Theranostics*, 12:15.

Livet, J., Weissman, T. A., Kang, H., Draft, R. W., Lu, J., Bennis, R. A., Sanes, J. R., and Lichtman, J. W. (2007). Transgenic strategies for combinatorial expression of fluorescent proteins in the nervous system. *Nature 2007 450:7166*, 450(7166):56–62.

Loosli, F., Köster, R. W., Carl, M., Kühnlein, R., Henrich, T., Mücke, M., Krone, A., and Wittbrodt, J. (2000). A genetic screen for mutations affecting embryonic

development in medaka fish (Oryzias latipes). *Mechanisms of Development*, 97(1-2):133–139.

Loosli, F., Winkler, S., Burgtorf, C., Wurmbach, E., Ansorge, W., Henrich, T., Grabher, C., Arendt, D., Carl, M., Krone, A., Grzebisz, E., and Wittbrodt, J. (2001). Medaka eyeless is the key factor linking retinal determination and eye growth. *Development*, 128(20):4035–4044.

Lust, K., Sinn, R., Pérez Saturnino, A., Centanin, L., and Wittbrodt, J. (2016). De novo neurogenesis by targeted expression of atoh7 to Müller glia cells. *Development*, 143(11):1874–1883.

Lust, K. and Wittbrodt, J. (2018). Activating the regenerative potential of Müller glia cells in a regeneration-deficient retina. *eLife*, 7.

Marcucci, F., Murcia-Belmonte, V., Wang, Q., Coca, Y., Ferreiro-Galve, S., Kuwajima, T., Khalid, S., Ross, M. E., Mason, C., and Herrera, E. (2016). The Ciliary Margin Zone of the Mammalian Retina Generates Retinal Ganglion Cells. *Cell Reports*, 17(12):3153–3164.

Marsh-Armstrong, N., Mccaffery, P., Gilbert, W., Dowling, J. E., and Draeger, U. C. (1994). Retinoic acid is necessary for development of the ventral retina in zebrafish. *Proceedings of the National Academy of Sciences of the United States of America*, 91(July):7286–7290.

Martin, F. J., Amode, M. R., Aneja, A., Austine-Orimoloye, O., Azov, A. G., Barnes, I., Becker, A., Bennett, R., Berry, A., Bhai, J., Bhurji, S. K., Bignell, A., Boddu, S., Branco Lins, P. R., Brooks, L., Ramaraju, S. B., Charkhchi, M., Cockburn, A., Da Rin Fiorretto, L., Davidson, C., Dodiya, K., Donaldson, S., El Houdaigui, B., El Naboulsi, T., Fatima, R., Giron, C. G., Genez, T., Ghattaoraya, G. S., Martinez, J. G., Guijarro, C., Hardy, M., Hollis, Z., Hourlier, T., Hunt, T., Kay, M., Kaykala, V., Le, T., Lemos, D., Marques-Coelho, D., Marugán, J. C., Merino, G. A., Mirabueno, L. P., Mushtaq, A., Hossain, S. N., Ogeh, D. N., Sakthivel, M. P., Parker, A., Perry, M., Piliota, I., Prosovetskaia, I., Perez-Silva, J. G., Salam, A. I. A., Saraiva-Agostinho, N., Schuilenburg, H., Sheppard, D., Sinha, S., Sipos, B., Stark, W., Steed, E., Sukumaran, R., Sumathipala, D., Suner, M. M., Surapaneni, L., Sutinen, K., Szpak, M., Tricomi, F. F., Urbina-Gómez, D., Veidenberg, A., Walsh, T. A., Walts, B., Wass, E., Willhoft, N., Allen, J., Alvarez-Jarreta, J., Chakiachvili, M., Flint, B., Giorgetti, S., Haggerty, L., Ilsley, G. R., Loveland, J. E., Moore, B., Mudge, J. M., Tate,

J., Thybert, D., Trevanion, S. J., Winterbottom, A., Frankish, A., Hunt, S. E., Ruffier, M., Cunningham, F., Dyer, S., Finn, R. D., Howe, K. L., Harrison, P. W., Yates, A. D., and Flicek, P. (2023). Ensembl 2023. *Nucleic Acids Research*, 51(D1):D933–D941.

Martinez-Morales, J. R., Cavodeassi, F., and Bovolenta, P. (2017). Coordinated Morphogenetic Mechanisms Shape the Vertebrate Eye. *Frontiers in Neuroscience*, 11(DEC).

Martinez-Morales, J. R., Del Bene, F., Nica, G., Hammerschmidt, M., Bovolenta, P., and Wittbrodt, J. (2005). Differentiation of the vertebrate retina is coordinated by an FGF signaling center. *Developmental Cell*, 8(4):565–574.

Martinez-Morales, J. R., Signore, M., Acampora, D., Simeone, A., and Bovolenta, P. (2001). Otx genes are required for tissue specification in the developing eye. *Development*, 128(11):2019–2030.

Martinez-Morales, J. R. and Wittbrodt, J. (2009). Shaping the vertebrate eye. *Current Opinion in Genetics & Development*, 19:1–7.

Mccaffery, P., Lee, M.-O., Wagner, M. A., Sladek, N. E., and Dräger, U. C. (1992). Asymmetrical retinoic acid synthesis in the dorsoventral axis of the retina. *Development*, 115(2):371–382.

Meyers, J. R., Hu, L., Moses, A., Kaboli, K., Papandrea, A., and Raymond, P. A. (2012). β-catenin/Wnt signaling controls progenitor fate in the developing and regenerating zebrafish retina. *Neural Development*, 7(1):1–18.

Mic, F. A., Molotkov, A., Fan, X., Cuenca, A. E., and Duester, G. (2000). RALDH3, a retinaldehyde dehydrogenase that generates retinoic acid, is expressed in the ventral retina, otic vesicle and olfactory pit during mouse development. *Mechanisms of Development*, 97(1-2):227–230.

Miles, A. and Tropepe, V. (2021). Retinal stem cell 'retirement plans': Growth, regulation and species adaptations in the retinal ciliary marginal zone. *International Journal of Molecular Sciences*, 22(12).

Milsom, M. D. and Essers, M. A. (2023). Recent advances in understanding the impact of infection and inflammation on hematopoietic stem and progenitor cells. Michael. *Cells and Development*.

Monteiro, R., Pinheiro, P., Joseph, N., Bonkhofer, F., Kirmizitas, A., and Correspondence, R. P. (2016). Transforming Growth Factor β Drives Hemogenic Endothelium Programming and the Transition to Hematopoietic Stem Cells. *Developmental Cell*, 38:358–370.

Moreb, J. (2008). Aldehyde dehydrogenase as a marker for stem cells. *Current stem cell research & therapy*, 3(4):237–246.

Moreno-Mármol, T., Ledesma-Terrón, M., Tabanera, N., Martin-Bermejo, M. J., Cardozo, M. J., Cavodeassi, F., and Bovolenta, P. (2021). Stretching of the retinal pigment epithelium contributes to zebrafish optic cup morphogenesis. *eLife*, 10.

Morris, V. B., Wylie, C. C., and Miles, V. J. (1976). The growth of the chick retina after hatching. *The Anatomical Record*, 184(1):111–113.

Moshiri, A. and Reh, T. A. (2004). Persistent Progenitors at the Retinal Margin of ptc+/- Mice. *The Journal of Neuroscience*, 24(1):229.

Motegi, H., Kamoshima, Y., Terasaka, S., Kobayashi, H., and Houkin, K. (2014). Type 1 collagen as a potential niche component for CD133-positive glioblastoma cells. *Neuropathology : official journal of the Japanese Society of Neuropathology*, 34(4):378–385.

Nicolás-Pérez, M., Kuchling, F., Letelier, J., Polvillo, R., Wittbrodt, J., and Martínez-Morales, J. R. (2016). Analysis of cellular behavior and cytoskeletal dynamics reveal a constriction mechanism driving optic cup morphogenesis. *eLife*, 5(OCTOBER2016).

Obermair, F. J., Fiorelli, R., Schroeter, A., Beyeler, S., Blatti, C., Zoerner, B., and Thallmair, M. (2010). A novel classification of quiescent and transit amplifying adult neural stem cells by surface and metabolic markers permits a defined simultaneous isolation. *Stem cell research*, 5(2):131–143.

Ohnuma, S. I., Hopper, S., Wang, K. C., Philpott, A., and Harris, W. A. (2002). Co-ordinating retinal histogenesis: early cell cycle exit enhances early cell fate determination in the Xenopus retina. *Development*, 129(10):2435–2446.

Ohnuma, S. I., Philpott, A., and Harris, W. A. (2001). Cell cycle and cell fate in the nervous system. *Current Opinion in Neurobiology*, 11(1):66–73.

Okuda, S., Takata, N., Hasegawa, Y., Kawada, M., Inoue, Y., Adachi, T., Sasai, Y., and Eiraku, M. (2018). Strain-triggered mechanical feedback in self-organizing optic-cup morphogenesis. *Science Advances*, 4(11).

Osei-Sarfo, K. and Gudas, L. J. (2014). Retinoic Acid Suppresses the Canonical Wnt Signaling Pathway in Embryonic Stem Cells and Activates the Noncanonical Wnt Signaling Pathway. *STEM CELLS*, 32:2061–2071.

Pardo-Saganta, A., Calvo, I. A., Saez, B., and Prosper, F. (2019). Role of the Extracellular Matrix in Stem Cell Maintenance. *Current Stem Cell Reports*, 5(1):1–10.

Pedersen, T. L. (2023). patchwork: The Composer of Plots.

Perron, M., Kanekar, S., Vetter, M., and Harris, W. (1998). The genetic sequence of retinal development in the ciliary margin of the Xenopus eye. *Developmental biology*, 199(2):185–200.

Peters, M. A. and Cepko, C. L. (2002). The dorsal-ventral axis of the neural retina is divided into multiple domains of restricted gene expression which exhibit features of lineage compartments. *Developmental Biology*, 251(1):59–73.

Pérez, A., Saturnino, P., Lust, K., and Wittbrodt, J. (2018). Notch signalling patterns retinal composition by regulating atoh7 during post-embryonic growth.

Picelli, S., Faridani, O. R., Björklund, . K., Winberg, G., Sagasser, S., and Sandberg, R. (2014). Full-length RNA-seq from single cells using Smart-seq2. *Nature Protocols*, 9(1):171–181.

Picker, A., Cavodeassi, F., Machate, A., Bernauer, S., Hans, S., Abe, G., Kawakami, K., Wilson, S. W., and Brand, M. (2009). Dynamic Coupling of Pattern Formation and Morphogenesis in the Developing Vertebrate Retina. *PLOS Biology*, 7(10):e1000214.

Pissarra, L., Henrique, D., and Duarte, A. (2000). Expression of hes6, a new member of the Hairy/Enhancer-of-split family, in mouse development. *Mechanisms of Development*, 95(1-2):275–278.

Post, Y. and Clevers, H. (2019). Defining Adult Stem Cell Function at Its Simplest: The Ability to Replace Lost Cells through Mitosis. *Cell stem cell*, 25(2):174–183.

Ptito, M., Bleau, M., and Bouskila, J. (2021). The Retina: A Window into the Brain. *Cells*, 10(12).

Pujic, Z., Omori, Y., Tsujikawa, M., Thisse, B., Thisse, C., and Malicki, J. (2006). Reverse genetic analysis of neurogenesis in the zebrafish retina. *Developmental Biology*, 293(2):330–347.

R Core Team (2022). R: A Language and Environment for Statistical Computing.

Ramamurthy, B., Yengo, C. M., Straight, A. F., Mitchison, T. J., and Sweeney, H. L. (2004). Kinetic mechanism of blebbistatin inhibition of nonmuscle myosin IIB. *Biochemistry*, 43(46):14832–14839.

Raymond, P. A., Barthel, L. K., Bernardos, R. L., and Perkowski, J. J. (2006). Molecular characterization of retinal stem cells and their niches in adult zebrafish. *BMC Developmental Biology*, 6(1).

Reh, T. A. (2002). Neural stem cells: form and function. *Nature neuroscience*, 5(5):392–394.

Reinhardt, R., Centanin, L., Tavhelidse, T., Inoue, D., Wittbrodt, B., Concordet, J., Martinez-Morales, J. R., and Wittbrodt, J. (2015). Sox2, Tlx, Gli3, and Her9 converge on Rx2 to define retinal stem cells in vivo. *The EMBO journal*, 34(11):1572–1588.

Rembold, M., Loosli, F., Adams, R. J., and Wittbrodt, J. (2006). Individual cell migration serves as the driving force for optic vesicle evagination. *Science (New York, N.Y.)*, 313(5790):1130–4.

Renn, J., Schaedel, M., Volff, J.-N., Goerlich, R., Schartl, M., and Winkler, C. (2006). Dynamic expression of sparc precedes formation of skeletal elements in the Medaka (Oryzias latipes).

Roselló-Díez, A. and Joyner, A. L. (2015). Regulation of Long Bone Growth in Vertebrates; It Is Time to Catch Up. *Endocrine Reviews*, 36(6):646–680.

Rotllant, J., Liu, D., Yan, Y. L., Postlethwait, J. H., Westerfield, M., and Du, S. J. (2008). Sparc (Osteonectin) functions in morphogenesis of the pharyngeal skeleton and inner ear. *Matrix Biology*, 27(6):561–572.

RStudio Team (2020). RStudio: Integrated Development Environment for R.

Sakai, Y., Luo, T., McCaffery, P., Hamada, H., and Dräger, U. C. (2004). CYP26A1 and CYP26C1 cooperate in degrading retinoic acid within the equatorial retina during later eye development. *Developmental biology*, 276(1):143–157.

Schindelin, J., Arganda-Carreras, I., Frise, E., Kaynig, V., Longair, M., Pietzsch, T., Preibisch, S., Rueden, C., Saalfeld, S., Schmid, B., Tinevez, J. Y., White, D. J., Hartenstein, V., Eliceiri, K., Tomancak, P., and Cardona, A. (2012). Fiji:

an open-source platform for biological-image analysis. *Nature Methods 2012 9:7*, 9(7):676–682.

Schröter, C., Ares, S., Morelli, L. G., Isakova, A., Hens, K., Soroldoni, D., Gajewski, M., Jülicher, F., Maerkl, S. J., Deplancke, B., and Oates, A. C. (2012). Topology and Dynamics of the Zebrafish Segmentation Clock Core Circuit. *PLOS Biology*, 10(7):e1001364.

Seleit, A., Aulehla, A., and Paix, A. (2021). Endogenous protein tagging in medaka using a simplified CRISPR/Cas9 knockin approach. *eLife*, 10.

Seleit, A., Krämer, I., Riebesehl, B. F., Ambrosio, E. M., Stolper, J. S., Lischik, C. Q., Dross, N., and Centanin, L. (2017). Neural stem cells induce the formation of their physical niche during organogenesis. *eLife*, 6.

Shilin, Z., Linlin, Y., Yan, G., Quanhu, S., and Yu, S. (2021). heatmap3: An Improved Heatmap Package.

Shima, A. and Mitani, H. (2004). Medaka as a research organism: past, present and future. *Mechanisms of Development*, 121(7-8):599–604.

Sidhaye, J. and Norden, C. (2017). Concerted action of neuroepithelial basal shrinkage and active epithelial migration ensures efficient optic cup morphogenesis. *eLife*, 6.

Sidney, L. E., Branch, M. J., Dunphy, S. E., Dua, H. S., Hopkinson, A., and E Dunphy, S. A. (2014). Concise Review: Evidence for CD34 as a Common Marker for Diverse Progenitors. *Stem cells (Dayton, Ohio)*, 32(6):1380–1389.

Sinn, R. and Wittbrodt, J. (2013). An eye on eye development. *Mechanisms of Development*, 130(6-8):347–358.

Soans, K. G., Ramos, A. P., Sidhaye, J., Krishna, A., Solomatina, A., Hoffmann, K. B., Schlüßler, R., Guck, J., Sbalzarini, I. F., Modes, C. D., and Norden, C. (2022). Collective cell migration during optic cup formation features changing cell-matrix interactions linked to matrix topology. *Current Biology*, 32(22):4817–4831.

Sokolova, N. (2019). Neuroepithelial flow and BMP signaling shape the optic cup in medaka.

Sokolova, N., Zilova, L., and Wittbrodt, J. (2023). Unravelling the link between embryogenesis and adult stem cell potential in the ciliary marginal zone: A comparative study between mammals and teleost fish. *Cells and Development*, 174.

Souren, M., Martinez-Morales, J. R., Makri, P., Wittbrodt, B., and Wittbrodt, J. (2009). A global survey identifies novel upstream components of the Ath5 neurogenic network. *Genome Biology*, 10(9):1–16.

Spence, J. R., Madhavan, M., Ewing, J. D., Jones, D. K., Lehman, B. M., and Del Rio-Tsonis, K. (2004). The hedgehog pathway is a modulator of retina regeneration. *Development*, 131(18):4607–4621.

Stolper, J., Ambrosio, E. M., Danciu, D.-P., Buono, L., Elliott, D. A., Naruse, K., Martínez-Morales, J. R., Marciniak-Czochra, A., and Centanin, L. (2019). Stem cell topography splits growth and homeostatic functions in the fish gill. *eLife*, 8.

Straight, A. F., Cheung, A., Limouze, J., Chen, I., Westwood, N. J., Sellers, J. R., and Mitchison, T. J. (2003). Dissecting temporal and spatial control of cytokinesis with a myosin II inhibitor. *Science*, 299(5613):1743–1747.

Straznicky, K. and Gaze, R. M. (1971). The growth of the retina in Xenopus laevis: an autoradiographic study. *Development*, 26(1):67–79.

Susaki, E. A., Tainaka, K., Perrin, D., Yukinaga, H., Kuno, A., and Ueda, H. R. (2015). Advanced CUBIC protocols for whole-brain and whole-body clearing and imaging. *Nature Protocols 2015 10:11*, 10(11):1709–1727.

Tainaka, K., Kubota, S. I., Suyama, T. Q., Susaki, E. A., Perrin, D., Ukai-Tadenuma, M., Ukai, H., and Ueda, H. R. (2014). Whole-body imaging with single-cell resolution by tissue decolorization. *Cell*, 159(4):911–924.

Tang, X., Gao, J., Jia, X., Zhao, W., Zhang, Y., Pan, W., and He, J. (2017). Bipotent progenitors as embryonic origin of retinal stem cells. *The Journal of Cell Biology*, 216(6):1833–1847.

Tomita, H., Tanaka, K., Tanaka, T., and Hara, A. (2016). Aldehyde dehydrogenase 1A1 in stem cells and cancer. *Oncotarget*, 7(10):11018.

Trimarchi, J. M., Cho, S. H., and Cepko, C. L. (2009). Identification of genes expressed preferentially in the developing peripheral margin of the optic cup. *Developmental dynamics : an official publication of the American Association of Anatomists*, 238(9):2327–2329.

Tropepe, V., Coles, B. L., Chiasson, B. J., Horsford, D. J., Elia, A. J., McInnes, R. R., and Van Der Kooy, D. D. (2000). Retinal stem cells in the adult mammalian eye. *Science (New York, N.Y.)*, 287(5460):2032–2036.

Tsingos, E., Höckendorf, B., Sütterlin, T., Kirchmaier, S., Grabe, N., Centanin, L., and Wittbrodt, J. (2019). Retinal stem cells modulate proliferative parameters to coordinate post-embryonic morphogenesis in the eye of fish. *eLife*, 8.

Tumbar, T., Guasch, G., Greco, V., Blanpain, C., Lowry, W. E., Rendl, M., and Fuchs, R. (2004). Defining the Epithelial Stem Cell Niche in Skin. *Science (New York, N.Y.)*, 303(5656):359.

Tworig, J. M. and Feller, M. B. (2022). Müller Glia in Retinal Development: From Specification to Circuit Integration. *Frontiers in Neural Circuits*, 15:815923.

Tzeng, S.-f. and Vellis, J. D. E. (1998). Id1, Id2, and Id3 Gene Expression in Neural Cells During Development. 381(October 1997):372–381.

Urbán, N., Blomfield, I. M., and Guillemot, F. (2019). Quiescence of Adult Mammalian Neural Stem Cells: A Highly Regulated Rest. *Neuron*, 104(5):834–848.

Van Raay, T. J. and Vetter, M. L. (2004). Wnt/frizzled signaling during vertebrate retinal development. *Developmental neuroscience*, 26(5-6):352–358.

Vasiliauskas, D. and Stern, C. D. (2000). Expression of mouse HES-6, a new member of the Hairy/Enhancer of split family of bHLH transcription factors. *Mechanisms of Development*, 98(1-2):133–137.

Veien, E. S., Rosenthal, J. S., Kruse-Bend, R. C., Chien, C. B., and Dorsky, R. I. (2008). Canonical Wnt signaling is required for the maintenance of dorsal retinal identity. *Development*, 135(24):4101–4111.

Wan, Y., Almeida, A. D., Rulands, S., Chalour, N., Muresan, L., Wu, Y., Simons, B. D., He, J., and Harris, W. A. (2016). The ciliary marginal zone of the zebrafish retina: Clonal and time-lapse analysis of a continuously growing tissue. *Development (Cambridge)*, 143(7):1099–1107.

Wetts, R., Serbedzija, G. N., and Fraser, S. E. (1989). Cell lineage analysis reveals multipotent precursors in the ciliary margin of the frog retina. *Developmental Biology*, 136(1):254–263.

Wickham, H. (2016). ggplot2: Elegant Graphics for Data Analysis. *Springer-Verlag New York*.

Wickham, H., Averick, M., Bryan, J., Chang, W., D', L., Mcgowan, A., François, R., Grolemund, G., Hayes, A., Henry, L., Hester, J., Kuhn, M., Lin Pedersen, T., Miller, E., Bache, S. M., Müller, K., Ooms, J., Robinson, D., Seidel, D. P., Spinu, V., Takahashi, K., Vaughan, D., Wilke, C., Woo, K., and Yutani, H. (2019). Welcome to the Tidyverse. *Journal of Open Source Software*, 4(43):1686.

Wickham, H., Vaughan, D., and Girlich, M. (2023). tidyr: Tidy Messy Data.

William, H. and Perron, M. (1998). Molecular recapitulation: The growth of the vertebrate retina Retinal determination in Xenopus View project. Technical report.

Winkler, S., Loosli, F., Henrich, T., Wakamatsu, Y., Wittbrodt, J., Henrich, T., Grabher, C., Arendt, D., Carl, M., Krone, A., Grzebisz, E., and Wittbrodt, J. (2000). The conditional medaka mutation eyeless uncouples patterning and morphogenesis of the eye. *Development (Cambridge, England)*, 127(9):1911–9.

Wittbrodt, J., Shima, A., and Schartl, M. (2002). Medaka — a model organism from the far east. *Nature Reviews Genetics*, 3(1):53–64.

Wong, L. L. and Rapaport, D. H. (2009). Defining retinal progenitor cell competence in Xenopus laevis by clonal analysis. *Development*, 136(10):1707–1715.

Wu, J. J., Weis, M. A., Kim, L. S., and Eyre, D. R. (2010). Type III Collagen, a Fibril Network Modifier in Articular Cartilage. *The Journal of Biological Chemistry*, 285(24):18537.

Xu, B., Tang, X., Jin, M., Zhang, H., Du, L., Yu, S., and He, J. (2020). Unifying developmental programs for embryonic and postembryonic neurogenesis in the zebrafish retina. *Development (Cambridge)*, 147(12).

Yip, H., Yeung, S., and Li, S. (2004). Expression of Id gene family in the retina during development. *Investigative Ophthalmology & Visual Science*, 45(13):5331–5331.

Yuzwa, S. A., Borrett, M. J., Innes, B. T., Voronova, A., Ketela, T., Kaplan, D. R., Bader, G. D., and Miller, F. D. (2017). Developmental Emergence of Adult Neural Stem Cells as Revealed by Single-Cell Transcriptional Profiling. *Cell Reports*, 21(13):3970–3986.

Zhang, H. (2023). SCP: Single Cell Pipeline. R package version 0.4.8.

Zhang, Y. V., Cheong, J., Ciapurin, N., McDermitt, D. J., and Tumbar, T. (2009). Distinct Self-renewal and Differentiation Phases in the Niche of Infrequently Dividing Hair Follicle Stem Cells. *Cell stem cell*, 5(3):267.

Zheng, B., Cao, B., Crisan, M., Sun, B., Li, G., Logar, A., Yap, S., Pollett, J. B., Drowley, L., Cassino, T., Gharaibeh, B., Deasy, B. M., Huard, J., and Péault, B. (2007). Prospective identification of myogenic endothelial cells in human skeletal muscle. *Nature biotechnology*, 25(9):1025–1034.

Zilova, L., Weinhardt, V., Tavhelidse, T., Schlagheck, C., Thumberger, T., and Wittbrodt, J. (2021). Fish primary embryonic pluripotent cells assemble into retinal tissue mirroring in vivo early eye development. *eLife*, 10.

List of Figures

List of Tables

Acknowledgements

First and most importantly - Jochen! Thank you for being my scientific advisor and welcoming me into the laboratory and onto the 5th floor 6 years ago. Not only have you inspired and supported my research over all these years, but my life circumstances have made me discover a different side of you. Whenever I came to you with one after another darker news, you were so generous in giving me time to be with my family. I am truly blessed that during these dark times, you had my back, even though it was clearly not beneficial for research. Of course, I will never forget our Zoom sessions when I was locked up in that hospital in Moscow, and you still found time to talk to me weekly and cheer me up. Besides, thank you a lot for all our scientific discussions, the endless cups of espresso you made for me, and for constantly pushing me to ask big and crazy questions.

I would like to thank Steffen Lemke for being my second supervisor and for all the discussions in my TACs and beyond. Your continuous optimism and support have helped me a lot throughout my PhD time.

I am very grateful to you, Lázaro, for all the fantastic feedback you gave me and all the ArCoS discussions we had over the last years.

I would like to thank Ana Martín-Villalba for agreeing to be part of my PhD committee.

I would like to thank my TAC members, Jochen Wittbrodt, Steffen Lemke, Carmen Ruiz de Almodóvar, Lázaro Centanin and Alexander Aulehla for all the constructive and clear feedback I have been receiving in the meetings over the years.

Besides, I thank Anette Kurz for patiently answering multiple questions regarding the submission of this thesis.

I would like to thank the fantastic team of 5th floor secretaries (past and present) – Frederike Seibold, Kevin Urbansky, and Ute Volbehr - for all the support with residence permit and beyond I have been receiving from you over the last years.

I thank Lucie for all the support and guidance I've received over the last three years. Your patience, expertise and, most importantly, genuine passion for the project made this journey so much more manageable and enriching for me. I have learned a lot from you and I hope this project will prosper and you will get to the gravel of life-long growth.

Venera, I can't thank you enough for all the things you have done for me in my

PhD time. From proofreading my reports to sending flowers to my mum, you were always there for me. The discussions with you and your honest feedback helped me become a much more constructive scientist.

I would like to extend my gratitude to Lucie Zilova, Venera Weinhardt and Tanja Kellner for the fantastic feedback I have received from you while writing this thesis. I also thank Bettina Welz, Philip Watson, Moritz Fuchs, and Cassian Afting for editing my "Zusammenfassung".

I am deeply grateful to Tanja and Beate for all the excellent technical support I have received from you throughout my time in the lab. Besonderer Dank geht an Tanja, die mir zugehört hat, als ich versucht habe, Deutsch zu sprechen =).

I thank all the 5th floor (past and present) people for all the support I have received from you, for all the fun we have shared and for creating the one and only home-like atmosphere of the 5th floor.

I am also grateful to the members of Bay 4 (ever) – past and present. Clara, Jørgen, Sevinç, Jana, and Rachel – you have made the lab time for me so much fun. I would like to especially thank Jørgen for all the work we have done together and the support I received from you.

I would like to thank Katha for all the scientific conversations we had and for all the valuable advice on HCR and beyond.

I thank Alex, Omar, and Colin for your support and advice.

I would like to extend my gratitude to Bettina, Leonie, Jasmin, Karen, Rashi and Bea. Talking to you has always been such a good support for me which helped me to go through this.

I thank Danila for your friendship and support throughout the years. Many thanks go to Alicia for all the support and advice I have received from you. I really like our tradition of breakfasting together :D

I want to thank my mum, dad, and stepdad for helping me become who I am today. I wish you were here to see this moment.

I thank Natasha, Philip, Polina, Stephan, and Sasha. Your unconditional support was my comfort during the tough times. Thank you.

I would like to thank Maja and Jørgen, for setting the standards of friendship high for me. I would also like to thank Nazrin and Asaf, Jafar, Toma, and Medina, for their warmth and always finding a good word for me.

Moritz, I thank you for your enduring patience and love. You made my last two years much brighter. I also thank Petra and Harry for their support.